AWARD NUMBER: W81XWH-14-1-0480

TITLE: Androgen Receptor Splice Variants and Resistance to Taxane Chemotherapy

PRINCIPAL INVESTIGATOR: Haitao Zhang, Ph.D.

CONTRACTING ORGANIZATION: Tulane University, New Orleans, LA

REPORT DATE: December 2018

TYPE OF REPORT: Final report

PREPARED FOR: U.S. Army Medical Research and Materiel Command
Fort Detrick, Maryland 21702-5012

DISTRIBUTION STATEMENT: Approved for Public Release;
Distribution Unlimited

REPORT DOCUMENTATION PAGE

Form Approved
OMB No. 0704-0188

1. REPORT DATE	2. REPORT TYPE	3. DATES COVERED
December 2018	Final	29Sep2014-28Sep2018

4. TITLE AND SUBTITLE

Androgen Receptor Splice Variants and Resistance to Taxane Chemotherapy

5a. CONTRACT NUMBER
W81XWH-14-1-0480

5b. GRANT NUMBER
PC130570

5c. PROGRAM ELEMENT NUMBER

6. AUTHOR(S)
Haitao Zhang, Ph.D.

E-Mail:hzhang@tulane.edu

5d. PROJECT NUMBER

5e. TASK NUMBER

5f. WORK UNIT NUMBER

7. PERFORMING ORGANIZATION NAME(S) AND ADDRESS(ES)

Tulane University
1430 Tulane Ave
New Orleans, LA 70112

8. PERFORMING ORGANIZATION REPORT NUMBER

9. SPONSORING / MONITORING AGENCY NAME(S) AND ADDRESS(ES)

U.S. Army Medical Research and Materiel Command
Fort Detrick, Maryland 21702-5012

10. SPONSOR/MONITOR'S ACRONYM(S)

11. SPONSOR/MONITOR'S REPORT NUMBER(S)

12. DISTRIBUTION / AVAILABILITY STATEMENT

Approved for Public Release; Distribution Unlimited

13. SUPPLEMENTARY NOTES

14. ABSTRACT

During the grant period, we have achieved the following: 1) Identified two regions in the AR ligand binding domain (LBD) that confer the microtubule binding activity; 2) Characterized the functional significance of the AR-microtubule interaction and provided compelling evidence to suggest that the intracellular localization and activity of AR microtubules is regulated by its association with the microtubules; 3) Provided a fundamental understanding of the constitutive activities of LBD-truncated AR splice variants, such as AR-V7 and ARv567es; 4) Developed and validated a whole-blood based assay for the detection of AR-V7 and ARv567es, and 5) Identified a profound interaction of AR LBD hotspot mutations.

15. SUBJECT TERMS
Castration-resistant prostate cancer; docetaxel; cabazitaxel; chemotherapy; androgen receptor splice variants; microtubule; ligand-binding domain; microtubule-associated sequence

16. SECURITY CLASSIFICATION OF:			17. LIMITATION OF ABSTRACT	18. NUMBER OF PAGES	19a. NAME OF RESPONSIBLE PERSON
a. REPORT	b. ABSTRACT	c. THIS PAGE			USAMRMC
Unclassified	Unclassified	Unclassified	Unclassified	68	19b. TELEPHONE NUMBER *(include area code)*

Table of Contents

Page

1. Introduction……. 1

2. Keywords……. 1

3. Accomplishments……..……... 1

4. Impact……...…… 9

5. Changes/Problems...…..…… 10

6. Products…….……..…..……. 10

7. Participants & Other Collaborating Organizations……. 11

8. Special Reporting Requirements…… 12

9. Appendices…… 12

I. Introduction

This project was initially designed to test the central hypothesis that constitutively active androgen receptor splice variants (AR-Vs) are associated with resistance to taxane chemotherapy in castration-resistant prostate cancer (CRPC). However, this hypothesis has been challenged by several clinical studies during the course of the study. Antonarakis et al first evaluated the associations between AR-V7 status and clinical responses in patients receiving taxane chemotherapy (1). The key response biomarkers, including PSA progression-free survival, clinical/radiographic progression-free survival, and overall survival, were comparable between patients with different AR-V7 expression status in circulating tumor cells (1). Furthermore, AR-V7-positive patients had superior responses to taxanes than to enzalutamide or abiraterone, suggesting taxane chemotherapy is a viable treatment option for these patients. Subsequently, a report by Scher et al confirmed that taxane is more efficacious than AR-directed therapies in AR-V7-positive patients, and that no significant differences in clinical responses to taxane are associated with AR-V7 status (2). Since our proposed clinical study in the original Aim 3 had a similar study design as these studies, we believe we will not be able to reach a different conclusion. In addition, we have encountered difficulty in patient accrual as few patients are treated with docetaxel or cabazitaxel alone at Tulane Cancer Center. Based on these considerations, we had requested and subsequently received approval to change the focus of the project. The restructured proposal consists of the following specific aims:

Aim 1. To understand the fundamental difference in nuclear translocation mechanisms of AR-FL and AR-Vs.

Aim 2. To functionally characterize the microtubule association sequences.

Aim 3. To develop a blood-based assay for detecting the expression of AR-Vs.

In this report, we will provide a comprehension summary of the work completed to date, organized around the revised specific aims and major tasks.

II. Keywords

Castration-resistant prostate cancer; docetaxel; cabazitaxel; chemotherapy; androgen receptor splice variants; microtubule; ligand-binding domain; microtubule-associated sequence

III. Accomplishments

What are the major goals/tasks of this project?

Major Task 1: To identify the microtubule-associated sequence (MTAS) on AR.
Major Task 2: To develop a blood-based assay for detecting the expression of AR-Vs.
Major Task 3: To determine the transcriptional activity of MTAS-truncated AR constructs.
Major Task 4: To determine the influence of recurring AR LBD mutations on microtubule association.

What was accomplished under these goals?

Major Task 1: To identify the microtubule-associated sequence (MTAS) on AR.

1. Identification of the microtubule-associated sequences (MTAS) on AR. We have previously demonstrated that the nuclear import of full-length AR (AR-FL) depends on a dynamic microtubule, whereas that of the AR-Vs is microtubule-independent (3). We hypothesize that this fundamental difference is caused by the different binding capacities to the microtubule cytoskeleton by the two types of receptors. This hypothesis was confirmed by using an *in vivo* microtubule-binding assay (3). In addition, we generated a series of deletion constructs encompassing different domains of AR. By using the *in vivo* microtubule-binding assay, we have demonstrated that the microtubule-binding is mediated by the ligand-binding domain (LBD) of AR (3). Consistent with this finding, we found that the LBD-truncated AR-V7 and AR^{v567es} both bind poorly to the microtubules (3).

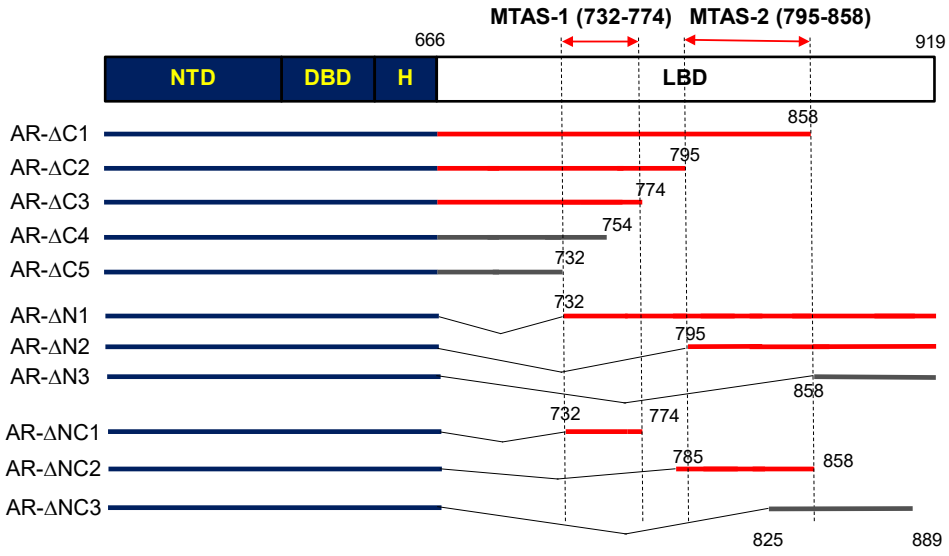

Figure 1. Diagram of the deletion constructs containing various fragments of the ligand-binding domain. Fragments with strong microtubule-binding activities are shown in red. Two putative microtubule association sequences (MTAS) are shown. The full summary of the binding activity is provided in Table 1.

To further map the region(s) within the LBD that is responsible for microtubule association, we generated a series of deletion constructs within the LBD (Fig. 1). COS-7 cells were transiently transfected with these plasmids, cultured in an androgen-deprived condition, and lysed for the *in vivo* microtubule-binding assay. This deletion analysis revealed that two regions in the AR LBD could potentially mediate the association with the microtubules (Fig. 1). These regions were termed *microtubule association sequence 1* (MTAS1, a.a. 732-774) and *2* (MTAS2, a.a. 795-858). Constructs retained one or both MTAS displayed strong binding activities, whereas those with both MTAS deleted or disrupted lost the ability to bind to the microtubules (Fig. 1). Interestingly, all constructs that were capable of microtubule binding showed similar binding activities, regardless of which or how many copies of MTAS they contain (Table 1 and Fig. 1), suggesting there is functional redundancy between MTAS1 and MTAS2.

2. Correlation of the microtubule-binding activity and the intracellular localization of AR proteins in the absence of ligand stimulation. To determine the localization of the aforementioned AR deletional mutants, COS-7 cells were transfected with plasmids and cultured in an androgen-depleted condition. Following fixation, the intracellular localization of the AR proteins was analyzed by immunofluorescence using an antibody recognizing the N-terminus of AR. The complete results were compiled in Table 1 and representative images were shown in Fig. 2. In summary, we observed a strong correlation of intracellular localization and microtubule-binding activity of these proteins in the absence of androgen stimulation. All mutants with strong microtubule-binding activities were localized to the cytoplasm, whereas those with weak binding activities were found in the nucleus. These results provide evidence supporting the notion that association with the microtubules is a mechanism for retaining AR in the cytoplasm.

Table 1. Summary of AR-LBD deletion analysis.

Name	LBD fragment	MT binding	Localization (w/o androgen)
AR-FL	666-919	++	Cytoplasmic
ΔC1	666-858	++	Cytoplasmic
ΔC2	666-795	++	Cytoplasmic
ΔC3	666-774	++	Cytoplasmic
ΔC4	666-754	-	Nuclear
ΔC5	666-732	-	Nuclear
ΔN1	732-919	++	Cytoplasmic
ΔN2	795-919	++	Cytoplasmic
ΔN3	858-919	-	Nuclear
ΔNC1	732-774	++	Cytoplasmic
ΔNC2	795-858	++	Cytoplasmic
ΔNC3	825-889	-	Nuclear

*, scored based on relative MT-binding activity compared to that of AR-FL. ++, >75%; +, 50-75%; -, <50%.

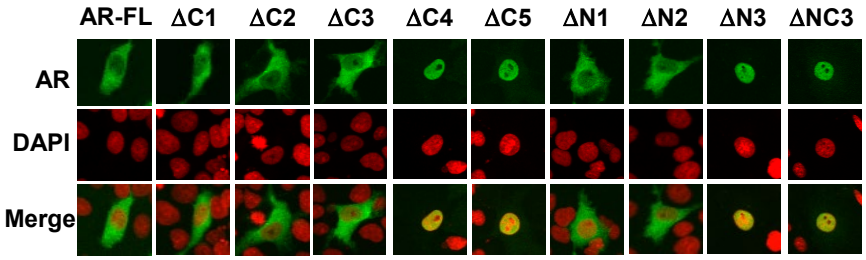

Fig. 2. The intracellular distribution of the AR LBD deletion mutants. Transfected COS7 cells were cultured on cover slips in androgen-free media and the intracellular localization of the proteins was detected by an antibody recognizes the N-terminus of AR. The nuclei were stained with DAPI (pseudo-colored red to enhance visualization).

3. Association with the microtubules traps nuclear-localized AR-Vs in the cytoplasm. The intracellular localization analysis above is consistent with what we have observed with AR-V7 and AR^{v567es}, which possess weak microtubule-binding activities and are predominantly nuclear-localized (3). We hypothesize that AR-V7 and AR^{v567es} gain constitutive nuclear localization by escaping microtubule-mediated cytoplasmic retention. To test this hypothesis we engineered chimeric proteins by appending MTAS1 (M1, a.a 732-744) or MTAS2 (M2, a.a. 795-858) to the

C-terminus of the variants. *In vivo* microtubule-binding assays confirmed that the ensuing fusion proteins gained microtubule-binding activities (data not shown). Next, the intracellular localization of the fusion proteins was examined in COS-7 cells by immunofluorescence as described above. As shown in Fig. 3A, AR-V7 was predominantly localized to the nucleus. However, after fusing M1 or M2, the chimeric protein were localized primarily to the cytoplasm. Similarly, the addition of M1 or M2 caused AR^{v567es} to be trapped in the cytoplasm. In addition, AR-V7 and AR^{v567es} lost its transcriptional activity when fused with M1 or M2 (Fig. 3B). Collectively, these results provide strong support for the role of MTAS in retaining AR in the cytoplasm.

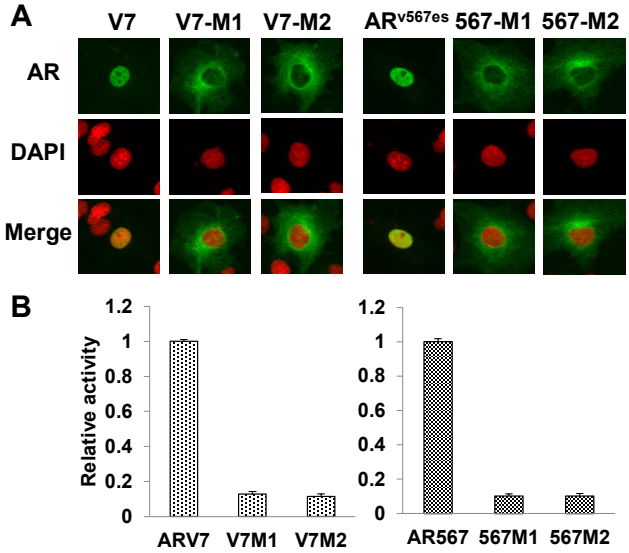

Fig. 3. Microtubule association traps AR-Vs in the cytoplasm. MTAS1 (M1, a.a 732-744) or MTAS2 (M2, a.a. 795-858) was fused to the c-terminus of AR-V7 or AR^{v567es}. **A, the localization of the fusion proteins**. Transfected COS-7 cells were cultured on cover slips in androgen-free media and the intracellular localization of the proteins was analyzed by immunofluorescence. The nuclei were stained with DAPI (pseudo-colored red to enhance visualization). **B, the transcriptional activity of the fusion proteins**. COS-7 cells were co-transfected with an ARE-luciferase reporter and one of the fusion proteins, and AR activity was determined by the luciferase assay.

4. MTAS1 and MTAS2 are highly conserved among nuclear receptors. MTAS1 is located within Exon 5, whereas MTAS is encoded by Exons 6 and 7. Sequence analysis revealed little homology between MTAS1 and MTAS2 (data not shown). However, both MTAS regions were highly conserved within the Type I nuclear receptor subfamily, particularly progesterone receptor (PR), mineralcorticoid receptor (MR), and glucocorticoid receptor (GR). In contrast, estrogen receptor alpha (ERα) only contains a region with modest homology with MTAS1. This is possibly due to the short C-terminus of ERα as compared to other Type I receptors. Nonetheless, the sequence analysis suggests that both MTAS are present in other Type I nuclear receptors.

MTAS1 (contained within Exon 5)

```
AR(732-774)   DDQMAVIQYSWMGLMVFAMGWRSFTNVNSRMLYFAPDLVFNEY
PR(745-787)   DDQITLIQYSWMSLMVFGLGWRSYKHVSGQMLYFAPDLILNEQ
MR(796-838)   EDQITLIQYSWMCLSSFALSWRSYKHTNSQFLYFAPDLVFNEE
GR(590-632)   DDQMTLLQYSWMFLMAFALGWRSYRQSSANLLCFAPDLIINEQ
ERα(373-403)  HDQVHLLECAWLEILMIGLVWRS--MEHPGKLLFAPNLLLDRN
```

MTAS2 (contained by Exons 6 and 7)

```
AR(795-858) FGWLQITPQEFLCMKALLLFSIIPVDGLKNQKFFDELRMNYIKELDRIIACKRKNPTSCSRRFY
GR(653-716) LHRLQVSYEEYLCMKTLLLLSSVPKDGLKSQELFDEIRMTYIKELGKAIVKREGNSSQNWQRFY
PR(808-871) FVKLQVSQEEFLCMKVLLLLNTIPLEGLRSQTQFEEMRSSYIRELIKAIGLRQKGVVSSSQRFY
MR(859-922) FVRLQLTFEEYTIMKVLLLLSTIPKDGLKSQAAFEEMRTNYIKELRKMVTKCPNNSGQSWQRFY
```

Fig. 4. MTAS1 and MTAS2 are highly conserved among nuclear receptors. Sequence analyses showed both MTAS1 and MTAS2 are highly conserved among members of the Type I nuclear receptor subfamily, including progesterone receptor (PR), glucocorticoid receptor (GR), mineralcorticoid receptor (MR). Identical amino acids among all members are highlighted in bold. The residue affected by the AR LBD hotspot mutation W742C is underlined.

Summary: we have completed the proposed experiment listed under Major Task 1. In addition, we have extended the scope of this task with additional experiments to better understand the functional significance of AR association with the microtubules.

Major Task 2: To develop a whole-blood-based assay for detecting the expression of AR-Vs.

1. Development of a blood-based assay for AR-V7 and AR^{v567es}. We first evaluated the whole-blood approach (whole-blood collected in Paxgene Blood RNA tubes, also referred to as the PAXgene approach) and the CTC negative selection approach based on depletion of CD45+ leukocytes (also referred to as the CD45-depletion approach). Ten heavily treated mCRPC patients were identified for this purpose and blood samples obtained from the same patient were analyzed by both approaches (Fig. 5). As shown in Table 2, AR-FL and AR-V7 transcripts were detected in all samples by both methods. AR^{v567es} was detected in 20% of the samples by the PAXgene approach, but only in 10% by the CD45-depletion, suggesting that the leukocyte depletion process may cause a loss of sensitivity. Indeed, the AR-Vs transcript levels measured by the CD45-depletion approach were always lower than those by the PAXgene approach: in the case of AR-V7, the estimated loss of sensitivity was ~40% (Table 3).

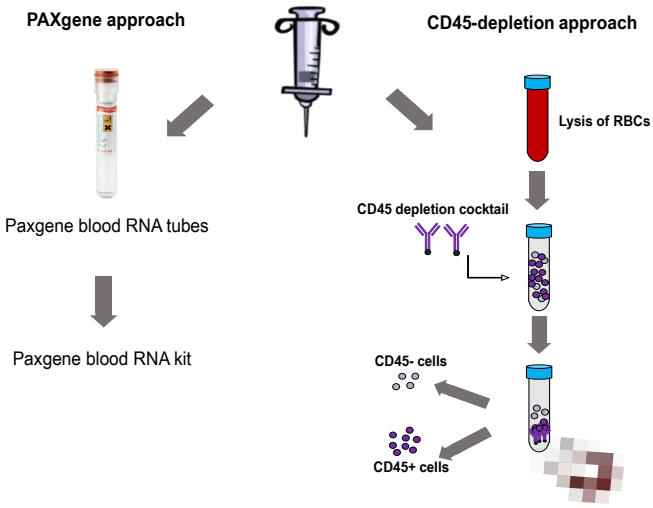

Fig. 5. Diagram of the experimental design to compare the PAXgene approach with the CD45-depleteion approach.

Table 2. Detection of AR transcripts by two approaches.

	PAXgene	CD45 depletion
AR-FL	10/10	10/10
AR-V7	10/10	10/10
AR^{v567es}	2/10	1/10

Table 3. Relative expression levels of AR-V transcripts by CD45-depletion approach as compared to the PAXgene approach.

Sample ID	Relative expression (%)*	
	AR-V7	AR^{v567es}
1	33.06	-
2	18.04	-
3	78.75	-
4	54.55	92.34
5	73.50	-
6	60.42	0
7	85.71	-
8	29.32	-
9	80.15	-
10	84.73	-
Mean±SD	59.82 ± 21.10	-

*The expression level detected by the PAXgene approach is set as 100%.

The separation of CD45- and CD45+ cells during the leukocyte depletion process provides an opportunity to investigate the sources of AR transcripts in the blood. As shown in Table 4, in the majority of the samples (8 out of 10), the AR-V7 transcript was exclusively from the CD45- fraction. Only 2 out of 10 samples were with detectable AR-V7 in the CD45+ fraction. The expression level, when compared to the CD45- fraction (i.e. CTC-enriched fraction), were markedly lower.

Similarly, the vast majority of AR^{v567es} transcript was found in the CD45- fraction. In contrast, AR-FL is abundantly expressed in the both fractions (Table 4).

Table 4. Distribution of AR transcripts in the CD45- and CD45+ fractions*.

ID	AR-V7		AR^{v567es}		AR-FL	
	CD45-	CD45+	CD45-	CD45+	CD45-	CD45+
1	100.00%	0.00%	-	-	46.05%	53.95%
2	100.00%	0.00%	-	-	29.21%	70.79%
3	100.00%	0.00%	-	-	63.96%	36.04%
4	85.93%	14.07%	96.16%	3.84%	55.55%	44.45%
5	100.00%	0.00%	-	-	65.27%	34.73%
6	100.00%	0.00%	-	-	54.75%	45.25%
7	100.00%	0.00%	-	-	20.02%	79.98%
8	91.65%	8.35%	-	-	76.71%	23.29%
9	100.00%	0.00%	-	-	75.59%	24.41%
10	100.00%	0.00%	-	-	31.34%	68.66%

*The percentage values were calculated from the expression ratio between the two fractions, with a total of 100%.

Collectively, these results suggest that the AR-Vs transcripts in the CD45+ fraction are below or slightly above the level of detection, suggesting that depleting the hematopoietic cells offers little or no improvement in specificity for the detection of AR-Vs. On the other hand, performing this procedure could lead to a loss of sensitivity, possibly due to RNA degradation during the process.

2. Sensitivity of the PAXgene assay. Based on the results above, we decided on the PAXgene approach for AR-V detection in blood. To estimate the sensitivity of this assay, fixed numbers of 22Rv1 cells, which express a number of AR-Vs including AR-V7, were spiked into 5 ml blood from a healthy donor. Fig. 6 shows that this assay has the sensitivity of detecting 5-50 AR-V7+ cells in 5 ml of blood, or 1-10 cells per ml of blood.

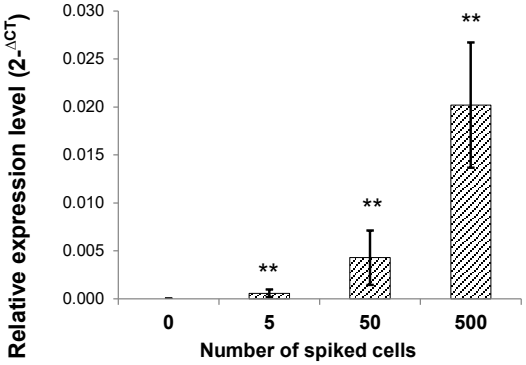

Fig. 6. Sensitivity of the PAXgene approach in detection of AR-V7 mRNA. Specified numbers of 22RV1 cells were spiked into 5 ml of blood from a healthy donor and transferred to PAXgene tubes. RNA was purified using the PAXgene Bloood RNA Kit and qRT-PCR was performed. Statistics analysis was performed using one-tailed Z-test. **, P<0.01.

3. The stability of AR transcripts in PAXgene tubes. An important question for the blood-based assay is the stability of AR transcripts in the PAXgene tubes. To answer this question, we spiked 100 22RV1 cells into PAXgene tubes containing 2.5 ml of blood from a healthy donor (AR-V negative). The tubes were stored at room temperature (RT), 4˚C or -20˚C for up to 4 days and the assay was performed as described. As shown in Fig. 7, AR-V7 transcript was fairly stable at room temperature for 24 h, but suffered a 30% loss of signal after 48 h. In contrast, AR-V7 was much more stable when stored at 4˚C or -20˚C, with more than 90% of signal remained after day 4. The stability of AR-FL transcript was similar to that of AR-V7. These results showed that the AR transcripts remain stable in Paxgene tubes stored at 4˚C or -20˚C for at least 4 days.

Summary: By developing and validating the whole-blood-based assay for detecting the expression of AR-V7 and AR^{v567es} in patients, we have completed Major Task #2. The addition work on the stability of AR-V7 in PAXgene tubes provides guidelines for sample collection from multiple centers, to be analyzed by a centralize lab.

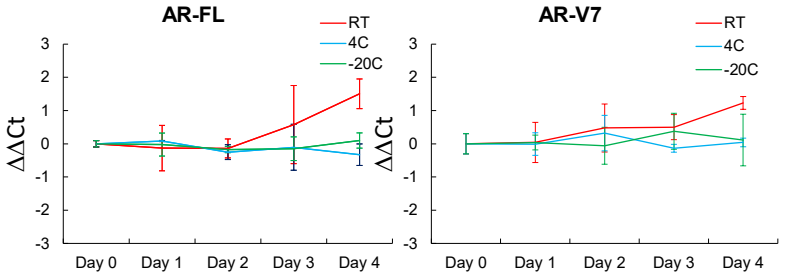

Fold relative to Day 0

	AR-FL			AR-V7		
	RT	4˚C	-20˚C	RT	4˚C	-20˚C
Day 1	1.09	0.94	1.02	0.97	1.01	0.97
Day 2	1.10	1.19	1.13	0.72	0.80	1.04
Day 3	0.67	1.08	1.11	0.71	1.10	0.77
Day 4	0.35	1.26	0.93	0.43	0.97	0.92

Fig. 7. Stability of the AR transcripts in Paxgene Tubes. One hundred (100) 22Rv1 cells were spike into 2.5 ml blood from a healthy donor drawn in Paxgene tubes in triplicates and stored at room temperature (RT), 4˚C, or -20˚C for up to 4 days. The assay was performed as described (Liu et al 2016), using RPL30 as the housekeeping gene. Top, the changes of ΔCt from Day 0. Bottom, relative levels of the transcripts compared to Day 0.

Major Task 3: To determine the transcriptional activity of MTAS-truncated AR constructs.

The transcriptional activity of several MTAS-truncated AR constructs, including AR-ΔC1, ΔC2, ΔC3, ΔC4, and ΔC5 (Table 1), were analyzed in COS-7 cells. Cells were transiently transfected with an androgen response element (ARE) luciferase construct (ARE-Luc) and pRL-TK, along with an AR construct, and cultured in the presence or absence of 1 nM R1881. After 24 hours, luciferase assay was performed using the Dual-Luciferase Reporter Assay System (Promega). The transcriptional activity of AR (measured by the firefly luciferase activity) was normalized by transfection efficiency (measured by Renilla luciferase activity). As shown in Fig. 8, constructs ΔC1, ΔC2, ΔC3, which are located in the cytoplasm in the absence of androgen (Table 1), showed little or no transcriptional activity in this condition. Adding androgen to the culture didn't stimulated the activity for these constructs, possibly due to the disruption of the ligand-binding capacity in these constructs. On the other hand, AR-ΔC5, which is localized to the nucleus in the absence of androgen stimulation (Table 1), showed strong constitutive activity and resistance to docetaxel treatment. These results are consisted with the microtubule-binding and nuclear localization date. However, one exception is AR-ΔC4. Despite being nuclear localized, this constructs exhibited little or no transcriptional activity in the presence or absence of androgen. One possible explanation is that there is a negative regulatory element in the region between 732-754 a.a in the AR LBD.

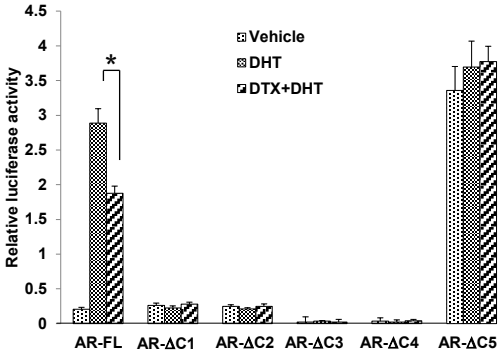

Fig. 8. Transcriptional activity of MTAS-truncated AR constructs.

Major Task 4: To determine the influence of recurring AR LBD mutations on microtubule association.

Recent studies using cutting edge next generation sequencing analysis have confirmed AR LBD as a mutational hotspot. Particularly, four missense mutations (L702H, W742C, H875Y, and T878A) have been identified as recurring mutations in mCRPC specimens (4). Clinically, all these mutations have been implicated in resistance to AR-targeted therapies (5). Interestingly, the W742C mutation is located within MTAS1 and affects a residue conserved among all Type I nuclear receptors (Fig. 4). The other mutations are located in close proximity to MTAS1 (L702H) or MTAS2 (H875Y and T878A). To explore the possibility that the W742C mutation, along or in combination with other mutations, may interfere with the microtubule-binding activity of AR, we carried out site-directed mutagenesis to introduce these mutations to the wild-type AR (Table below).

Template	Mutation(s) introduced	Designation
AR-WT	W742C	AR-W742C
AR-WT	T878A	AR-T878A
AR-T878A	W742C	AR-W742C/T878A

We first analyzed the microtubule-binding activity of these plasmids by the *in vivo* microtubule-binding assay. Surprisingly, all these AR mutants showed similar microtubule-binding activity as the wild-type AR (data not shown). However, when the luciferase reporter assay was performed, the W742C/T878A AR-DM showed a much stronger activity in the androgen-depleted condition when compared with the wildtype AR (~30x) (Fig. 9). Furthermore, the AR-DM was responsive to androgen stimulation but refractory to the antiandrogen MDV-3100 (Fig. 9). When treated with docetaxel, this AR-DM was partially inhibited but the activity remained high (Fig. 9). In contrast, the W742C and T878 single mutants showed similar activities as the wildtype AR under these conditions.

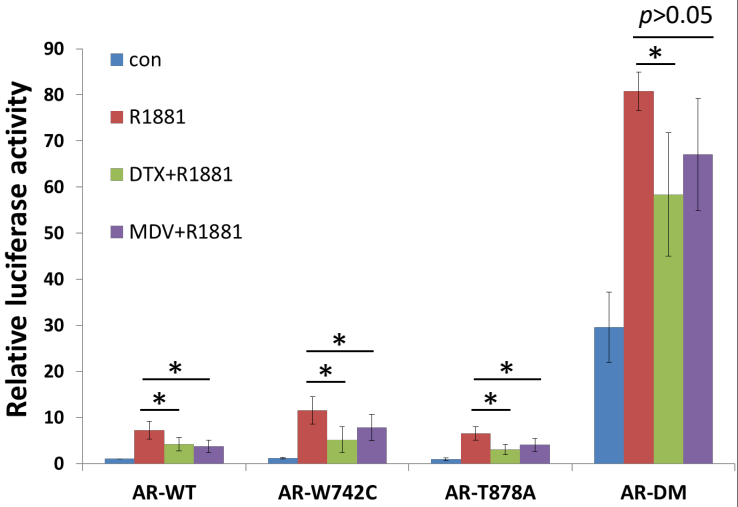

Fig 9. Transcriptional activity of different AR isoforms. COS-7 cells were transfected with AR plasmids and luciferase reporter assay was carried out to determine the transcriptional activities. R1881, 1 nM; DTX, docetaxel (20 nM); MDV, MDV-3100 (10 μM). *, $p<0.05$. AR-DM, AR-W742C/T878A double mutant.

We further examined the intracellular localization of the AR mutants under these conditions, and the results are shown in Fig.10. In the absence of androgen, AR-WT was primarily

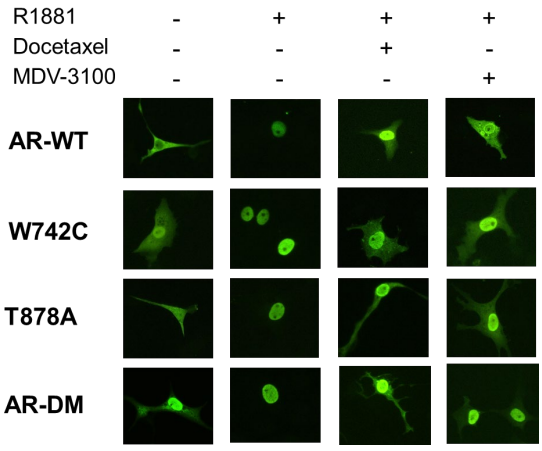

Fig 10. Intracellular localization of AR mutants. COS-7 cells were transfected with AR mutants and cultured in an androgen-depleted condition. Cells were fixed 4 h after R1881 treatment and analyzed by immuno-fluorescence using an anti-AR (N20).

localized in the cytoplasm, whereas W742C and T878A were partially nuclear. Upon androgen stimulation, all 3 underwent nuclear translocation. Consistent with the luciferase assay results, AR-DM was predominantly located in the nucleus in the absence of androgens, and become completely nuclear after androgen stimulation. While MDV3100 inhibited the nuclear translocation all other AR isoforms, it had little or no effect on that of AR-DM.

Taken together, the results shown under Major Task 4 suggest that *there is a profound interaction between the W742C and T878A mutations to alter the ligand specificity of AR, allowing the receptor harboring both mutations to become constitutively active and refractory to both MDV-3100 (enzalutamide) and docetaxel.*

What opportunities for training and professional development has the project provided?

This project has provided research training and professional development for 2 PhD students (Guanyi Zhang and Jizhuo Li) and 1 postdoctoral fellow (Dr. Dongying Li). Dr. Guanyi Zhang is now a postdoctoral at Louisiana State University Health Sciences Center. Dr. Jianzhuo Li joined MD Anderson Cancer Center as a staff scientist after graduation. Dr. Dongying Li is now a staff scientist in the National Center for Toxicological Research (NCTR) at FDA.

How were the results disseminated to communities of interest?

Nothing to report.

What do you plan to do during the next reporting period to accomplish the goals?

Nothing to report.

IV. Impact

What was the impact on the development of the principal discipline(s) of the project?

The impact of the project is several fold. First, we have developed and validate a whole-blood assay for the detection of AR-V7 and AR^{v567es}, without the need for isolation of or enrichment for circulating tumor cells. This is important because constitutively active AR-Vs have been associated with resistance to hormonal therapies. Compared to other liquid biospy assays for AR-

V7, our assays are easy to implement due to its sensitivity, specificity, and cost effectiveness. Second, we have demonstrated that the AR transcripts remain stable in PAXgene tubes for at least 4 days at 4˚C or -20˚C, suggesting it is feasible to collect samples from multiple locations to be analyzed in a central lab, allowing more patients to have access to this assay. Third, the work on the functional significance of AR-microtubule association provided strong evidence that the microtubule cytoskeleton plays an important role in regulating the intracellular localization and trafficking of AR. Constitutively active AR-Vs are able to escape such regulation due to the truncation of the ligand-binding domain. Finally, our study identified potential interactions between AR LBD hotspot mutations, which could uncover a previously unrecognized resistance mechanism to anti-AR therapies.

What was the impact on other disciplines?
Nothing to report.

What was the impact on technology transfer?
Nothing to report.

What was the impact on society beyond science and technology?
Nothing to report.

V. Changes/Problems

As mentioned in the Introduction, we have proposed to change the direction of the research to focus on the functional significance of AR-microtubule association. The previously proposed clinical study and animal experiment will not be carried out. These changes have been approved by the DOD-PCRP.

VI. Products

Publications, conference papers, and presentations

- **Journal publications.** The following paper was published:

  Zhang G, Liu X, Li J, Ledet E, Alvarez X, Qi Y, et al. Androgen receptor splice variants circumvent AR blockade by microtubule-targeting agents. Oncotarget. 2015;6:23358–71. Status: Published; Acknowledgement of federal support: yes.

  Xu D, Zhan Y, Qi Y, Cao B, Bai S, Xu W, et al. Androgen Receptor Splice Variants Dimerize to Transactivate Target Genes. Cancer Res. 2015;75:3663–71. Status: Published; Acknowledgement of federal support: yes.

  Xichun Liu, Elisa Ledet, Dongying Li, Ary Dotiwala, Allie Steinberger, Jianzhuo Li, Yanfeng Qi, Yan Dong, Jonathan Silberstein, Benjamin Lee, Oliver Sartor, and Haitao Zhang. A Whole Blood-Based Detection Assay for AR-V7 and AR^{v567es} in Patients with Advanced

Prostate Cancer. Journal of Urology 2016;196:1758-1763. Status: Published; Acknowledgement of federal support: yes.

Jianzhuo Li, Xueqi Fu, Subing Cao, Jing Li, Shu Xing, Dongying Li, Yan Dong, Derrick Cardin, Hee-Won Park, Franck Mauvais-Jarvis, and Haitao Zhang. Membrane-associated androgen receptor (AR) potentiates its transcriptional activities by activating heat shock protein 27 (HSP27). J. Biol. Chem. (2018) 293(33):12719–12729. Status: Published; Acknowledgement of federal support: yes.

- **Books or other non-periodical, one-time publications.** Nothing to report.

- **Other publications, conference papers, and presentations.** Nothing to report

Website(s) or other Internet site(s)
Nothing to report.

Technologies or techniques
Nothing to report.

Inventions, patent applications, and/or licenses
Nothing to report.

Others
Nothing to report.

VII. Participants & Other Collaborating Organizations

What individuals have worked on the project?

Name	Haitao Zhang	Guanyi Zhang	Dongying Li
Project role	PI	Technician/PhD trainee	Postdoc Fellow
Researcher Identifier (ORCID ID)	0000-0002-5969-1024	N.A.	N.A.
Nearest person month worked	12	20	7
Contribution to project	Conception and project design; data analysis; Study coordination and supervision; manuscript writing; report	Characterization of MTAS	Development of the PAXgene assay
Funding support	American Cancer Society	American Cancer Society	American Cancer Society

Name	Jianzhuo Li	Xichun Liu	Elisa Ledet	Brian Lewis
Project role	Technician/PhD trainee	Postdoc Fellow	Study coordinator	Co-investigator
Researcher Identifier (ORCID ID)	N.A.	N.A.	N.A.	N.A.
Nearest person month worked	11	3	1	1
Contribution to project	Functional characterization of MTAS;	Developing sample collection and ddPCR protocols	Clinical study coordinator	Patient recruitment and consent
Funding support	American Cancer Society	American Cancer Society	DOD-PCRP postdoctoral	

Has there been a change in the active other support of the PD/PI(s) or senior/key personnel since the last reporting period?

Nothing to report.

What other organizations were involved as partners?

Nothing to report.

VIII. Special Reporting Requirements: not applicable.

IX. Appendices

Reference Cited:

1. Antonarakis ES, Lu C, Luber B, et al. Androgen receptor splice variant 7 and efficacy of taxane chemotherapy in patients with metastatic castration-resistant prostate cancer. JAMA Oncol. 2015;1:582–91.
2. Scher HI, Lu D, Schreiber NA, Louw J, Graf RP, Vargas HA, et al. Association of AR-V7 on Circulating Tumor Cells as a Treatment-Specific Biomarker With Outcomes and Survival in Castration-Resistant Prostate Cancer. JAMA Oncol. 2016;2:1441–9.
3. Zhang G, Liu X, Li J, Ledet E, Alvarez X, Qi Y, et al. Androgen receptor splice variants circumvent AR blockade by microtubule-targeting agents. Oncotarget. 2015;6:23358–71.
4. Robinson D, Van Allen EM, Wu Y-M, Schultz N, Lonigro RJ, Mosquera J-M, et al. Integrative clinical genomics of advanced prostate cancer. Cell. 2015;161:1215–28.
5. Watson PA, Arora VK, Sawyers CL. Emerging mechanisms of resistance to androgen receptor inhibitors in prostate cancer. Nat Rev Cancer. 2015;15:701–11.

Publications (pdf files)

Androgen receptor splice variants circumvent AR blockade by microtubule-targeting agents

Guanyi Zhang[1,2,6], Xichun Liu[2,6], Jianzhuo Li[1,2,6], Elisa Ledet[4,5,6], Xavier Alvarez[7], Yanfeng Qi[3,6], Xueqi Fu[1], Oliver Sartor[4,5,6], Yan Dong[1,3,6], Haitao Zhang[2,6]

[1]College of Life Sciences, Jilin University, Changchun, P.R. China

[2]Department of Pathology, Tulane University School of Medicine, New Orleans, Louisiana, USA

[3]Department of Structural and Cellular Biology, Tulane University School of Medicine, New Orleans, Louisiana, USA

[4]Department of Medicine, Tulane University School of Medicine, New Orleans, Louisiana, USA

[5]Department of Urology, Tulane University School of Medicine, New Orleans, Louisiana, USA

[6]Tulane Cancer Center, Tulane University School of Medicine, New Orleans, Louisiana, USA

[7]Division of Comparative Pathology, Tulane National Primate Research Center, Covington, Louisiana, USA

Correspondence to:
Haitao Zhang, **e-mail:** hzhang@tulane.edu

Keywords: *androgen receptor, splice variants, prostate cancer, taxane chemotherapy, microtubule*

Received: *April 24, 2015* ***Accepted:*** *June 09, 2015* ***Published:*** *June 22, 2015*

ABSTRACT

Docetaxel-based chemotherapy is established as a first-line treatment and standard of care for patients with metastatic castration-resistant prostate cancer. However, half of the patients do not respond to treatment and those do respond eventually become refractory. A better understanding of the resistance mechanisms to taxane chemotherapy is both urgent and clinical significant, as taxanes (docetaxel and cabazitaxel) are being used in various clinical settings. Sustained signaling through the androgen receptor (AR) has been established as a hallmark of CRPC. Recently, splicing variants of AR (AR-Vs) that lack the ligand-binding domain (LBD) have been identified. These variants are constitutively active and drive prostate cancer growth in a castration-resistant manner. In taxane-resistant cell lines, we found the expression of a major variant, AR-V7, was upregulated. Furthermore, ectopic expression of two clinically relevant AR-Vs (AR-V7 and AR^{V567es}), but not the full-length AR (AR-FL), reduced the sensitivities to taxanes in LNCaP cells. Treatment with taxanes inhibited the transcriptional activity of AR-FL, but not those of AR-Vs. This could be explained, at least in part, due to the inability of taxanes to block the nuclear translocation of AR-Vs. Through a series of deletion constructs, the microtubule-binding activity was mapped to the LBD of AR. Finally, taxane-induced cytoplasm sequestration of AR-FL was alleviated when AR-Vs were present. These findings provide evidence that constitutively active AR-Vs maintain the AR signaling axis by evading the inhibitory effects of microtubule-targeting agents, suggesting that these AR-Vs play a role in resistance to taxane chemotherapy.

INTRODUCTION

Prostate cancer is the most common non-skin cancer and the second leading cause of cancer mortality in men in the United States. Androgen deprivation therapy, which disrupts androgen receptor (AR) signaling by reducing androgen levels through surgical or chemical castration, or by administration of anti-androgens that compete with androgens for binding to AR [1], is the first-line treatment for metastatic and locally advanced prostate cancer. While this regimen is effective initially, progression to the presently incurable and lethal stage, termed castration-resistant prostate cancer (CRPC), invariably occurs. In 2004, docetaxel-based chemotherapy is established as a first-line treatment and standard of care for patients with metastatic CRPC [2]. However, about half of the patients

do not respond to treatment and those do respond become refractory within one year. Several new treatments, including the new taxane cabazitaxel [3], the CYP17A1 inhibitor abiraterone [4], and the potent antiandrogen enzalutamide [5], have received FDA approval as second-line treatments for metastatic CRPC in recent years. However, the survival benefits are relatively small (< = 5 months) and patients eventually become refractory to treatments. Therefore, breakthroughs in the treatment of prostate cancer hinge upon better understandings of the mechanisms of therapeutic resistance of CRPC.

Paclitaxel, docetaxel, and cabazitaxel belong to the taxane family of chemotherapeutic agents. Taxanes bind to the microtubules and prevent their disassembly, thereby suppressing microtubule dynamics, leading to mitotic arrest and apoptosis [6]. This was believed to be the mechanism of action of taxanes in prostate cancer until recently when it was demonstrated by several groups that taxanes in fact inhibit the AR signaling pathway in prostate cancer. Taxanes have been shown to block the nuclear translocation of AR and inhibit the expression of AR-regulated genes [7, 8]. Additionally, Gan et al. showed that taxanes inhibit the transcriptional activity of AR by inducing FOXO1, a transcriptional repressor of AR [9]. It is well-established that CRPC cells remain addicted to AR signaling; therefore, the inhibitory effect on AR, rather than the antimitotic activity, could possibly be the predominant mechanism of action for taxanes in prostate cancer.

Sustained signaling through AR has been established as a hallmark of CRPC. Recently, alternative splicing variants of AR (AR-Vs) that lack the ligand-binding domain (LBD) have been identified [10–13]. These splice variants remain transcriptionally active in the absence of androgens and drive prostate cancer growth in a castration-resistant manner. In addition, these variants are reported to be prevalently upregulated in CRPC compared to hormone-naïve prostate cancer [10–13]. AR-Vs can regulate the expression of canonical androgen-responsive genes, as well as a unique set of target genes [12, 14]. In a significant portion of metastatic CRPC tissues, the variants proteins are expressed at a level comparable to that of the canonical, full-length AR (AR-FL) [15, 16]. Patients with high expression of two major AR-Vs, AR-V7 (also known as AR3) and AR^{v567es}, have shorter cancer-specific survival than other CRPC patients [15]. In addition, recent studies have provided strong support for a critical role of these AR-Vs in resistance to hormonal therapies, including enzalutamide and abiraterone [17–20].

Recently, laboratory and clinical studies have suggested the existence of a cross-resistance mechanism between taxane-based chemotherapy and second-line hormonal therapies [21–25]. In this study, we set out to test the potential roles of AR-Vs in modulating the response to taxane-based chemotherapy.

RESULTS

Taxane-resistant prostate cancer cell lines express higher levels of AR-V7

We first established taxane-resistant 22Rv1 and LNCaP95 lines by culturing cells in escalating doses of paclitaxel and docetaxel over a period of 2 months. The response to taxanes were determined by the MTT assay (Fig. 1, A–C). Western blotting analyses showed that the expression of AR-FL was reduced, whereas the expression of AR-V7 was robustly induced, in the 22Rv1 resistant lines in comparison with the passage-matched parental line (Fig. 1D). A similar, albeit less pronounced, induction of AR-V7 was observed in the LNCaP95 docetaxel-resistant line (Fig. 1E). These results suggest that the constitutive active AR-V7 was selectively up-regulated in taxane-resistant prostate cancer cells.

Expression of constitutively active AR-Vs impairs the cytotoxicity of taxanes

To directly test the roles of constitutively active AR-Vs in resistance to taxanes, we transfected AR-V7 and AR^{v567es} into the AR-V-null LNCaP cells, and measured the responses to taxanes. As shown in Fig. 2A, cell viability after docetaxel treatment was markedly higher in cells expressing AR-V7 or AR^{v567es}, but not in those overexpressing AR-FL, than in vector-transfected cells. Similar observations were made with paclitaxel and cabazitaxel (Supplementary Figure S1). In LNCaP95 cells, when the expression of AR-V7 was silenced by a V7-specific shRNA, cells became more sensitive to docetaxal and cabazitaxel (Fig. 2B). Taken together, these results suggest the expression of constitutively active AR-Vs negatively impacts the efficacies of taxanes in prostate cancer cells.

Transcriptional activities of the constitutively active AR-Vs are refractory to the taxanes

To understand the difference between AR-V7/AR^{v567es} and the AR-FL in cytoprotection against the taxanes, we investigated the influence of taxane treatment on the transactivation activities of these AR isoforms. COS-7, which does not express any AR proteins, was chosen in this experiment to avoid interference from the endogenous AR. As shown in Fig. 3, treatment with docetaxel or paclitaxel dose-dependently inhibited the ligand-dependent transcriptional activity of AR-FL, but neither drug was able to inhibit the constitutive activities of AR-V7 and AR^{v567es}. This disparity can't be attributed to the down-regulation of AR-FL expression, as all AR proteins were not affected by the treatments (Supplementary Figure S2). These results suggest that the transcriptional activities of the AR variants are refractory to the inhibitory effects of taxanes.

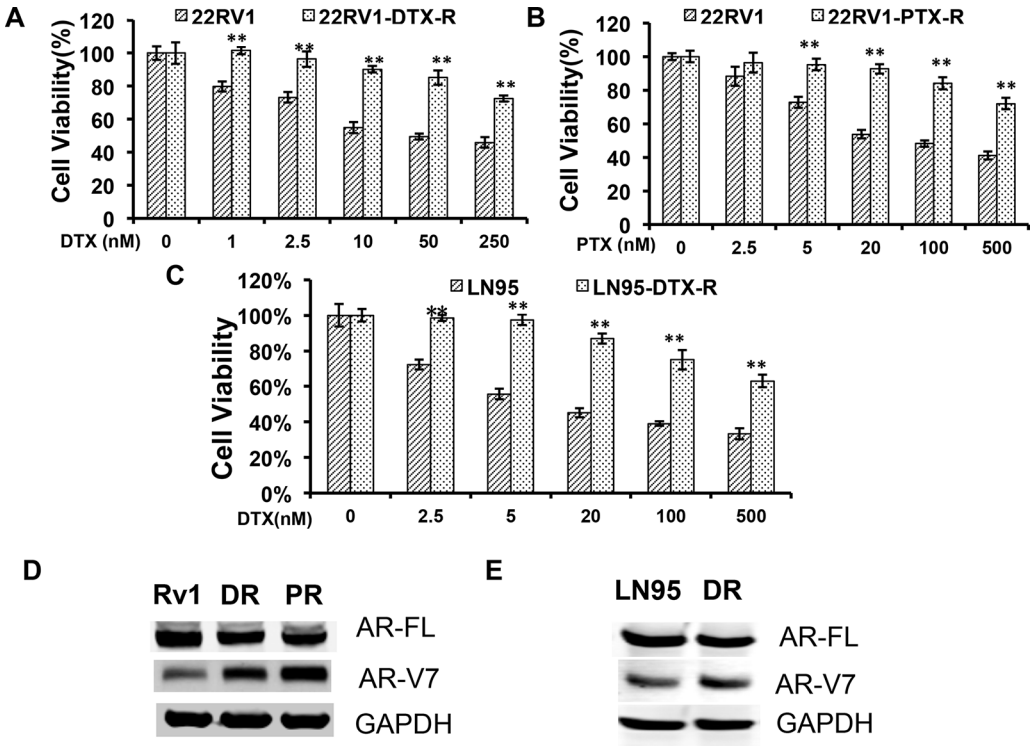

Figure 1: Upregulation of AR-V7 in taxane-resistant prostate cancer cells. A. and **B.** 22Rv1 with acquired resistance to taxanes were established by culturing in escalating doses of docetaxel (DTX) or paclitaxel (PTX). MTT assays were performed in passage-matched 22Rv1 or 22Rv1 resistant cells to determine the responses to taxanes. **C.** The response of DTX-resistant LNCaP95 to docetaxel treatment. **D.** and **E.** Western blotting using an anti-N terminal antibody or an AR-V7-specific antibody in 22Rv1 (D) or LNCaP95 (E) resistant cells. Rv1/LN95, passage-matched parental line; DR, docetaxel-resistant; PR, paclitaxel-resistant. The *P* values were determined by the *Student's t*-tests, ** denotes $P < 0.01$. The results presented are mean ± SEM from three experiments.

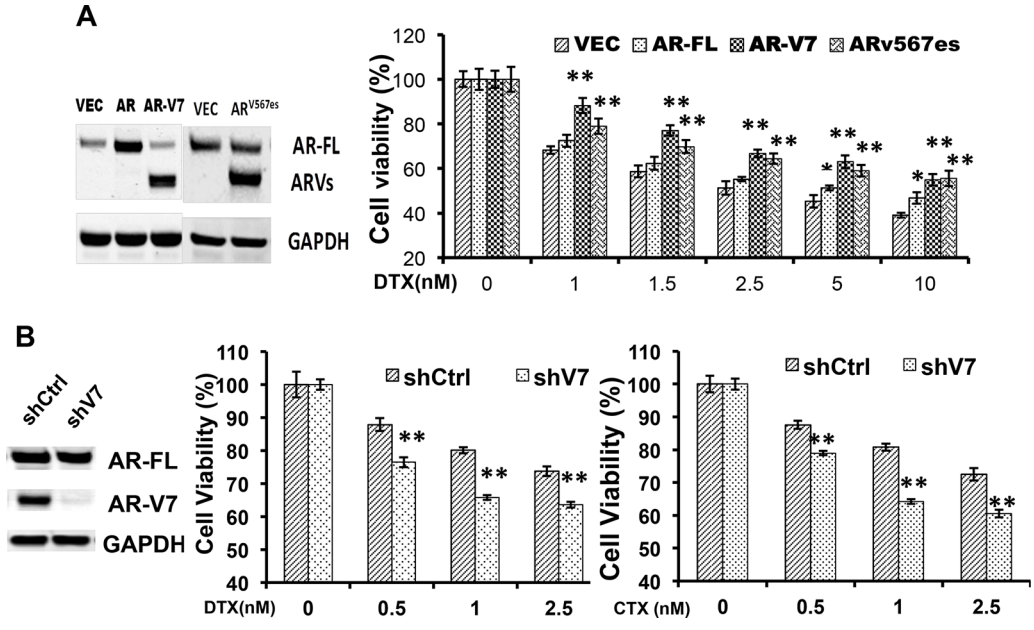

Figure 2: Expression of constitutively active AR-Vs negatively impact the cytotoxicities of taxanes. A. LNCaP cells were transfected with vector, AR-FL, AR-V7, or AR^{v567es}, and cell viability was determined by the MTT assay after 48 h of treatment with docetaxel. Western analysis was performed with an antibody recognizes the N-terminus of AR. The *P* values were determined by the *Student's t*-tests. *$P < 0.05$; **$P < 0.01$ vs vector. **B.** LNCaP95 cells were cultured in an androgen-depleted condition, and transfected with a control or an AR-V7-specific shRNA. **$P < 0.01$. CTX, cabazitaxel. The results presented are mean ± SEM.

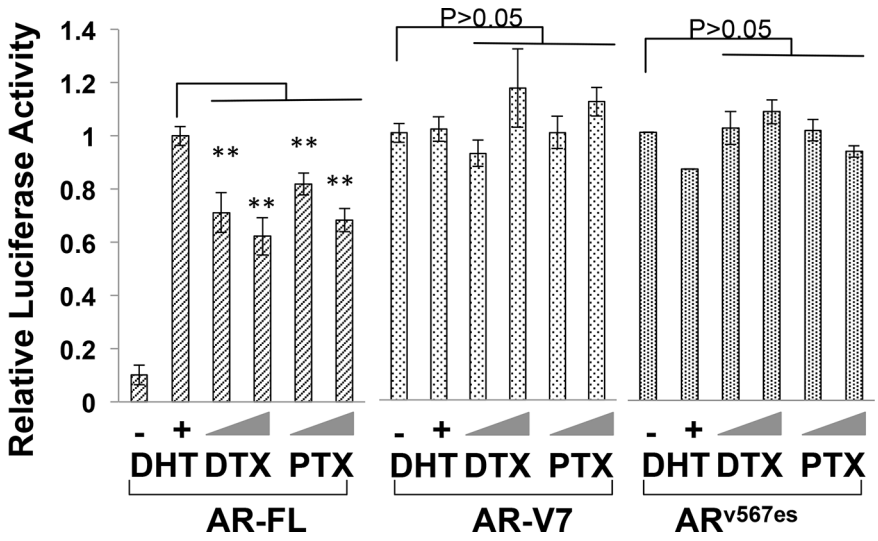

Figure 3: Transcriptional activities of constitutively active AR-Vs are refractory to taxane treatment. COS-7 cells were transfected with the ARR3-luc reporter plasmid along with a plasmid encoding AR-FL, AR-V7, or AR^{v567es}. The luciferase reporter assay was performed after 24 h treatment. The *P* values were determined by the *Student's t*-tests. $^{**}P < 0.01$ vs untreated. Doses: DTX, 1 and 2.5 nM; PTX, 2.5 and 5 nM. The results presented are mean ± SEM from three experiments.

Nuclear imports of constitutively active AR-Vs are microtubule-independent

Next, we investigated the influence of the taxanes on nuclear translocation of AR-V7 and AR^{v567es}, as these agents have been shown to block that of AR-FL [7, 8]. Enhanced green fluorescent protein (EGFP)-tagged AR-FL and AR-V7 were expressed in COS-7 cells and the localization of the fusion proteins was analyzed by fluorescence microscopy. Unlike EGFP-AR-FL, which required androgen stimulation for nuclear import, EGFP-AR-V7 spontaneously translocated to the nucleus (Supplementary Figure S3). When docetaxel and paclitaxel were added to the culture medium following androgen stimulation, accumulation of AR-FL in the cytoplasm was observed after 24 h of treatment (Supplementary Figure S3). However, treatment with the taxanes had no effect on the subcellular distribution of AR-V7.

To validate the results above, we performed fluorescence recovery after photobleaching (FRAP) assays in COS-7 cells expressing fluorescence-tagged AR proteins. Following treatment with docetaxel, selected nuclei were photobleached and the cells were imaged at regular intervals. Nuclear translocation is indicated by recovery of the nuclear to cytoplasmic fluorescence ratio (Fn/c). As indicated by the confocal images (Fig. 4A) and the fractional recovery plots (Fig. 4B), nuclear import of AR-FL was greatly deterred by docetaxel. In contrast, the nuclear translocations of AR-V7 and AR^{v567es} were not affected by docetaxel, evidenced by similar Fn/c recovery curves in control and treated cells (Fig. 4B). To substantiate these findings, we performed FRAP assays with additional microtubule inhibitors. KX-01 is a novel peptidomimetic inhibitor of Src family of kinases, but also inhibits tubulin polymerization [26], and nocodazole causes microtubule disassembly [27]. Once again, these drugs inhibited the nuclear import of AR-FL, but not that of AR-V7 or AR^{v567es} (Fig. 4B). Collectively, these results suggest the nuclear translocation of AR-V7 or AR^{v567es} are not mediated by the microtubules.

AR associates with the microtubules through the LBD

Proteins that use the microtubule pathway for nuclear import are known to bind to the microtubules [28, 29]. To test whether AR binds to the microtubules, we conducted *in vivo* microtubule-binding assays in COS-7 cells ectopically expressing AR. Under the condition in which the microtubules were stabilized, the majority of AR-FL co-precipitated with the microtubules and was found in the pellet (Fig. 5). Importin β was used as a negative control as previously described [29], and p53, which is known to be a microtubule-binding protein [30], was used as the positive control. The microtubule-binding activity was quantitated by the pellet to supernatant (P/S) ratio [29]. In contrast, when nocodazole, $CaCl_2$, or low temperature was employed to disrupt microtubule integrity, AR-FL shifted from the pellet to the supernatant, leading to marked decreases of the P/S ratios. These results suggest the AR-FL is a microtubule-associated protein.

To map the region responsible for microtubule-binding on AR, we generated a series of deletion constructs encompassing different domains of AR (Fig. 6, left panel). These constructs were analyzed by the microtubule binding assay. As shown in

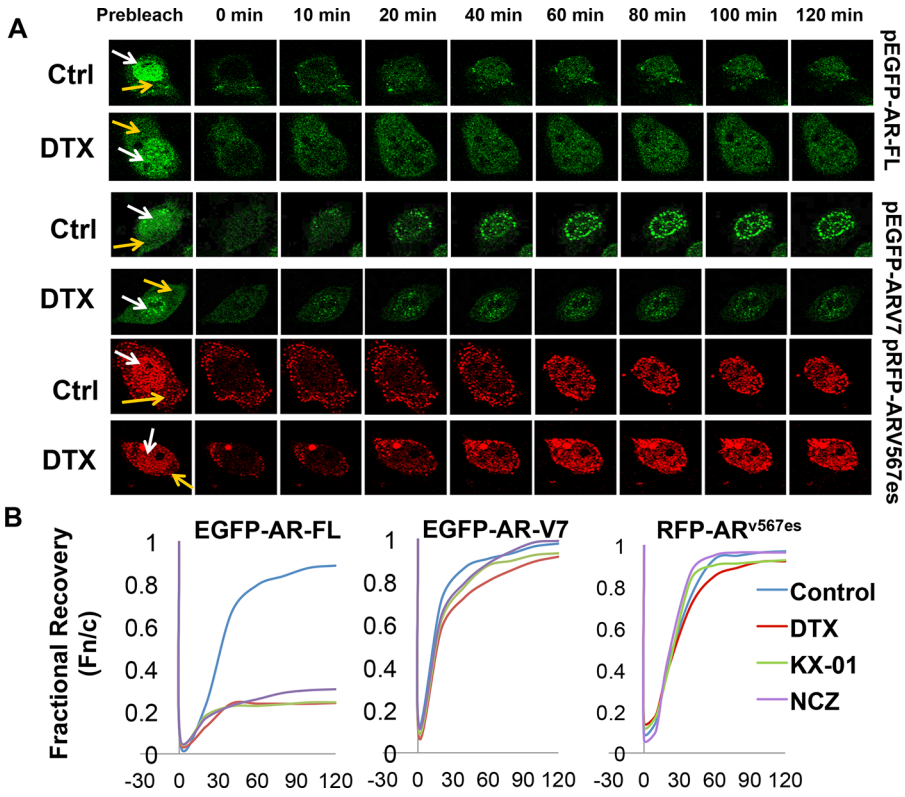

Figure 4: Nuclear imports of constitutively active AR-Vs are microtubule-independent. FRAP assays were performed in COS-7 cells expressing different fluorescence-tagged AR proteins. Cells transfected with EGFP-AR-FL were cultured in the presence of androgen. Cells were treated with 20 nM docetaxel for 2 h before photobleaching. **A.** Confocal images taken at different intervals after photobleaching of the nuclei. White and yellow arrows indicate the nucleus and the cytoplasm, respectively. **B.** Recovery plot of the nuclear:cytoplamic fluorescence ratio (Fn/c) over time in cells treated with different microtubule inhibitors. Fn/c ratios are expressed as fractions of the pre-photobleach Fn/c. Nocodazole (NCZ) was used at 5 μg/ml and KX-01 was at 100 nM. FRAP images for NCZ and KX-01 are in Supplementary Figure S4.

Supplementary Figure S4A and Figure 6 (right panel), all constructs lacking the LBD have poor microtubule-binding activities. In contrast, those retaining the LBD have similar binding activities as that of AR-FL (Supplementary Figure S4B and Figure 6). These results indicate that microtubule association is mediated by the LBD. Consistent with this finding, we found that the LBD-truncated AR-V7 and AR^{v567es} both bind poorly to the microtubules (Fig. 7).

AR-Vs interfere with docetaxel-mediated AR-FL cytoplasmic retention

It has been previously shown that both AR-V7 and AR^{v567es} facilitate AR-FL nuclear translocation in the absence of androgen [13, 19]. To investigate whether AR-Vs mitigate the inhibitory effect of AR-FL nuclear translocation by docetaxel, we expressed EGFP-AR-FL with or without TurboFP635-tagged AR-V7 or AR^{v567es} in the AR-null COS-7 cells. When co-expressed with TurboFP635, EGFP-AR-FL was retained in the cytoplasm following docetaxel treatment (Fig. 8A). However, in the presence of AR-V7-TurboFP635 or AR^{v567es}-TurboFP635, the inhibitory effect of docetaxel was significantly attenuated (Fig. 8A & 8B).

To further understand how AR-Vs circumvent docetaxel-mediated cytoplasmic sequestration of AR-FL, we conducted the microtubule-binding assay in COS-7 cells co-transfected with AR-FL and an AR-V. As shown in Fig. 8C, the binding of AR-FL to the microtubules was markedly reduced when it was co-expressed with AR-V7 or AR^{v567es}. Taken together, these results suggest that the constitutively active AR-V7 or AR^{v567es} could divert AR away from the microtubules, and facilitate its nuclear translocation in a microtubule-independent manner.

Nuclear import of AR-Vs is blocked by an importin β inhibitor

As an initial attempt to elucidate the nuclear translocation mechanisms of AR-V7 and AR^{v567es}, we investigated the involvement of the importin α/β machinery. FRAP assay was conducted in COS-7 transfected with EGFP-AR-V7 and treated with importazole, a specific inhibitor of importin β [31] . As shown by Fig. 9A & 9B, treatment with importazole

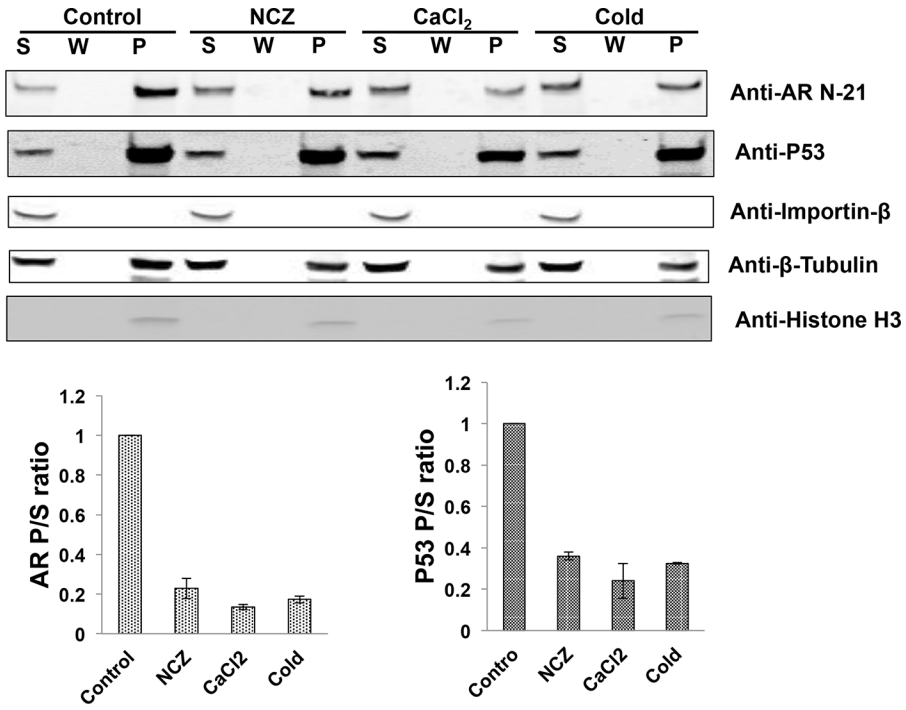

Figure 5: The full-length AR associates with the microtubules. COS-7 cells were transfected with an expression vector for AR-FL and *in vivo* microtubule binding assay was performed with a commercial kit (Cytoskeleton, BK038). Nocodazole (NCZ), $CaCl_2$, and low temperature (cold) were used to disrupt microtubule integrity. Assembled microtubules were precipitated by ultracentrifugation and the pellet was resuspended and analyzed by Western blot (Top). Importin β and p53 were used as negative and positive controls, respectively, and histone H3 was used to detect nuclear contamination. P, pellet; W, wash; S, supernatant. Bottom, the microtubule-binding activities for AR and p53 were quantitated by the P/S ratios. The results presented are mean ± SEM from three experiments.

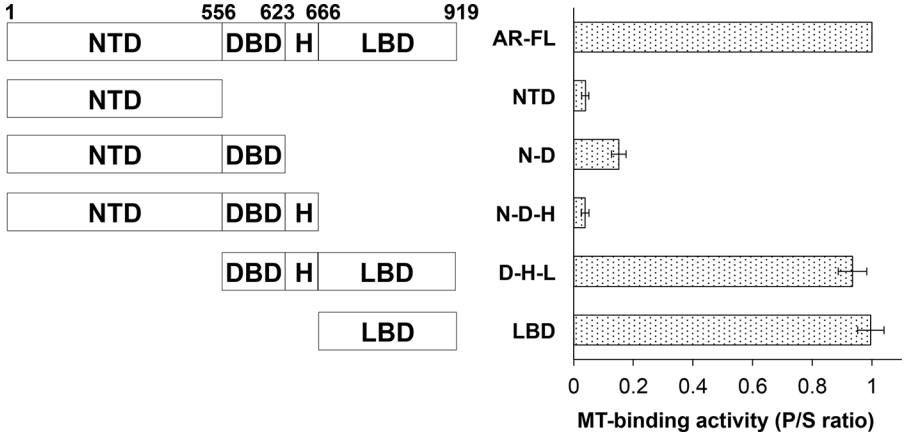

Figure 6: Microtubule-binding activity is mapped to the ligand-binding domain of AR. Left panel, a series of deletion constructs encompassing different domains of AR were generated and expressed in COS-7 cells. Right panel, the microtubule-binding activities of these constructs were analyzed by the *in vivo* microtubule binding assay and the Western blots (Supplementary Figure S5) were quantitated to calculate the P/S ratios. The results presented are mean ± SEM from three experiments. MT, microtubule.

significantly reduced the recovery of AR-V7 in the nucleus. Consistently, AR-V7 was found to accumulate in the cytoplasm following importazole treatment (Fig. 9C). FRAP assay showed a similar inhibition by importazole on the nuclear recovery of TurboFP635-tagged AR^{v567es} (Fig. 9D & 9E), suggesting that both variants are imported to the nucleus by the importin α/β machinery.

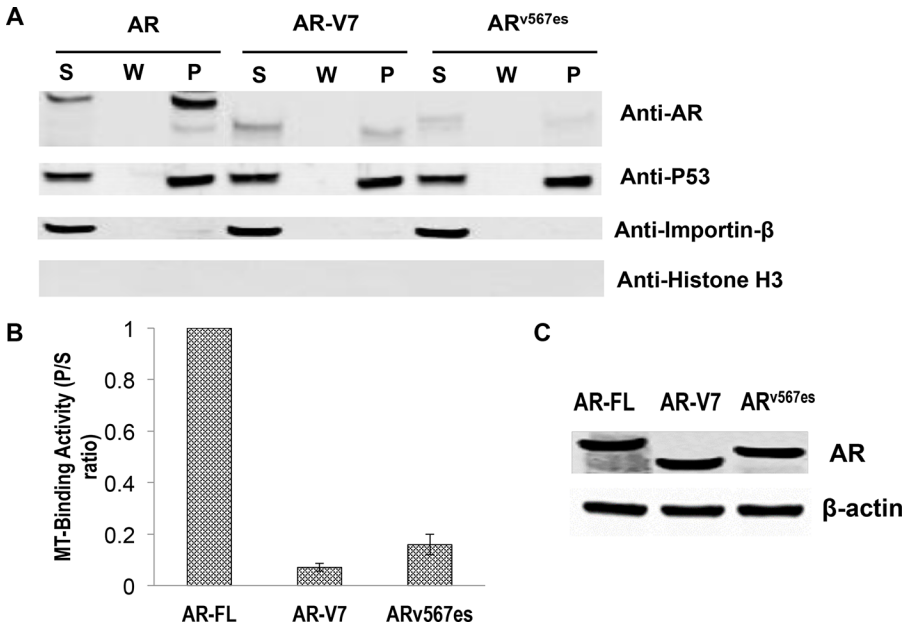

Figure 7: Poor microtubule-binding activities of the AR-Vs. COS-7 cells were transfected with an expression vector for AR-FL, AR-V7, and AR^{v567es} and cultured in an androgen-deprived condition. **A.** *In vivo* MT-binding assays. **B.** quantitation of the results in A. The results presented are mean ± SEM from three experiments. **C.** Western blot showing that the proteins were expressed at similar levels after transfection.

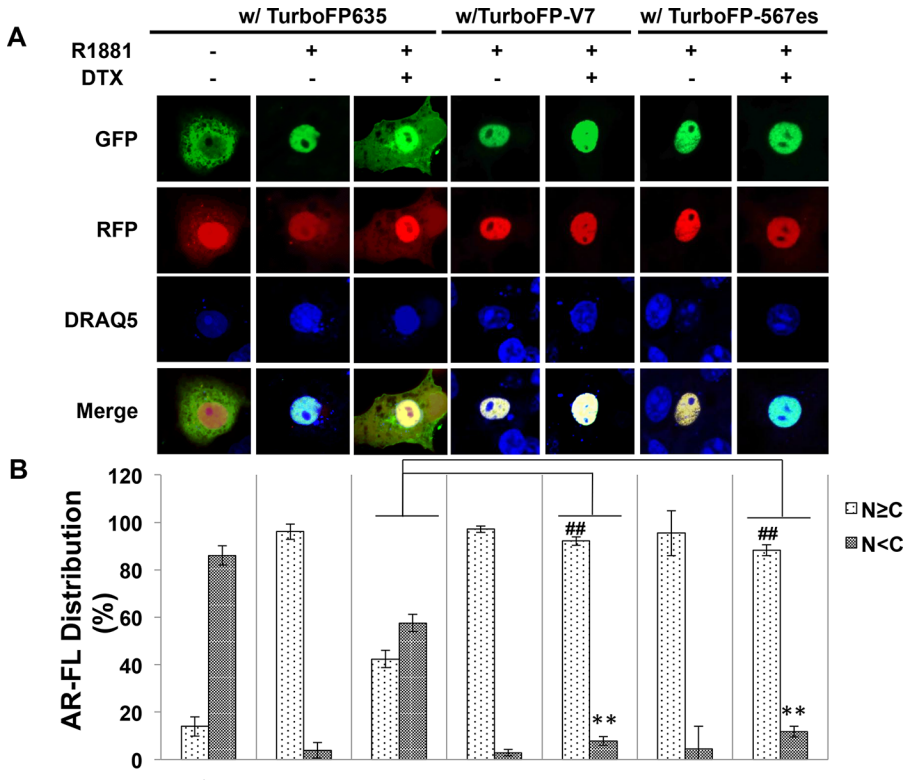

Figure 8: Cytoplasmic sequestration of AR-FL by docetaxel is attenuated by AR-V7 and AR^{v567es}. A. Confocal fluorescence microscopy of EGFP-AR-FL subcellular localization when it was expressed with TurboFP or with a TurboFP-tagged AR-V in COS-7 cells. **B.** Based on distribution of the green fluorescence signal, cells were categorized into cytoplasmic (N < C), or nuclear and equally nuclear and cytoplasmic (N ≥ C).% of cells in each category were quantified. DRAQ5 was used to stain the nuclei. Cells cultured in an androgen-deprived condition were pre-treated with 10 nM docetaxel for 6 hr, followed by treatment with 1 nM R1881 for 4 hr. ** and ## $P < 0.01$.

(*continued*)

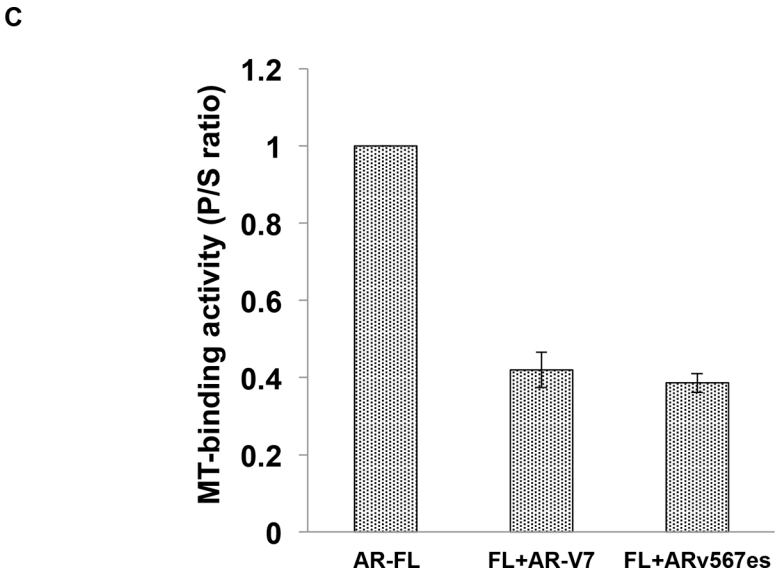

Figure 8: C. (*Continued*) *In vivo* MT-binding assay in COS-7 cells expressing AR-FL alone, or with AR-V7 or AR^{v567es}.

DISCUSSION

To date, docetaxel and cabazitaxel are the only chemotherapeutic agents that have been shown to offer survival benefits for patients with mCRPC. Even in today's rapidly evolving landscape of treatment options for mCRPC, taxane-based chemotherapy continues to be an important component of the treatment regimens. Recently, a randomized phase III trial supports the expansion of the indications of taxanes to earlier disease stages. The CHARRTED trial demonstrated that the addition of docetaxel to ADT in patients with high-volume, metastatic, hormonal-sensitive disease improves overall survival by 17 months (49.2 vs 32.2, $P = 0.0013$) than ADT alone [32]. With taxane chemotherapy projected to remain a mainstay in the treatment of prostate cancer, it is imperative to derive a better understanding of the mechanisms underlying the inherent and acquired taxane resistances, both of which are commonly observed in the clinic.

Resistance to taxanes could be multifactorial, involving general mechanisms of chemoresistance as well as mechanisms intrinsic to prostate cancer [33]. Existing literature focuses primarily on mechanisms common to many cancer types, including unfavorable tumor microenvironment, expression of drug efflux proteins, alterations in microtubule structure and/or function, expression of anti-apoptotic and cytoprotective proteins [34]. However, mechanisms that are specific to prostate cancer remain poorly understood. Recent clinical observations provided evidence for a cross-resistance of CRPC to hormonal therapy and taxane-based chemotherapy [21–25], suggesting a common culprit may underlie such a cross-resistance phenotype.

Our study represents a step forward in this direction. Herein, we present evidence that expression of constitutively active AR-Vs, but not over-expression of the canonical full-length receptor, protects prostate cancer cells from the cytotoxic effects of taxanes. We further show that taxane treatment selectively inhibits androgen-induced nuclear translocation and transactivation activity of AR-FL, while exerting no such inhibitory effects on the AR-Vs. These results reveal a fundamental difference in the nuclear translocation mechanisms of AR-FL and AR-Vs. AR-FL, as shown by this and other studies, utilizes a microtubule-facilitated pathway for nuclear translocation. This trafficking mechanism is shared by several nuclear proteins including glucocorticoid receptor (GR), p53, Rb, and parathyroid hormone-related protein (PTHrP) [29]. On the other hand, the nuclear import of AR-V7 and AR^{v567es} is not mediated by the microtubule pathway. The independence of the microtubule pathway enables the variants to evade taxane-induced cytoplasmic retention. Finally, we show that sequestration of AR-FL in the cytoplasm by taxanes is alleviated when AR-V7 or AR^{v567es} is present. This is likely caused by AR-V steering AR-FL away from the microtubules, as shown by reduced binding to the microtubules when AR-Vs are co-expressed. As an initial attempt to unveil the nuclear translocation mechanisms of the AR-Vs, we found that nuclear import of AR-V7 and AR^{v567es} is possibly mediated by the importin α/β machinery. Elucidation of the upstream events will likely lead to opportunities to design novel strategies to target this variant.

The clinical relevance of AR-Vs has been demonstrated by a myriad of studies. Higher expression of AR-V7 in hormone-naïve prostate tumors predicts increased risk of biochemical recurrence following radical

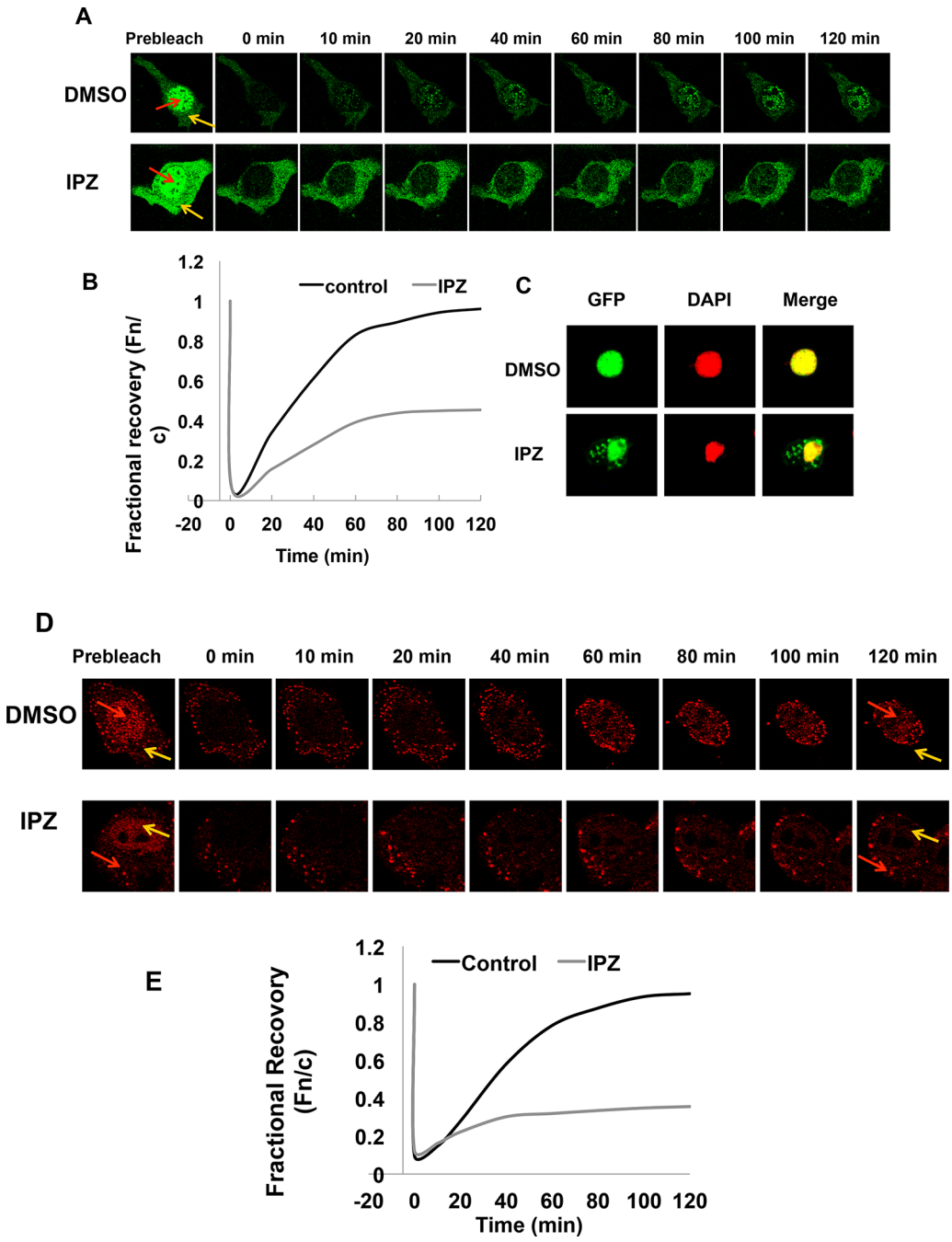

Figure 9: Nuclear translocation of AR-Vs is importin β-dependent. A. FRAP assays were performed in COS-7 cells expressing EGFP-tagged AR-V7. Cells were treated with DMSO or 50 μM importazole (IPZ) for 2 h before photobleaching. Confocal images taken at different intervals after photobleaching of the nuclei. Red and yellow arrows indicate nucleus and cytoplasm, respectively. **B.** Fn/c recovery plot for EGFP-AR-V7. **C.** COS-7 cells transfected with pEGFP-AR-V7 were treated with DMSO or 10 μM importazole for 48 h. DAPI was used for staining the nuclei. **D.** & **E.** confocal images (D) and Fn/c recovery plot (E) of FRAP assays in COS-7 cells expressing TurboFP635-tagged AR^{v567es} and treated with IPZ.

prostatectomy [11, 12], and patients with high levels of expression of AR-V7 or detectable expression of AR^{v567es} have a significantly shorter survival than other CRPC patients [15], indicating an association between AR-Vs expression and a more lethal form of prostate cancer. Studies have indicated that AR-Vs play important roles in resistance to androgen-directed therapies [17–19]. Particularly, a recent groundbreaking study by Antonarakis et al. showed that

patients positive for AR-V7 expression in circulating tumor cells have significantly worse responses to enzalutamide or abiraterone than AR-V7-negative patients [20].

While the roles of AR-Vs are well recognized in resistance to hormonal therapies, evidence has just started to accumulate to support their involvement in resistance to taxane chemotherapy. Thadani-Mulero and colleagues are the first to show evidence supporting a role of AR-V7 in resistance to taxane chemotherapy [35]. In addition, the study by Martin et al. [36] showed that in cells harboring AR-Vs, targeting the AR N-terminal domain of with a small molecule inhibitor enhances the therapeutic response to docetaxel [36]. A clinical study by Steinestel et al. showed expression of AR-V7 in circulating cancer cells significantly correlates with prior treatment with docetaxel [37]. Very recently, a clinical study presented at the American Society of Clinical Oncology Genitourinary Cancers Symposium investigated the responses to taxane chemotherapy in mCRPC patients with different AR-V7 status in circulating tumor cells [38]. Although all the clinical outcomes are worse in patients in the AR-V7(+) arm, the differences are not statistically significant [38]. The insignificant differences could result from the small sample size or due to a "threshold effect" of AR-V7. In other words, the influence of AR-V7 on taxane response may be manifested only when it is expressed above a certain level. Hence, the association of AR-Vs and sensitivity to taxane chemotherapy warrants further investigation in a larger cohort.

The main disparity between our study and that of Thadani-Mulero et al. [35] is on whether AR^{v567es} is inhibited by the taxanes. In contrast to the data present herein, Thadani-Mulero and colleagues showed that AR^{v567es} associates with the microtubules and that the nuclear translocation of AR^{v567es} is inhibited by taxanes. In addition, the microtubule-binding activity is mapped to the DNA-binding and hinge domains of AR [35]. One possible explanation for these discrepancies is the use of different assays. Thadani-Mulero et al. performed *in vitro* assays in which cell lysates containing AR proteins tagged by GFP or hemagglutinin were incubated with purified tubulin in a cell-free system to allow microtubule polymerization and association. In contrast, we conducted *in vivo* microtubule-binding assays in which the microtubules and associated proteins were extracted from cells expressing untagged AR isoforms. Another major difference between the two studies is the dosage of taxanes. Docetaxel was applied at a concentration of 1 μM in the cell culture studies by Thadani-Mulero et al., in contrast to the clinically attainable [39] nanomolar concentrations used in our studies. We demonstrated that treatment with taxanes, at the low nanomolar concentrations, fail to inhibit the transcriptional activity or nuclear import of AR^{v567es}.

The canonical AR nuclear localization signal (NLS) is located in the hinge domain, encoded by exons 3 and 4. Sequence analysis predicted that this NLS is truncated in AR-V7. However, the study by Chan et al. demonstrated that splicing of exon 3 with cryptic exon 3 in AR-V7 reconstitutes this bipartite NLS, which mediates the nuclear import of AR-V7 [40]. In addition, expression of a dominant negative mutant of Ran protein (RanQ69L) which causes premature dissociation of the importin/cargo complex, reduced nuclear localization of AR-V7 and AR^{v567es}. These findings are consistent with our importazole data, suggesting that the nuclear import of the AR-Vs is mediated by the importin α/β pathway. They also found that unlike AR-FL, the nuclear localization of AR-V7 and AR^{v567es} is not affected by an inhibitor for heat shock protein 90. Together, this study and our data present herein suggest a fundamental difference between AR-FL and AR-Vs in the events upstream of importin α/β-mediated nuclear entry.

In summary, our study provides support for the involvement of AR-V7 and AR^{v567es} in attenuating the response to taxane-based chemotherapy. Mechanistically, we demonstrated that both variants translocate to the nucleus in a microtubule-independent manner. Additionally, these variants can reduce the microtubule-binding activity of AR-FL, thus circumventing its cytoplasm sequestration triggered by taxanes. These findings have important clinical implications. The expression status of these AR variants could potentially be used as a biomarker to aid treatment selection and sequencing. More importantly, targeting AR-Vs could be a fruitful direction to pursue to enhance the efficacy of taxane chemotherapy. To this end, several small molecule inhibitors at various stages of clinical development have shown promises against AR-Vs [41–43], opening doors for novel therapeutic strategies.

MATERIALS AND METHODS

Cell lines and reagents

LNCaP, 22Rv1, and COS-7 cells were obtained from American Type Culture Collection. With the exception of drug-resistant lines, cells used in this study were within 20 passages (~3 months of non-continuous culturing). All cell lines were tested and authenticated by the method of short tandem repeat profiling. Docetaxel, cabazitaxel, and paclitaxel were purchased from Selleck Chemicals (Houston, TX). Nocodazole was from Sigma Aldrich, and KX-01 was provided by Kinex Pharmaceuticals. The following antibodies were used in Western blot analysis: anti-GAPDH, anti-AR (N-terminus-directed, PG-21; Millipore), anti-importin β1, anti-β-actin (Santa Cruz), anti-p53 (Calbiochem), anti-histone H3 (Cell Signaling), and anti-AR-V7 (Precision Antibody).

Selection of taxane resistant cell lines

22Rv1 cells were initially treated with 10 nM paclitaxel for 72 hours and the surviving cells were re-seeded and allowed to recover for 1 week.

Paclitaxel-resistant cells were developed over a period of 2 months by stepwise increasing concentrations of paclitaxel (5–50 nM). Age-matched parental cells which did not receive treatments were maintained in parallel. Docetaxel-resistant 22Rv1 and LNCaP95 lines were generated in a similar manner, but with different doses of docetaxel (5 nM initially, 2.5–20 nM for selection). The resistant cells were continuously maintained in the highest concentration of the taxane in which they selected.

Western blotting

Cells were washed with ice-cold phosphate-buffered saline (PBS) and lysed with 2X Cell Lysis Buffer (Cell Signaling) containing a phosphatase inhibitor and the protease inhibitor cocktail (Sigma). After incubating the cells on ice for 30 min, lysates were collected by centrifugation at 10, 000 rpm for 10 minutes. Protein concentrations were determined by the BCA Protein Assay kit (Pierce). The samples were separated on 10% SDS-polyacrylamide gels and transferred onto polyvinylidene fluoride (PVDF) membranes. After blocking in TBS buffer (150 mM NaCl, 10 mM Tris, pH 7.4) containing 5% nonfat milk, the blots were incubated with a primary antibody overnight at 4°C and a fluorescent-labeled secondary antibody for 1 h at room temperature. The fluorescent signals were obtained by the Odyssey Infrared Imaging System (LI-COR Bioscience).

Transient transfection and reporter gene assay

COS-7 cells were seeded in 10-cm dishes at a density to reach 80–90% confluency at time of transfection. Transient transfection was performed by using the Lipofectamine and Plus reagents following the manufacturer's instructions (Invitrogen). Cells were co-transfected with ARR3-luc luciferase reporter contruct and pRL-TK, along with a plasmid encoding for AR-FL, AR-V7 or AR^{v567es}. After incubating with the transfection mixture for 4 h, cells were re-plated in RPMI 1640 containing 10% charcoal-stripped fetal bovine serum (cs-FBS). Cells were allowed to recover overnight before treated with DTX (1 and 2.5 nM) or PTX (2.5 or 5 nM) in the presence or absence of 10 nM DHT. Dual-luciferase assay was performed at 24 h post treatment using the Dual-luciferase Reporter Assay System (Promega). The renilla luciferase activity was used to normalize that of firefly luciferase.

Confocal fluorescence microscopy

Subcellular localization of AR proteins was analyzed by confocal fluorescence microscopy. The pTurboFP635-AR-V7 and pTurboFP635-AR^{v567es} plasmids were generated by cloning the cDNA fragments for AR-V7 and AR^{v567es}, respectively, into the pCMV-TurboFP635 vector. COS-7 cells were transfected with indicated plasmids and cultured in phenol red-free RPMI-1640 supplemented with 10% cs-FBS. At 40 hr after transfection, cells were pre-treated with or without 10 nM docetaxel for 6 hr, followed by treatment with or without 1 nM R1881 for 4 hr. COS-7 cells were subsequently fixed with 2% paraformaldehyde, and the nuclei were stained with 2.5 μM DRAQ5 (Cell Signaling). Confocal images were obtained by using a Leica TCS SP2 system with a 63X oil-immersion objective on a Z-stage, and an average of 6 fields with ~10 cells per field were captured for each group. Data quantitation was performed as described [44].

Fluorescence recovery after photobleaching (FRAP) assay

FRAP assay was performed using a Leica TCS SP2 microscope equipped with 20X, 40X and 63X oil immersion lenses (Nikon) in combination with a heated stage (Delta T Open Dish System, Bioptechs), as described by Roth et al. [45] with modifications. Briefly, three images were obtained before photobleaching using 10% of total laser power with excitation at 488 nm, scanning at a rate of 8 μs/pixel. Photobleaching was performed by scanning an area covering the entire nucleus 10 times at a rate of 12.5 μs/pixel, applying 100% of the laser power. After bleaching, the recovery of fluorescence was monitored by scanning the cells at 1 minute intervals for up to 2 hours, using detector and laser settings identical to those prior to photobleaching. Image analysis was carried out by using the NIH Image J Software to quantitate the nuclear (Fn) and cytoplasmic (Fc) fluorescence signals. The ratios of Fn to Fc (Fn/c) were calculated and the extent of recovery was determined by fractional recovery of Fn/c, which is the Fn/c at each time point divided by the prebleach Fn/c. The data were fitted exponentially to generate the fractional recovery plot.

In vivo microtubule binding assay

The AR deletion constructs were generated by inserting PCR products of the corresponding cDNA regions into the pcDNA3.1(-) vector. The resulting plasmids were sequenced to confirm sequence accuracy and in-frame reading. COS-7 cells were transfected with indicated plasmids and cultured in RPMI 1640 medium supplemented with 10% cs-FBS. Microtubule-binding assay was performed by using the Microtubule/Tubulin *In Vivo* Assay Kit (Cytoskeleton Inc., Cat.# BK038) following the manufacturer's instructions. Briefly, 3×10^6 cells were lysed in 4 mL pre-warmed (37°C) Lysis and Microtubule Stabilization 2 (LMS2) buffer (100 mM PIPES, pH 6.9, 5 mM $MgCl_2$, 1mM EGTA, 30% (v/v) glycerol, 0.1% Nonidet P40, 0.1% Triton X-100, 0.1% Tween 20, 0.1% β-mercaptoethanol, 0.001% Antifoam, 100 μM GTP, 1 mM ATP, 1 × protease inhibitors cocktail) in a 10-cm cell culture dish. The lysates were collected

and spun at 2,000 g for 10 min at 37°C to remove nuclei and unbroken cells. The supernatants were then subjected to ultracentrifugation at 100, 000 g for 30 min at 37°C to separate the microtubules from the soluble, unpolymerized tubulin. The pellet was washed with pre-warmed LMS2 buffer and centrifuged at 100, 000 g for 30 min at 37°C. For microtubule destabilization conditions, LMS2 buffer containing nocodazole (5 μg/ml) or $CaCl_2$ (2 mM), or ice-cold LMS2 buffer were used in the above procedure. The pellets were resuspended in ice-cold 2 mM $CaCl_2$ and incubated in room temperature for 15 min to depolymerize microtubules. The supernatant (S), wash solution (W), and resuspended pellet (P) were adjusted to equal volumes and analyzed by Western blotting.

Statistical analysis

Statistical analysis was performed using Microsoft Excel. The *Student's* two-tailed *t*-test was used to determine the difference in means between two groups. $P < 0.05$ is considered significant. Data are presented as mean ± standard error of men (SEM).

ACKNOWLEDGMENTS

We are indebted to Dr. Yun Qiu for providing the AR-FL and AR-V7 cDNA constructs, to Dr. Stephen R. Plymate for the AR^{v567es} cDNA construct, to Dr. Jun Luo for the EGFP-AR-FL and EGFP-AR-V7 expression vectors, and to Dr. Rebecca Heald for providing importazole.

GRANT SUPPORT

This work was supported by the following grants: ACS RSG-07-218-01-TBE, DOD W81XWH-12-1-0275 and W81XWH-14-1-0480, NIH/NCI R01CA188609, Louisiana Board of Regents LEQSF(2012-15)-RD-A-25, NIH/NIGMS 5P20GM103518-10, Louisiana Cancer Research Consortium Fund, Oliver Sartor Prostate Cancer Research Fund, National Natural Science Foundation of China Projects 81272851 and 81430087.

CONFLICTS OF INTEREST

No conflicts of interest to declare.

REFERENCES

1. Harris WP, Mostaghel EA, Nelson PS, Montgomery B. Androgen deprivation therapy: progress in understanding mechanisms of resistance and optimizing androgen depletion. Nat Clin Pract Urol. 2009; 6:76–85.
2. Tannock IF, de WR, Berry WR, Horti J, Pluzanska A, Chi KN, Oudard S, Theodore C, James ND, Turesson I, Rosenthal MA, Eisenberger MA. Docetaxel plus prednisone or mitoxantrone plus prednisone for advanced prostate cancer. N Engl J Med. 2004; 351:1502–1512.
3. De Bono JS, Oudard S, Ozguroglu M, Hansen S, Machiels JP, Kocak I, Gravis G, Bodrogi I, Mackenzie MJ, Shen L, Roessner M, Gupta S, Sartor AO. Prednisone plus cabazitaxel or mitoxantrone for metastatic castration-resistant prostate cancer progressing after docetaxel treatment: a randomised open-label trial. Lancet. 2010; 376:1147–1154.
4. De Bono JS, Logothetis CJ, Molina A, Fizazi K, North S, Chu L, Chi KN, Jones RJ, Goodman OB, Saad F, Staffurth JN, Mainwaring P, Harland S, Flaig TW, Hutson TE, Cheng T, Patterson H, Hainsworth JD, Ryan CJ, Sternberg CN, Ellard SL, Flechon A, Saleh M, Scholz M, Efstathiou E, Zivi A, Bianchini D, Loriot Y, Chieffo N, Kheoh T, Haqq CM, Scher HI. Abiraterone and increased survival in metastatic prostate cancer. N Engl J Med. 2011; 364:1995–2005.
5. Scher HI, Fizazi K, Saad F, Taplin M-E, Sternberg CN, Miller K, de Wit R, Mulders P, Chi KN, Shore ND, Armstrong AJ, Flaig TW, Fléchon A, Mainwaring P, Fleming M, Hainsworth JD, Hirmand M, Selby B, Seely L, de Bono JS. Increased survival with enzalutamide in prostate cancer after chemotherapy. N Engl J Med. 2012; 367:1187–1197.
6. Jordan MA, Wilson L. Microtubules as a target for anticancer drugs. Nat Rev Cancer. 2004; 4:253–265.
7. Zhu ML, Horbinski CM, Garzotto M, Qian DZ, Beer TM, Kyprianou N. Tubulin-targeting chemotherapy impairs androgen receptor activity in prostate cancer. Cancer Res. 2010; 70:7992–8002.
8. Darshan MS, Loftus MS, Thadani-Mulero M, Levy BP, Escuin D, Zhou XK, Gjyrezi A, Chanel-Vos C, Shen R, Tagawa ST, Bander NH, Nanus DM, Giannakakou P. Taxane-induced blockade to nuclear accumulation of the androgen receptor predicts clinical responses in metastatic prostate cancer. Cancer Res. 2011; 71:6019–6029.
9. Gan L, Chen S, Wang Y, Watahiki A, Bohrer L, Sun Z, Wang Y, Huang H. Inhibition of the androgen receptor as a novel mechanism of taxol chemotherapy in prostate cancer. Cancer Res. 2009; 69:8386–8394.
10. Dehm SM, Schmidt LJ, Heemers HV, Vessella RL, Tindall DJ. Splicing of a novel androgen receptor exon generates a constitutively active androgen receptor that mediates prostate cancer therapy resistance. Cancer Res. 2008; 68:5469–5477.
11. Hu R, Dunn TA, Wei S, Isharwal S, Veltri RW, Humphreys E, Han M, Partin AW, Vessella RL, Isaacs WB, Bova GS, Luo J. Ligand-independent androgen receptor variants derived from splicing of cryptic exons signify hormone-refractory prostate cancer. Cancer Res. 2009; 69:16–22.
12. Guo Z, Yang X, Sun F, Jiang R, Linn DE, Chen H, Chen H, Kong X, Melamed J, Tepper CG, Kung HJ, Brodie AM, Edwards J, Qiu Y. A novel androgen receptor splice variant

is up-regulated during prostate cancer progression and promotes androgen depletion-resistant growth. Cancer Res. 2009; 69:2305–2313.

13. Sun S, Sprenger CC, Vessella RL, Haugk K, Soriano K, Mostaghel EA, Page ST, Coleman IM, Nguyen HM, Sun H, Nelson PS, Plymate SR. Castration resistance in human prostate cancer is conferred by a frequently occurring androgen receptor splice variant. J Clin Invest. 2010; 120:2715–2730.
14. Hu R, Lu C, Mostaghel EA, Yegnasubramanian S, Gurel M, Tannahill C, Edwards J, Isaacs WB, Nelson PS, Bluemn E, Plymate SR, Luo J. Distinct transcriptional programs mediated by the ligand-dependent full-length androgen receptor and its splice variants in castration-resistant prostate cancer. Cancer Res. 2012; 72:3457–3462.
15. Hornberg E, Ylitalo EB, Crnalic S, Antti H, Stattin P, Widmark A, Bergh A, Wikstrom P. Expression of androgen receptor splice variants in prostate cancer bone metastases is associated with castration-resistance and short survival. PLoS One. 2011; 6:e19059.
16. Zhang X, Morrissey C, Sun S, Ketchandji M, Nelson PS, True LD, Vakar-Lopez F, Vessella RL, Plymate SR. Androgen receptor variants cccur frequently in castration resistant prostate cancer metastases. PLoS ONE. 2011; 6:e27970.
17. Mostaghel EA, Marck BT, Plymate SR, Vessella RL, Balk S, Matsumoto AM, Nelson PS, Montgomery RB. Resistance to CYPA1 inhibition with abiraterone in castration-resistant prostate cancer: induction of steroidogenesis and androgen receptor splice variants. Clin Cancer Res. 2011; 17:5913–5925.
18. Li Y, Chan SC, Brand LJ, Hwang TH, Silverstein KAT, Dehm SM. Androgen receptor splice variants mediate enzalutamide resistance in castration-resistant prostate cancer Cell Lines. Cancer Res. 2013; 73:483–489.
19. Cao B, Qi Y, Zhang G, Xu D, Zhan Y, Alvarez X, Guo Z, Fu X, Plymate SR, Sartor O, Zhang H, Dong Y. Androgen receptor splice variants activating the full-length receptor in mediating resistance to androgen-directed therapy. Oncotarget. 2014; 5:1646–1656.
20. Antonarakis ES, Lu C, Wang H, Luber B, Nakazawa M, Roeser JC, Chen Y, Mohammad TA, Chen Y, Fedor HL, Lotan TL, Zheng Q, De Marzo AM, Isaacs JT, Isaacs WB, Nadal R, Paller CJ, Denmeade SR, Carducci MA, Eisenberger MA, Luo J. AR-V7 and resistance to enzalutamide and abiraterone in prostate cancer. N Engl J Med. 2014; 371:1028–1038.
21. Mezynski J, Pezaro C, Bianchini D, Zivi A, Sandhu S, Thompson E, Hunt J, Sheridan E, Baikady B, Sarvadikar A, Maier G, Reid AHM, Mulick Cassidy A, Olmos D, Attard G, de Bono J. Antitumour activity of docetaxel following treatment with the CYP17A1 inhibitor abiraterone: clinical evidence for cross-resistance? Ann Oncol Off J Eur Soc Med Oncol ESMO. 2012; 23:2943–2947.
22. Schweizer MT, Zhou XC, Wang H, Bassi S, Carducci MA, Eisenberger MA, Antonarakis ES. The influence of prior abiraterone treatment on the clinical activity of docetaxel in men with metastatic castration-resistant prostate cancer. Eur Urol. 2014; 66:646–652.
23. Van Soest RJ, van Royen ME, de Morrée ES, Moll JM, Teubel W, Wiemer EAC, Mathijssen RHJ, de Wit R, van Weerden WM. Cross-resistance between taxanes and new hormonal agents abiraterone and enzalutamide may affect drug sequence choices in metastatic castration-resistant prostate cancer. Eur J Cancer. 2013; 49:3821–3830.
24. Nadal R, Zhang Z, Rahman H, Schweizer MT, Denmeade SR, Paller CJ, Carducci MA, Eisenberger MA, Antonarakis ES. Clinical activity of enzalutamide in docetaxel-naïve and docetaxel-pretreated patients with metastatic castration-resistant prostate cancer. The Prostate. 2014; 74:1560–1568.
25. Cheng HH, Gulati R, Azad A, Nadal R, Twardowski P, Vaishampayan UN, Agarwal N, Heath EI, Pal SK, Rehman HT, Leiter A, Batten JA, Montgomery RB, Galsky MD, Antonarakis ES, Chi KN, Yu EY. Activity of enzalutamide in men with metastatic castration-resistant prostate cancer is affected by prior treatment with abiraterone and/or docetaxel. Prostate Cancer Prostatic Dis. 2015; 18:122–127.
26. Anbalagan M, Ali A, Jones RK, Marsden CG, Sheng M, Carrier L, Bu Y, Hangauer D, Rowan BG. Peptidomimetic Src/pretubulin inhibitor KX-01 alone and in combination with paclitaxel suppresses growth, metastasis in human ER/PR/HER2-negative tumor xenografts. Mol Cancer Ther. 2012; 11:1936–1947.
27. Cassimeris LU, Wadsworth P, Salmon ED. Dynamics of microtubule depolymerization in monocytes. J Cell Biol. 1986; 102:2023–2032.
28. Roth DM, Moseley GW, Glover D, Pouton CW, Jans DA. A microtubule-facilitated nuclear import pathway for cancer regulatory proteins. Traffic. 2007; 8:673–686.
29. Roth DM, Moseley GW, Pouton CW, Jans DA. Mechanism of microtubule-facilitated “fast track” nuclear import. J Biol Chem. 2011; 286:14335–14351.
30. Giannakakou P, Sackett DL, Ward Y, Webster KR, Blagosklonny MV, Fojo T. p53 is associated with cellular microtubules and is transported to the nucleus by dynein. Nat Cell Biol. 2000; 2:709–717.
31. Soderholm JF, Bird SL, Kalab P, Sampathkumar Y, Hasegawa K, Uehara-Bingen M, Weis K, Heald R. Importazole, a small molecule inhibitor of the transport receptor importin-β. ACS Chem Biol. 2011; 6:700–708.
32. Sweeney C, Chen Y-H, Carducci MA, Liu G, Jarrard DF, Eisenberger MA, Wong Y-N, Hahn NM, Kohli M, Vogelzang NJ, Cooney MM, Dreicer R, Picus J, Shevrin DH, Hussain M, Garcia JA, DiPaola RS. Impact on overall survival (OS) with chemohormonal therapy versus hormonal therapy for hormone-sensitive newly

metastatic prostate cancer (mPrCa): An ECOG-led phase III randomized trial. J Clin Oncol. 2014; 32:5s.

33. Seruga B, Ocana A, Tannock IF. Drug resistance in metastatic castration-resistant prostate cancer. Nat Rev Clin Oncol. 2011; 8:12–23.

34. Antonarakis ES, Armstrong AJ. Evolving standards in the treatment of docetaxel-refractory castration-resistant prostate cancer. Prostate Cancer Prostatic Dis. 2011; 14:192–205.

35. Thadani-Mulero M, Portella L, Sun S, Sung M, Matov A, Vessella RL, Corey E, Nanus DM, Plymate SR, Giannakakou P. Androgen receptor splice variants determine taxane sensitivity in prostate cancer. Cancer Res. 2014; 74:2270–2282.

36. Martin SK, Banuelos CA, Sadar MD, Kyprianou N. N-terminal targeting of androgen receptor variant enhances response of castration resistant prostate cancer to taxane chemotherapy. Mol Oncol. 2015; 9:628–639.

37. Steinestel J, Luedeke M, Arndt A, Schnoeller TJ, Lennerz JK, Wurm C, Maier C, Cronauer MV, Steinestel K, Schrader AJ. Detecting predictive androgen receptor modifications in circulating prostate cancer cells. Oncotarget. . Published online Apr 23, 2015.

38. Antonarakis ES, Lu C, Chen Y, Luber B, Wang H, Nakazawa M, Marzo AMD, Isaacs WB, Nadal R, Paller CJ, Denmeade SR, Carducci MA, Eisenberger MA, Luo J. AR splice variant 7 (AR-V7) and response to taxanes in men with metastatic castration-resistant prostate cancer (mCRPC). J Clin Oncol. 2015; 33 .

39. Clarke SJ, Rivory LP. Clinical pharmacokinetics of docetaxel. Clin Pharmacokinet. 1999; 36:99–114.

40. Chan SC, Li Y, Dehm SM. Androgen receptor splice variants activate androgen receptor target genes and support aberrant prostate cancer cell growth independent of canonical androgen receptor nuclear localization signal. J Biol Chem. 2012; 287:19736–19749.

41. Andersen RJ, Mawji NR, Wang J, Wang G, Haile S, Myung JK, Watt K, Tam T, Yang YC, Banuelos CA, Williams DE, McEwan IJ, Wang Y, Sadar MD. Regression of castrate-recurrent prostate cancer by a small-molecule inhibitor of the amino-terminus domain of the androgen receptor. Cancer Cell. 2010; 17:535–546.

42. Liu C, Lou W, Zhu Y, Nadiminty N, Schwartz CT, Evans CP, Gao AC. Niclosamide inhibits androgen receptor variants expression and overcomes enzalutamide resistance in castration-resistant prostate cancer. Clin Cancer Res. 2014; 20:3198–3210.

43. Purushottamachar P, Godbole AM, Gediya LK, Martin MS, Vasaitis TS, Kwegyir-Afful AK, Ramalingam S, Ates-Alagoz Z, Njar VCO. Systematic structure modifications of multi-target prostate cancer drug candidate galeterone to produce novel androgen receptor down-regulating agents as an approach to treatment of advanced prostate cancer. J Med Chem. 2013; 56:4880–4898.

44. Li J, Cao B, Liu X, Fu X, Xiong Z, Chen L, Sartor O, Dong Y, Zhang H. Berberine suppresses androgen receptor signaling in prostate cancer. Mol Cancer Ther. 2011; 10:1346–1356.

45. Roth DM, Harper I, Pouton CW, Jans DA. Modulation of nucleocytoplasmic trafficking by retention in cytoplasm or nucleus. J Cell Biochem. 2009; 107:1160–1167.

Published OnlineFirst June 9, 2015; DOI: 10.1158/0008-5472.CAN-15-0381

Tumor and Stem Cell Biology

Cancer Research

Androgen Receptor Splice Variants Dimerize to Transactivate Target Genes

Duo Xu[1,2,3], Yang Zhan[2], Yanfeng Qi[2], Bo Cao[1,2], Shanshan Bai[1,2], Wei Xu[4], Sanjiv S. Gambhir[5], Peng Lee[6], Oliver Sartor[7,8], Erik K. Flemington[9], Haitao Zhang[9], Chang-Deng Hu[10], and Yan Dong[1,2,11]

Abstract

Constitutively active androgen receptor splice variants (AR-V) lacking the ligand-binding domain have been implicated in the pathogenesis of castration-resistant prostate cancer and in mediating resistance to newer drugs that target the androgen axis. AR-V regulates expression of both canonical AR targets and a unique set of cancer-specific targets that are enriched for cell-cycle functions. However, little is known about how AR-V controls gene expression. Here, we report that two major AR-Vs, termed AR-V7 and AR^{v567es}, not only homodimerize and heterodimerize with each other but also heterodimerize with full-length androgen receptor (AR-FL) in an androgen-independent manner. We found that heterodimerization of AR-V and AR-FL was mediated by N- and C-terminal interactions and by the DNA-binding domain of each molecule, whereas AR-V homodimerization was mediated only by DNA-binding domain interactions. Notably, AR-V dimerization was required to transactivate target genes and to confer castration-resistant cell growth. Our results clarify the mechanism by which AR-Vs mediate gene regulation and provide a pivotal pathway for rational drug design to disrupt AR-V signaling as a rational strategy for the effective treatment of advanced prostate cancer. *Cancer Res; 75(17); 3663–71. ©2015 AACR.*

Introduction

Recurrence with lethal castration-resistant prostate cancer (CRPC) after androgen deprivation therapy remains the major challenge in treatment of advanced prostate cancer (1, 2). Significant advances in our understanding of continued androgen receptor (AR) signaling in CRPC have led to the development and FDA approval of two next-generation androgen-directed therapies, the androgen biosynthesis inhibitor abiraterone and the potent AR antagonist enzalutamide (3, 4). These drugs heralded a new era of prostate cancer therapy. However, some patients present with therapy-resistant disease, and most initial responders develop acquired resistance within months of therapy initiation (3, 4). The resistance is typically accompanied by increased prostate-specific antigen (PSA), indicating reactivated AR signaling (3, 4). Accumulating evidences indicate that prostate tumors can adapt to these androgen-directed therapies, including abiraterone and enzalutamide, by signaling through constitutively active alternative splicing variants of AR (AR-V; refs. 5–17).

To date, 15 AR-Vs have been identified (18). Structurally, AR-Vs have insertions of cryptic exons downstream of the exons encoding the DNA-binding domain (DBD) or deletions of the exons encoding the ligand-binding domain (LBD), resulting in a disrupted AR open reading frame and expression of LBD-truncated AR (6, 7, 9, 15, 19, 20). Because the N-terminal domain, which contains the most critical transactivation domain of the receptor (AF1), and the DBD remain intact in the majority of the AR-Vs, many AR-Vs display ligand-independent transactivation. AR-V7 (aka AR3) and AR^{v567es} (aka AR-V12) are two major AR-Vs expressed in clinical specimens (7–10, 15, 17). They localize primarily to the nucleus, activate target gene expression in a ligand-independent manner, and promote castration-resistant growth of prostate cancer cells both *in vitro* and *in vivo* (7, 9, 15, 19–21). Strikingly, patients with high levels of expression of AR-V7 or detectable expression of AR^{v567es} in prostate tumors have a shorter survival than other CRPC patients (8). Moreover, AR-V7 expression in circulating tumor cells of CRPC patients is associated with resistance to both abiraterone and enzalutamide (17). These findings indicate an association between AR-V expression and a more lethal form of prostate cancer, and also highlight the importance of AR-Vs in limiting the efficacy of androgen-directed therapies.

[1]College of Life Sciences, Jilin University, Changchun, China. [2]Department of Structural and Cellular Biology, Tulane University School of Medicine, Tulane Cancer Center, New Orleans, Louisiana. [3]School of Nursing, Jilin University, Changchun, China. [4]McArdle Laboratory for Cancer Research, University of Wisconsin, Madison, Wisconsin. [5]Bio-X Program and Department of Radiology, Stanford University School of Medicine, Stanford, California. [6]Department of Pathology, New York University School of Medicine, New York, New York. [7]Department of Urology, Tulane University School of Medicine, Tulane Cancer Center, New Orleans, Louisiana. [8]Department of Medicine, Tulane University School of Medicine, Tulane Cancer Center, New Orleans, Louisiana. [9]Department of Pathology and Laboratory Medicine, Tulane University School of Medicine, Tulane Cancer Center, New Orleans, Louisiana. [10]Department of Medicinal Chemistry and Molecular Pharmacology, Purdue University, West Lafayette, Indiana. [11]National Engineering Laboratory for AIDS Vaccine, Jilin University, Changchun, China.

Note: Supplementary data for this article are available at Cancer Research Online (http://cancerres.aacrjournals.org/).

D. Xu and Y. Zhan contributed equally to this article.

Corresponding Author: Yan Dong, Tulane University School of Medicine, 1430 Tulane Avenue SL-49, New Orleans, LA 70112. Phone: 504-988-4761; Fax: 504-988-0468; E-mail: ydong@tulane.edu

doi: 10.1158/0008-5472.CAN-15-0381

Published OnlineFirst June 9, 2015; DOI: 10.1158/0008-5472.CAN-15-0381

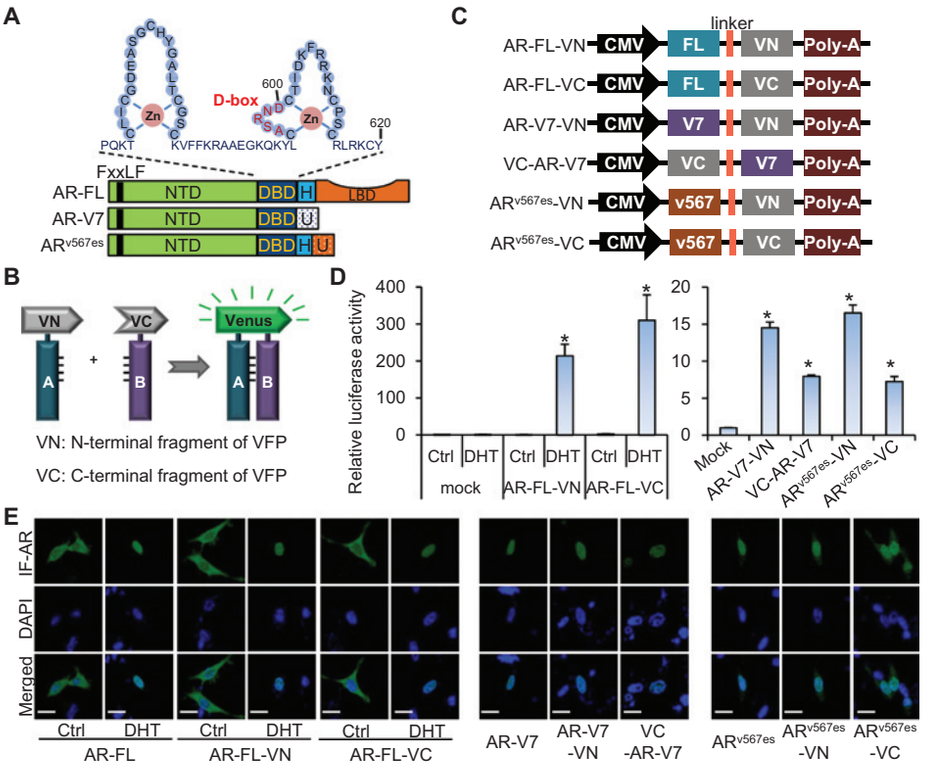

Figure 1.
AR-FL and AR-Vs in BiFC fusion proteins are functional. A, schematic representation of AR-FL, AR-V7, and AR^{v567es} protein structure. The DBD is composed of two zinc fingers. NTD, N-terminal domain; H, hinge region; U, unique C-terminal sequence. D-box and FxxLF motif mediate AR-FL dimerization. B, a schematic of the principle of the BiFC assay. VFP, Venus fluorescent protein. C, schematic diagram of the constructs used in the BiFC assay. D, luciferase assay showing AR transactivating activity in PC-3 cells cotransfected with the indicated BiFC construct and the ARE-luc plasmid. *, $P < 0.05$ from mock control. E, immunofluorescent (IF) staining showing protein fusion does not change subcellular localization of AR-FL, AR-V7, or AR^{v567es}. The indicated expression construct or BiFC fusion construct was transfected into PC-3 cells, and immunofluorescent staining was conducted at 48 hours after transfection. DAPI, nuclear stain. Scale bars, 10 μm. Cells were cultured under androgen-deprived condition unless specified. DHT, 1 nmol/L for 24 hours.

AR-V7 and AR^{v567es} can regulate the expression of both canonical AR targets and a unique set of targets enriched for cell-cycle function independent of the full-length AR (AR-FL; refs. 7, 10, 15). AR-V7 and AR^{v567es} can also activate AR-FL in the absence of androgen by facilitating AR-FL nuclear localization and coregulate the expression of canonical AR targets (5). It has long been appreciated that dimerization is required for AR-FL to regulate target gene expression (22), but little is known about AR-V dimerization. Coimmunoprecipitation of endogenous AR^{v567es} and AR-FL (15) and co-occupancy of the PSA promoter by AR-V7 and AR-FL (5) suggest that AR-Vs may form heterodimers with AR-FL. However, whether AR-Vs homodimerize or heterodimerize with each other and whether the dimerization is required for AR-Vs to regulate target genes and to confer castration-resistant cell growth are currently unknown.

Dimerization of AR-FL is mediated mainly through N/C-terminal interactions, via the FxxLF motif in the N-terminal domain and the coactivator groove in the LBD, and DBD/DBD interactions, via the dimerization box (D-box; ref. 22). Because the FxxLF motif and the D-box (Fig. 1A) are maintained in the majority of the AR-Vs identified, we hypothesize that these AR-Vs can form heterodimers with each other as well as homodimers via DBD/DBD interactions and that they can also form heterodimers with AR-FL via DBD/DBD and N/C interactions. In the current study, we tested this hypothesis by using the bimolecular fluorescence complementation (BiFC) and bioluminescence resonance energy transfer (BRET) assays, which have complementary capabilities for characterizing protein–protein interactions in live cells. BiFC allows direct visualization of subcellular locations of the interactions (23), while BRET allows real-time detection of complex formation (24, 25).

Materials and Methods

Cell lines and reagents

LNCaP, PC-3, DU145, VCaP, and HEK-293T cells were obtained from the ATCC, and cultured as described (26). C4-2 was provided by Dr. Shahriar Koochekpour (Roswell Park Cancer Institute, Buffalo, NY). All the cell lines were authenticated on April 1, 2015 by the method of short tandem repeat profiling at the Genetica DNA Laboratories. Enzalutamide was purchased from Selleck Chemicals.

Plasmid construction

To generate different BiFC fusion constructs of AR-FL, AR-V7, and AR^{v567es}, we PCR amplified the AR-FL, AR-V7, and AR^{v567es} cDNAs from their respective expression construct, and cloned the PCR amplicons separately into a TA-cloning vector (Promega). Fusion constructs of AR-FL, AR^{v567es}, and AR-V7 with either VN or VC were generated by subcloning the cDNAs from the TA plasmids into the SalI and XhoI sites of the pBiFC-VN155 and pBiFC-VC155 vectors. The mutant BiFC-AR-V and BiFC-AR-FL constructs with mutations at the FxxLF motif (F23,27A/L26A) and/or D-box (A596T/S597T) were generated by site-directed mutagenesis by using the Q5 site-Directed Mutagenesis Kit (New England BioLabs). BRET-fusion constructs of AR-FL, AR-V7, and AR^{v567es} were generated by subcloning the AR-FL, AR-V7, and AR^{v567es} cDNA from the respective TA plasmids into the BamHI and XbaI sites of the pcDNA3.1-RLuc8.6 and TurboFP635 vectors (24). The doxycycline-inducible AR^{v567es} lentiviral construct was generated by subcloning the AR^{v567es} cDNA from its TA plasmid first into the pDONR221 vector (Invitrogen) and subsequently into the doxycycline-inducible pHAGE-Ind-EF1a-DEST-GH lentiviral construct

Published OnlineFirst June 9, 2015; DOI: 10.1158/0008-5472.CAN-15-0381

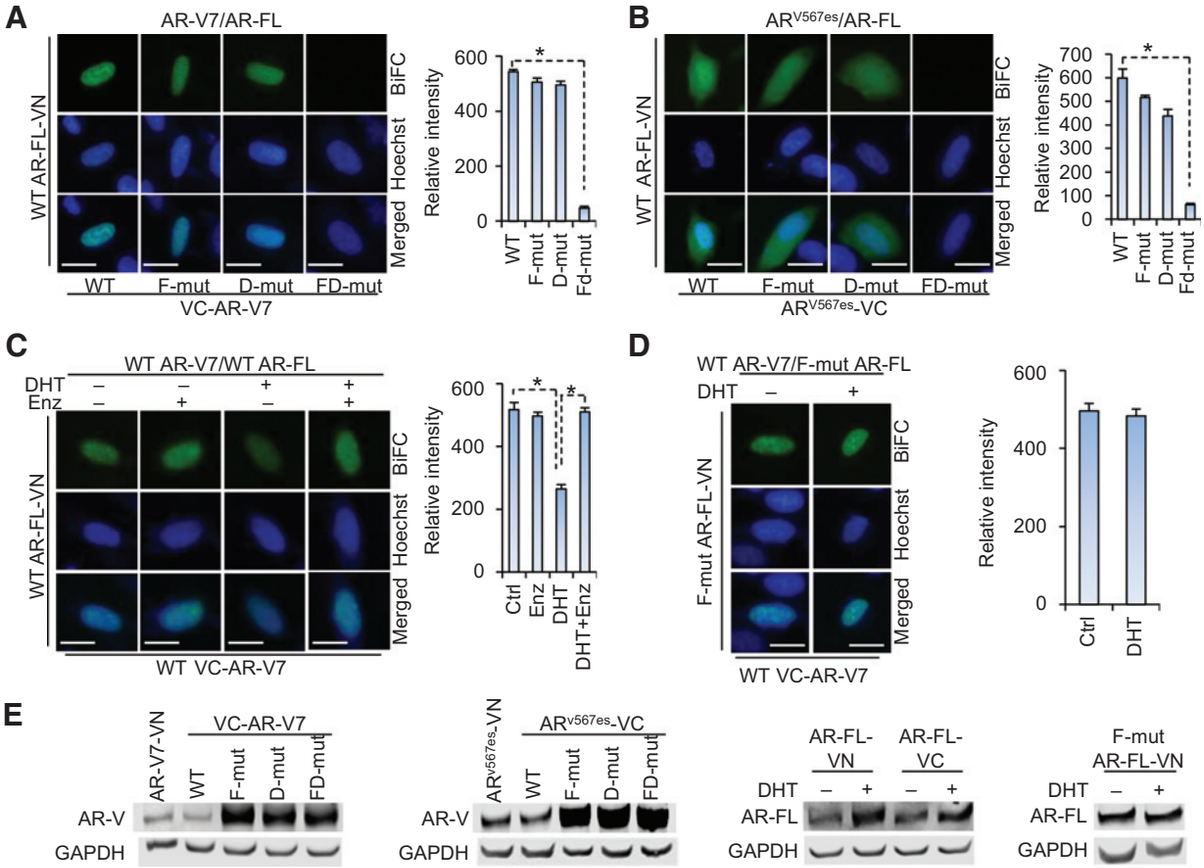

Figure 2.
AR-V7 and AR^{V567es} heterodimerize with AR-FL through both N/C and DBD/DBD interactions. wt, wild-type; F-mut, FxxLF-motif mutant; D-mut, D-box mutant; FD-mut, FxxLF-motif and D-Box double mutant. Hoechst, nuclear stain. Scale bars, 10 μm. *, $P < 0.05$. A and B, dimerization was detected by the BiFC assay in PC-3 cells under androgen-deprived condition. Right, quantitation of BiFC signals by flow cytometry. C and D, pretreatment with androgen attenuates the dimerization between AR-V7 and wt AR-FL (C) but not the dimerization between AR-V7 and F-mut AR-FL (D). PC-3 cells were treated with 1 nmol/L DHT with or without 10 μmol/L enzalutamide (Enz) right after transfection with the indicated BiFC constructs, and BiFC signal was assessed at 48 hours after transfection. Right, quantitation of BiFC signals by flow cytometry. E, Western blotting with a pan-AR antibody showing expression of the BiFC-fusion proteins. Individual fusion construct was transfected into PC-3 cells cultured under androgen-deprived condition unless specified. DHT, 1 nmol/L for 24 hours.

by using the Gateway Cloning System (Invitrogen). All plasmids were sequence verified.

DNA transfection and reporter gene assay

PC-3 and HEK-293T cells were transfected by using the TransIT-2020 (Mirus Bio LLC) and TurboFect reagents (Thermo Scientific), respectively, per instruction of the manufacturer. DU145, C4-2, and LNCaP cells were transfected by using the Lipofectamine 2000 and Plus reagent (Invitrogen) as described (27). Reporter gene assay was performed as previously described (28) with either an androgen-responsive element-luciferase plasmid (ARE-luc) containing three ARE regions ligated in tandem to the luciferase reporter or a luciferase construct driven by three repeats of an AR-V–specific promoter element of the ubiquitin-conjugating enzyme E2C (UBE2C) gene (UBE2C-luc). To ensure an even transfection efficiency, we conducted the transfection in bulk and then split the transfected cells for luciferase assay.

Immunofluorescence staining

Cells were transfected with indicated plasmids on Poly-D-Lysine–coated coverslips (neuVitro) and cultured in phenol red–free medium supplemented with 10% charcoal-stripped FBS. For the dihydrotestosterone (DHT) groups, 1 nmol/L DHT was added at 24 hours after transfection. At 48 hours after transfection, cells were fixed with 70% ethanol, and incubated with a pan-AR antibody (PG-21, Millipore; 1:200) overnight at 4°C and subsequently with Alexa Fluor 488–conjugated secondary antibody (Invitrogen; 1:1,000) for 1 hour at room temperature in the dark. Nuclei were then stained with 4′,6-diamidino-2-phenylindole (DAPI). Confocal images were obtained by using a Leica TCS SP2 system with a 40× oil-immersion objective on a Z-stage.

BiFC analysis

Cells were cotransfected with different BiFC fusion constructs. At 48 hours after transfection, cells were incubated with Hoechst33342 (Invitrogen) and observed by fluorescence microscopy (Olympus). For flow cytometry quantitation of BiFC signals, the pDsRed2-C1 construct (Clontech) was cotransfected with the BiFC fusion constructs. At 48 hours after transfection, cells were trypsinized, and the Venus and DsRed fluorescence were analyzed by flow cytometry.

Published OnlineFirst June 9, 2015; DOI: 10.1158/0008-5472.CAN-15-0381

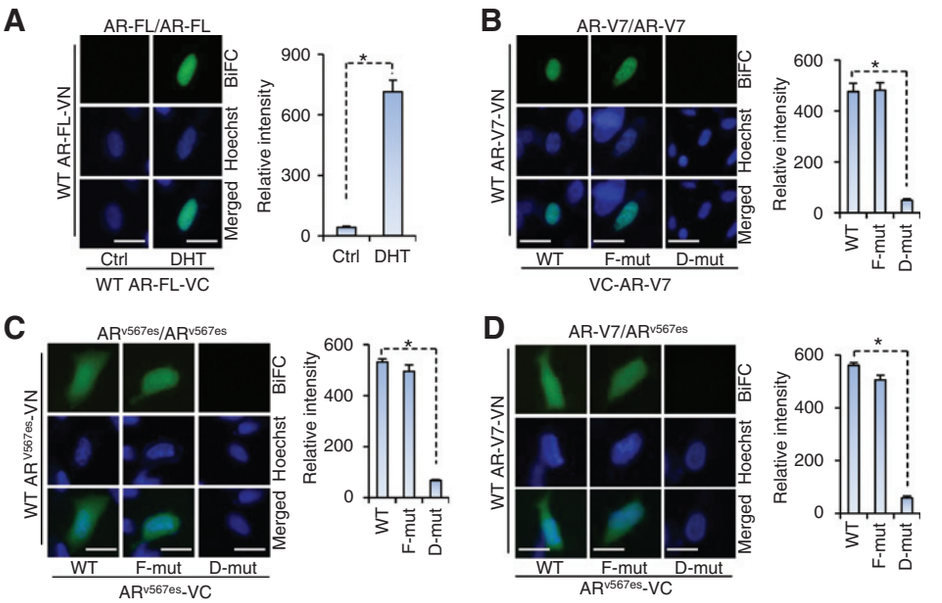

Figure 3.
AR-V and AR-V dimerize through DBD/DBD interactions. AR-FL homodimerization (A), AR-V7 homodimerization (B), AR^{v567es} homodimerization (C), and AR-V7/AR^{v567es} heterodimerization (D) were detected by BiFC assay in PC-3 cells under androgen-deprived condition unless specified. DHT, 1 nmol/L for 24 hours. Right panels, quantitation of BiFC signals by flow cytometry. wt, wild-type; F-mut, FxxLF-motif mutant; D-mut, D-box mutant. Hoechst, nuclear stain. Scale bars, 10 μm. *, $P < 0.05$. In contrast to AR-FL/AR-FL and AR-V7/AR-V7 dimerization, which were detected mainly in the nucleus (>90%), AR^{v567es}/AR^{v567es} and AR-V7/AR^{v567es} dimerization were observed in both the nucleus (37% and 57%, respectively) and the cytoplasm (63% and 43%, respectively).

Western blot analysis

The procedure was described previously (29). The anti-GAPDH (Millipore), anti-AR (N-20, Santa Cruz Biotechnology), anti-HSP70 (Abcam), anti-Turbo-red fluorescent protein (Abcam), and anti-*Renilla*-luciferase (Thermo Scientific) antibodies were used.

Quantitative RT-PCR and cell growth assay

Quantitative RT-PCR (qRT-PCR) was performed as described (30), and the qPCR primer probe sets were from IDT. Cell growth was determined by the sulforhodamine (SRB) assay as described (31). To ensure an even transduction efficiency, we conducted the transduction of the cells with packaged lentivirus in bulk, and then split the transduced cells for qRT-PCR and SRB assays.

BRET assay

Cells were either transfected with an RLuc BRET fusion plasmid or cotransfected with an RLuc and a TFP BRET fusion plasmid. At 72 hours after transfection, cells were detached with 5 mmol/L EDTA in PBS and resuspended in PBS with 1% sucrose. Cells were counted and seeded in triplicate into a 96-well white-wall microplate at 10^5 cells per well. Freshly prepared coelenterazine (Nanolight Technology) in water was added to the cells at a final concentration of 25 μmol/L. BRET readings at 528 nm and 635 nm were obtained immediately with a Synergy 2 microplate reader (BioTek). The BRET ratio was calculated by subtracting the ratio of 635-nm emission and 528-nm emission obtained from cells coexpressing the RLuc and TFP fusion proteins from the background BRET ratio resulting from cells expressing the RLuc fusion protein alone in the same experiment: BRET ratio = (emission at 635 nm)/(emission at 528 nm) − (emission at 635 nm RLuc only)/(emission at 528 nm RLuc only).

Statistical analysis

The Student two-tailed *t* test was used to determine the mean differences between two groups. $P < 0.05$ is considered significant. Data are presented as mean ± SEM.

Results

Characterization of AR-FL and AR-Vs in BiFC fusion proteins

For BiFC analysis of interaction between proteins A and B, the two proteins are fused separately to either the N- or C-terminal fragment of the Venus fluorescent protein (VN or VC, Fig. 1B). If the two proteins dimerize, the interaction allows regeneration of the Venus fluorescent protein to emit fluorescent signal (23). Because BiFC depends on the relative orientation of the fusion proteins (23), we generated all possible combinations of N- and C-terminal fusions by cloning the AR-FL, AR^{v567es}, or AR-V7 cDNA either in front of or after VN or VC. Different pairs of fusion protein constructs were transfected into the AR-null PC-3 cells (to avoid confounding effect of endogenous AR), and the fusion protein constructs exhibiting the highest BiFC signals (Fig. 1C) were chosen for further analysis. The transactivating abilities of the fusion proteins were tested by the reporter gene assay. Although the protein fusion affected the relative activities of the fusion proteins (Figs. 1D and Supplementary Fig. S1), all the fusion proteins can transactivate target genes. Immunofluorescence assay further showed that the AR-FL and AR-Vs in the fusion proteins have the same subcellular localizations as the respective nonfusion AR isoform (Fig. 1E). Collectively, the data indicated that AR-FL and AR-Vs are functional in the fusion proteins.

BiFC detection of AR-V/AR-FL heterodimerization

To assess the ability of AR-V7 and AR^{v567es} to heterodimerize with AR-FL, we cotransfected the AR-V- and AR-FL BiFC fusion constructs into PC-3 cells and quantitated the Venus fluorescence signal by flow cytometry. Both AR-V7 and AR^{v567es} dimerized with AR-FL, and the dimerization did not require androgen (Fig. 2A and B). To delineate the dimerization interface, we generated mutant BiFC-AR-V constructs with mutations at the FxxLF motif (F23,27A/L26A) and/or D-box (A596T/S597T). FxxLF motif and D-box mediate AR-FL homodimerization through N/C and DBD/DBD interactions, respectively (22). Only mutating both motifs abolished AR-V/AR-FL dimerization (Fig. 2A and B), indicating that both N/C and DBD/DBD interactions mediate

Published OnlineFirst June 9, 2015; DOI: 10.1158/0008-5472.CAN-15-0381

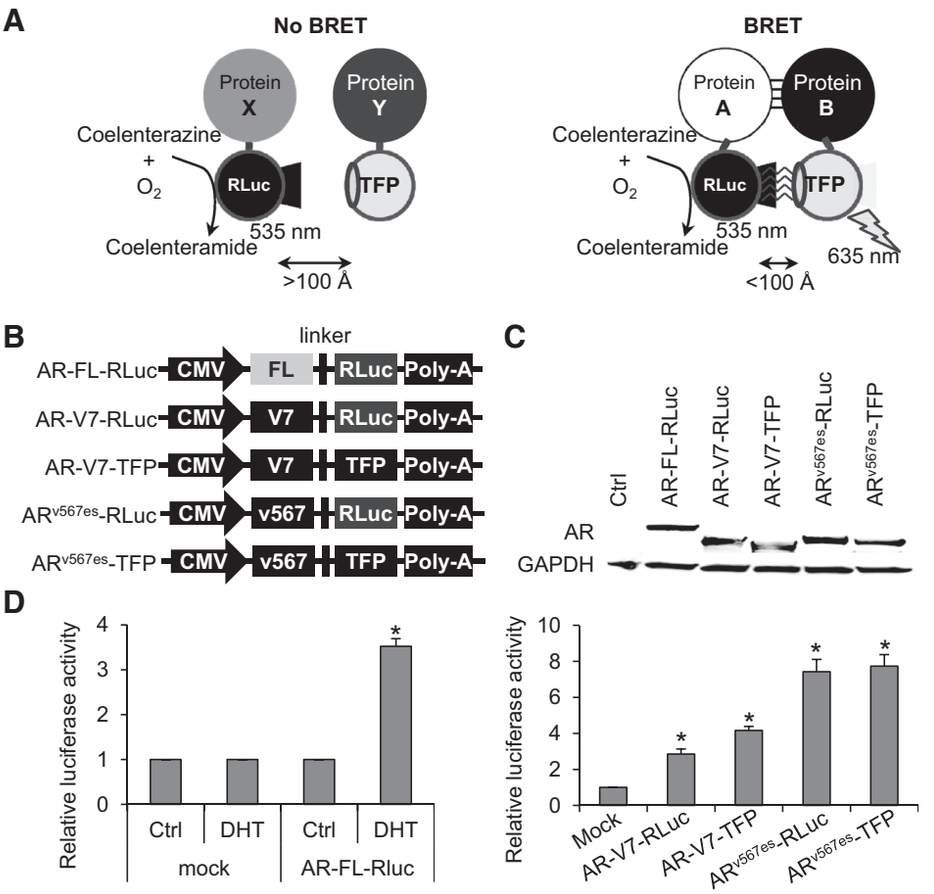

Figure 4.
AR-FL and AR-Vs in BRET fusion proteins are functional. A, a schematic of the principle of the BRET assay. B, schematic diagram of the constructs used in the BRET assay. RLuc, RLuc8.6 luciferase; TFP, TurboFP635 fluorescent protein. C, Western blotting with a pan-AR antibody showing expression of the BRET-fusion proteins. Individual fusion construct was transfected into HEK-293T cells cultured under androgen-deprived condition. D, luciferase assay showing AR *trans*-activating activity in HEK-293T cells cotransfected with the indicated BRET construct and the ARE-luc plasmid. Cells were cultured under androgen-deprived condition unless specified. DHT, 1 nmol/L for 24 hours. *, $P < 0.05$ from mock control.

the dimerization. Mutating one motif did not lead to significant change of BiFC signal (Fig. 2A and B), likely due to compensation of the loss of one mode of interaction by the other. Similar results were obtained in DU145 and HEK-293T cells (Supplementary Figs. S2 and S3). Intriguingly, although AR^{v567es}/AR-FL dimerization was observed in both the cytoplasm and the nucleus, AR-V7/AR-FL dimerization was detected primarily in the nucleus in the vast majority of the cells (Figs. 2A and B, Supplementary Figs. S2A, S2B, S3A, and S3B).

Pretreatment of cells with DHT attenuated AR-V7/AR-FL dimerization, and this effect was blocked by the antiandrogen enzalutamide (Fig. 2C). Conversely, DHT pretreatment produced minimal effect on the dimerization of AR-V7 and the FxxLF-motif–mutated AR-FL (Fig. 2D), which lost the ability to homodimerize upon androgen treatment (Supplementary Fig. S4B; ref. 32). These data indicate that AR-V7 may compete with AR-FL for dimerizing with AR-FL. Notably, the expression of each of the wild-type and mutant fusion proteins was confirmed by Western blotting (Fig. 2E). Collectively, our data demonstrated androgen-independent dimerization between AR-V and AR-FL, and indicated that AR-V/AR-FL dimerization may attenuate androgen induction of AR-FL homodimerization.

BiFC detection of AR-V/AR-V dimerization

We further showed that, like liganded AR-FL (Figs. 3A and Supplementary Fig. S4), both AR-Vs can form a homodimer when expressed alone (Figs. 3B and C and Supplementary Figs. S2C, S2D, S3C, and S3D). The homodimerization can also occur when AR-V is coexpressed with AR-FL and even when it is expressed at a much lower level than AR-FL (Supplementary Fig. S5). Moreover, AR-V7 and AR^{v567es} can heterodimerize (Fig. 3D). Mutating D-box, but not the FxxLF motif, abolished AR-V/AR-V interactions, indicating that AR-Vs homodimerize and heterodimerize with each other through DBD/DBD interactions. Interestingly, similar to AR-V7/AR-FL dimerization, AR-V7/AR-V7 dimerization was detected primarily in the nucleus (Figs. 3B and Supplementary Figs. S2C and S3C). However, AR^{v567es}/AR^{v567es} and AR-V7/AR^{v567es} dimerization were observed in both the nucleus and the cytoplasm (Fig. 3C and D and Supplementary Figs. S2D and S3D).

Characterization of AR-FL and AR-Vs in BRET fusion proteins

We then used the newest BRET system, BRET6 (24), to confirm the BiFC results. BRET6 is based on energy transfer between the Rluc8.6 *Renilla* luciferase (Rluc) energy donor and the turbo red fluorescent protein (TFP) energy acceptor when the donor and acceptor are brought into close proximity by their fused proteins (Fig. 4A). Similar to BiFC, BRET also depends on the relative orientation of the fusion proteins. We therefore generated all possible combinations of N- and C-terminal fusions by cloning the AR-FL, AR^{v567es}, or AR-V7 cDNA either in front of or after Rluc

Published OnlineFirst June 9, 2015; DOI: 10.1158/0008-5472.CAN-15-0381

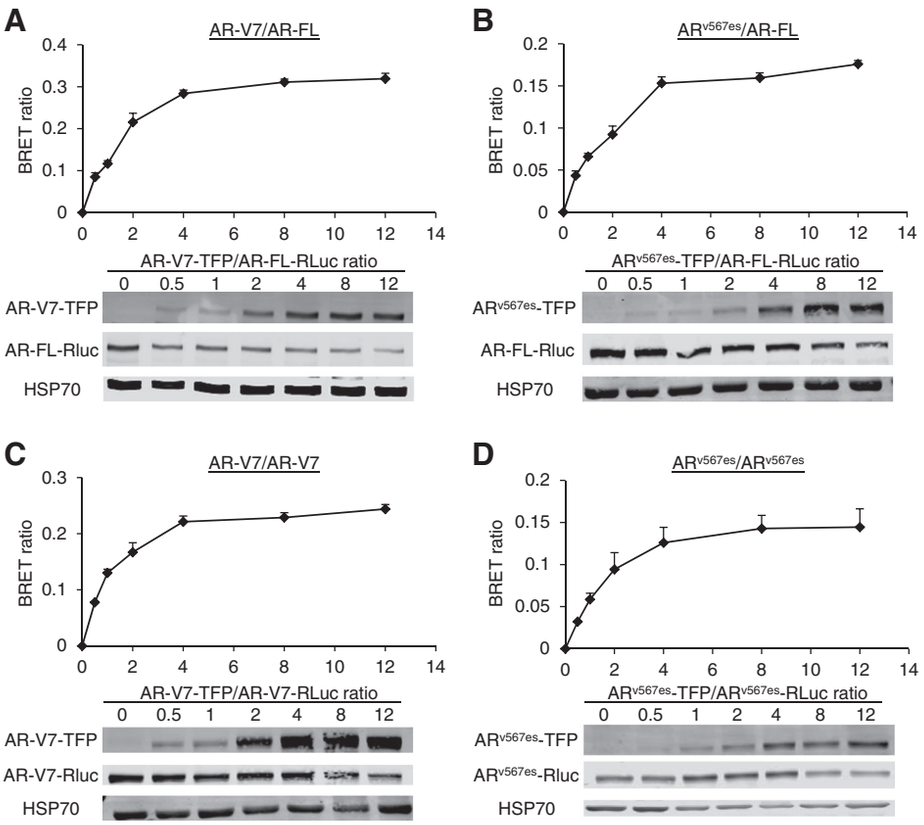

Figure 5.
BRET assay confirmation of AR-V/AR-FL and AR-V/AR-V dimerization. Indicated BRET fusion constructs were cotransfected into HEK-293T cells at different ratios, and BRET signal was measured after the addition of the coelenterazine substrate. Lower panels, Western blotting with an antibody against TFP, RLuc, or HSP70 showing the levels of the fusion proteins expressed. Cells were cultured under androgen-deprived condition.

or TFP. Different pairs of the fusion protein constructs were transfected into the AR-null HEK-293T cells (to avoid confounding effect of endogenous AR), and the fusion protein constructs exhibiting the highest BRET signals (Fig. 4B) were chosen for further analysis. The expression of these fusion proteins was confirmed by Western blotting (Fig. 4C). Furthermore, their abilities to transactivate were validated by luciferase assay with the cotransfection of the ARE-luc plasmid (Fig. 4D), indicating that AR-FL and AR-Vs are functional in the BRET fusion proteins.

BRET confirmation of AR-V/AR-FL and AR-V/AR-V dimerization

Figure 5 shows the BRET saturation curves for different combinations of the BRET fusion proteins in HEK-293T cells. The BRET ratios increased hyperbolically and rapidly saturated with the increase in the ratio of energy acceptor to energy donor, indicating specific protein–protein interaction (33). Similar to the BiFC data, mutating the FxxLF-motif and/or the D-box inhibited AR-V/AR-FL and AR-V/AR-V dimerization (Supplementary Fig. S6). Thus, the BRET data confirmed the BiFC results, showing the ability of AR-Vs to heterodimerize with AR-FL and to homodimerize. AR^{v567es}/AR^{v567es} interaction was further demonstrated by coimmunoprecipitation assay (Supplementary Fig. S7).

Dimerization is required for AR-V action

To assess the requirement of dimerization for AR-V action, we first performed reporter gene assay with the wild-type or the dimerization mutants of AR-V. As shown in Fig. 6A, the dimerization mutants completely lost the ability to transactivate, indicating a requirement of dimerization for AR-V transactivation. We then analyzed the ability of the wild-type and dimerization mutants of AR-Vs to regulate target gene expression and castration-resistant growth of prostate cancer cells. To this end, we infected the AR-FL–expressing LNCaP cells with lentivirus encoding AR-V7 or doxycycline-inducible AR^{v567es}. Mutation of the FxxLF motif alone or both the FxxLF motif and D-box attenuated AR-V induction of androgen-independent expression of the canonical AR target PSA and the AR-V–specific target UBE2C (Fig. 6B) as well as castration-resistant cell growth (Fig. 6C). The data indicated the requirement of dimerization for AR-Vs to regulate target genes and to confer castration-resistant cell growth.

Discussion

The current study represents the first to show the dimeric nature of AR-Vs in live cells. Using BiFC and BRET assays, we showed that AR-V7 and AR^{v567es} not only homodimerize and heterodimerize with each other but also heterodimerize with AR-FL. The dimerization does not require androgen. By mutating the FxxLF motif in the N-terminal domain and/or D-box in DBD of AR-Vs, we further showed that AR-V/AR-FL dimerization is mediated by both N/C and DBD/DBD interactions, whereas AR-V/AR-V dimerization is through DBD/DBD interactions. Because AR-Vs lack the C-terminal domain, the N/C interactions between AR-V and AR-FL is mediated presumably via the FxxLF motif of AR-V and the C-terminal domain of AR-FL. Significantly, dimerization mutants of AR-Vs lose the ability to transactivate target genes and to confer

Published OnlineFirst June 9, 2015; DOI: 10.1158/0008-5472.CAN-15-0381

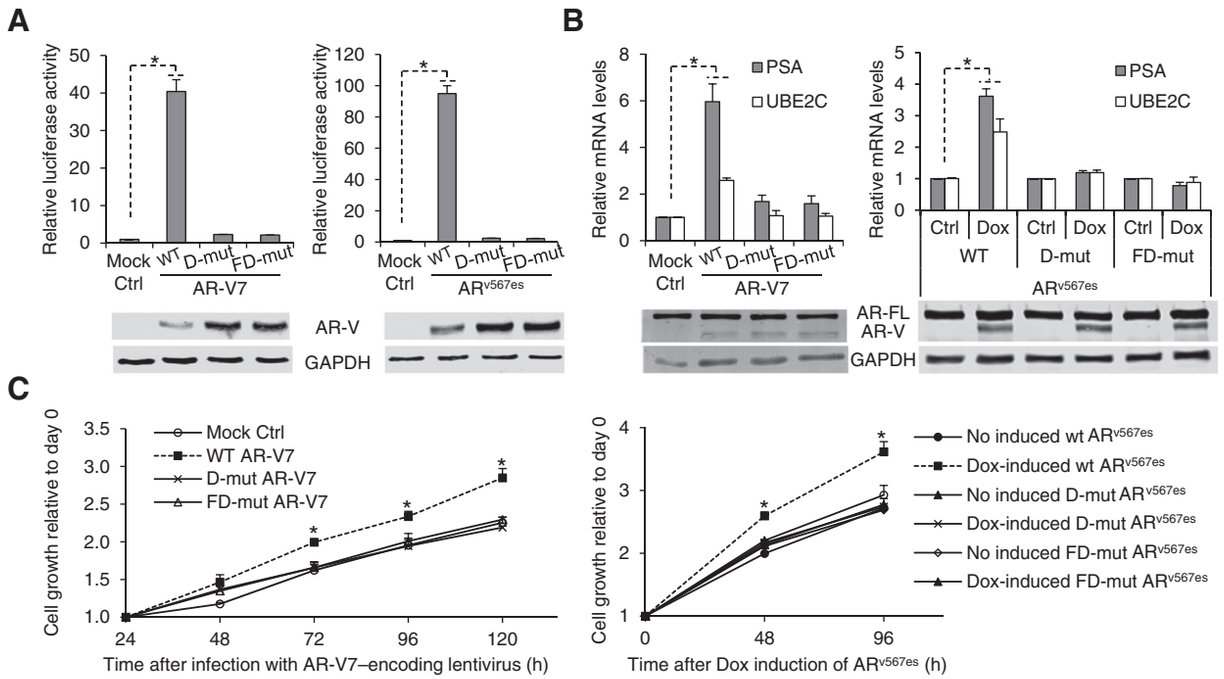

Figure 6.
Dimerization mutants of AR-Vs lose ability to transactivate and to promote castration-resistant cell growth. A, wild-type or dimerization mutant of AR-V was cotransfected with the ARE-luc plasmid, and cells were cultured under androgen-deprived condition. B and C, LNCaP cells were infected in bulk with lentivirus encoding wild-type or dimerization mutant of AR-V7 (left) or doxycycline-inducible wild-type or dimerization mutant of AR^{v567es} (right). At 24 hours after infection, cells were reseeded and treated with or without 200 ng/mL doxycycline and incubated for an additional 48 hours for qRT-PCR analysis of target genes (B) or for the indicated time for SRB assay of cell growth (C). Western blotting confirmed AR-V expression. *, $P < 0.05$ from control cells.

castration-resistant cell growth, indicating the requirement of dimerization for important functions of AR-Vs.

Our finding on AR-V/AR-FL interaction is in accordance with the previous reports on AR^{v567es} and AR-FL coimmunoprecipitation (15) as well as on AR-V7 and AR-FL co-occupancy of the PSA promoter (5), providing a direct evidence for their dimerization. Interestingly, we found that the androgen-independent dimerization between AR-V and AR-FL may mitigate androgen induction of AR-FL homodimerization. This could constitute a mechanistic basis for the ability of AR-Vs to attenuate androgen induction of AR-FL activity (5). To date, functional studies of AR-Vs have been focused mostly on their ability to regulate gene expression independent of AR-FL. Because AR-Vs are often coexpressed with AR-FL in biologic contexts, it is conceivable that the ability of AR-Vs to heterodimerize with and activate AR-FL in an androgen-independent manner could be equally important as their AR-FL–independent activity to castration resistance.

We and others showed previously that AR-V7 and AR^{v567es} localize constitutively to the nucleus and can facilitate AR-FL nuclear entry (5, 15), indicating that the initial interaction between AR-V and AR-FL is likely to be in the cytoplasm. This is supported by our data showing both cytoplasmic and nuclear localization of AR^{v567es}/AR-FL dimerization. Intriguingly, AR-V7/AR-FL dimerization is detected primarily in the nucleus in the vast majority of the cells. This may be due to the regeneration of the Venus fluorescent protein from the VN and VC fragments being slower than AR-V7/AR-FL nuclear translocation. Interestingly, AR-V7/AR-V7 dimerization was also detected primarily in the nucleus, whereas AR^{v567es}/AR^{v567es} and AR-V7/AR^{v567es} dimerization were observed in both the nucleus and the cytoplasm. Whether this is also due to slower regeneration of the Venus fluorescent protein than AR-V7/AR-V7 nuclear translocation or AR-V7 entering the nucleus as a monomer requires further investigation. In addition, the majority of the posttranslational modification sites of AR-FL are retained in AR-Vs (34). These posttranslational modifications regulate AR-FL transactivating activity, possibly via the interaction of AR-FL with other proteins or with itself (34). It is very likely that these posttranslational modifications may impact AR-V dimerization and transactivation and therefore deserve further investigation.

We reported previously that AR-V binds to the promoter of its specific target UBE2C without AR-FL, but co-occupies the promoter of the canonical AR target PSA with AR-FL in a mutually dependent manner (5). Furthermore, knockdown of AR-FL and AR-V both result in reduced androgen-independent PSA expression, but only AR-V knockdown downregulates UBE2C expression (5). The data, together with the findings from the current study, indicate that AR-Vs regulate their specific targets as an AR-V/AR-V dimer but control the expression of canonical AR targets as an AR-V/AR-FL dimer. Interestingly, while mutating D-box alone does not significantly mitigate AR-V/AR-FL dimerization, the mutation abolishes the ability of AR-V to induce the expression of PSA and UBE2C as well as to promote castration-resistant cell growth. A plausible explanation is that, although D-box–mutated AR-V can dimerize with AR-FL, the dimer cannot bind to DNA to regulate the expression of target genes. This, together with the finding that D-box–D-box interactions are required for the formation of androgen-induced AR-FL intermolecular N/C

Published OnlineFirst June 9, 2015; DOI: 10.1158/0008-5472.CAN-15-0381

interactions (32), indicates that disrupting D-box–D-box interactions could lead to inhibition of not only AR-V/AR-V dimerization and transactivation but also AR-FL activation induced by either AR-Vs or androgens. Thus, disrupting D-box–D-box interactions may represent a more effective means to suppress AR signaling than targeting the LBD of AR.

In summary, we demonstrated the dimeric nature of AR-Vs in live cells and identified the dimerization interface. Significantly, we showed that proper dimerization is required for AR-V functions. The research therefore represents a key step in delineating the mechanism by which AR-Vs mediate gene regulation. This is vital for developing effective therapeutic strategies to disrupt AR-V signaling and provide more effective treatments for prostate cancer.

Disclosure of Potential Conflicts of Interest

O. Sartor is a consultant/advisory board member for Astellas, Janssen, and Medivation. No potential conflicts of interest were disclosed by the other authors.

Authors' Contributions

Conception and design: D. Xu, Y. Zhan, Y. Qi, B. Cao, H. Zhang, Y. Dong
Development of methodology: D. Xu, Y. Zhan, Y. Qi, S.S. Gambhir, H. Zhang
Acquisition of data (provided animals, acquired and managed patients, provided facilities, etc.): D. Xu, S. Bai
Analysis and interpretation of data (e.g., statistical analysis, biostatistics, computational analysis): D. Xu, Y. Qi, S. Bai, P. Lee, Y. Dong
Writing, review, and/or revision of the manuscript: D. Xu, Y. Zhan, B. Cao, W. Xu, S.S. Gambhir, P. Lee, O. Sartor, E.K. Flemington, H. Zhang, Y. Dong
Administrative, technical, or material support (i.e., reporting or organizing data, constructing databases): D. Xu
Study supervision: Y. Qi, W. Xu, Y. Dong
Other (provided BiFC plasmids and suggestions to conduct the BiFC experiments. Also, reviewed the manuscript with comments): C.-D. Hu

Acknowledgments

The authors thank Dr. Yun Qiu (University of Maryland, College Park, MD) for the human AR-FL and AR-V7 expression constructs, Dr. Stephen Plymate (University of Washington, Seattle, WA) for the human AR^{v567es} expression construct, Dr. Jun Luo (Johns Hopkins University, Baltimore, MD) for the pEGFP-AR construct, Drs. Zhou Songyang and Nancy L. Weigel (Baylor College of Medicine, Houston, TX) for the pHAGE-Ind-EF1a-DEST-GH construct, and Dr. Shahriar Koochekpour (Roswell Park Cancer Institute, Buffalo, NY) for C4-2 cells. The authors appreciate the excellent technical assistance from Ms. Mary Price at the Louisiana Cancer Research Consortium FACS Core.

Grant Support

This work was supported by the following grants: NIH/NCI R01CA188609, NIH/NIGMS P20GM103518, DOD W81XWH-12-1-0112, W81XWH-14-1-0485, and W81XWH-12-1-0275; Louisiana Board-of-Regents LEQSF (2012–15)-RD-A-25; the Louisiana Cancer Research Consortium Fund; the Tulane University School of Medicine Research Bridge Fund; and the National Natural Science Foundation of China Projects 81272851 and 81430087.

The costs of publication of this article were defrayed in part by the payment of page charges. This article must therefore be hereby marked *advertisement* in accordance with 18 U.S.C. Section 1734 solely to indicate this fact.

Received February 6, 2015; revised May 7, 2015; accepted May 27, 2015; published OnlineFirst June 9, 2015.

References

1. Egan A, Dong Y, Zhang H, Qi Y, Balk SP, Sartor O. Castration-resistant prostate cancer: adaptive responses in the androgen axis. Cancer Treat Rev 2014;40:426–33.
2. Knudsen KE, Scher HI. Starving the addiction: new opportunities for durable suppression of AR signaling in prostate cancer. Clin Cancer Res 2009;15:4792–8.
3. Fizazi K, Scher HI, Molina A, Logothetis CJ, Chi KN, Jones RJ, et al. Abiraterone acetate for treatment of metastatic castration-resistant prostate cancer: final overall survival analysis of the COU-AA-301 randomised, double-blind, placebo-controlled phase 3 study. Lancet Oncol 2012;13:983–92.
4. Scher HI, Fizazi K, Saad F, Taplin ME, Sternberg CN, Miller K, et al. Increased survival with enzalutamide in prostate cancer after chemotherapy. N Engl J Med 2012;367:1187–97.
5. Cao B, Qi Y, Zhang G, Xu D, Zhan Y, Alvarez X, et al. Androgen receptor splice variants activating the full-length receptor in mediating resistance to androgen-directed therapy. Oncotarget 2014;5:1646–56.
6. Dehm SM, Schmidt LJ, Heemers HV, Vessella RL, Tindall DJ. Splicing of a novel androgen receptor exon generates a constitutively active androgen receptor that mediates prostate cancer therapy resistance. Cancer Res 2008;68:5469–77.
7. Guo Z, Yang X, Sun F, Jiang R, Linn DE, Chen H, et al. A novel androgen receptor splice variant is up-regulated during prostate cancer progression and promotes androgen depletion-resistant growth. Cancer Res 2009;69:2305–13.
8. Hornberg E, Ylitalo EB, Crnalic S, Antti H, Stattin P, Widmark A, et al. Expression of androgen receptor splice variants in prostate cancer bone metastases is associated with castration-resistance and short survival. PLoS ONE 2011;6:e19059.
9. Hu R, Dunn TA, Wei S, Isharwal S, Veltri RW, Humphreys E, et al. Ligand-independent androgen receptor variants derived from splicing of cryptic exons signify hormone-refractory prostate cancer. Cancer Res 2009;69:16–22.
10. Hu R, Lu C, Mostaghel EA, Yegnasubramanian S, Gurel M, Tannahill C, et al. Distinct transcriptional programs mediated by the ligand-dependent full-length androgen receptor and its splice variants in castration-resistant prostate cancer. Cancer Res 2012;72:3457–62.
11. Li Y, Chan SC, Brand LJ, Hwang TH, Silverstein KA, Dehm SM. Androgen receptor splice variants mediate enzalutamide resistance in castration-resistant prostate cancer cell lines. Cancer Res 2012;73:483–9.
12. Liu LL, Xie N, Sun S, Plymate S, Mostaghel E, Dong X. Mechanisms of the androgen receptor splicing in prostate cancer cells. Oncogene 2014;33:3140–50.
13. Mostaghel EA, Marck BT, Plymate SR, Vessella RL, Balk S, Matsumoto AM, et al. Resistance to CYP17A1 inhibition with abiraterone in castration-resistant prostate cancer: induction of steroidogenesis and androgen receptor splice variants. Clin Cancer Res 2011;17:5913–25.
14. Nadiminty N, Tummala R, Liu C, Yang J, Lou W, Evans CP, et al. NF-kappaB2/p52 induces resistance to enzalutamide in prostate cancer: role of androgen receptor and its variants. Mol Cancer Ther 2013;12:1629–37.
15. Sun S, Sprenger CC, Vessella RL, Haugk K, Soriano K, Mostaghel EA, et al. Castration resistance in human prostate cancer is conferred by a frequently occurring androgen receptor splice variant. J Clin Invest 2010;120:2715–30.
16. Zhang X, Morrissey C, Sun S, Ketchandji M, Nelson PS, True LD, et al. Androgen receptor variants occur frequently in castration resistant prostate cancer metastases. PLoS ONE 2011;6:e27970.
17. Antonarakis ES, Lu C, Wang H, Luber B, Nakazawa M, Roeser JC, et al. AR-V7 and resistance to enzalutamide and abiraterone in prostate cancer. N Engl J Med 2014;371:1028–38.
18. Zhang H, Zhan Y, Liu X, Qi Y, Zhang G, Sartor O, et al. Splicing variants of androgen receptor in prostate cancer. Am J Clin Exp Urol 2013;1:18–24.
19. Hu R, Isaacs WB, Luo J. A snapshot of the expression signature of androgen receptor splicing variants and their distinctive transcriptional activities. Prostate 2011;71:1656–67.
20. Watson PA, Chen YF, Balbas MD, Wongvipat J, Socci ND, Viale A, et al. Constitutively active androgen receptor splice variants expressed in castration-resistant prostate cancer require full-length androgen receptor. Proc Natl Acad Sci U S A 2010;107:16759–65.

21. Chan SC, Li Y, Dehm SM. Androgen receptor splice variants activate androgen receptor target genes and support aberrant prostate cancer cell growth independent of canonical androgen receptor nuclear localization signal. J Biol Chem 2012;287:19736–49.
22. Centenera MM, Harris JM, Tilley WD, Butler LM. Minireview: the contribution of different androgen receptor domains to receptor dimerization and signaling. Mol Endocrinol 2008;22:2373–82.
23. Hu CD, Grinberg AV, Kerppola TK. Visualization of protein interactions in living cells using bimolecular fluorescence complementation (BiFC) analysis. Curr Protoc Cell Biol 2006; Chapter 21:Unit 21.3.
24. Dragulescu-Andrasi A, Chan CT, De A, Massoud TF, Gambhir SS. Bioluminescence resonance energy transfer (BRET) imaging of protein–protein interactions within deep tissues of living subjects. Proc Natl Acad Sci U S A 2011;108:12060–5.
25. Pfleger KDG, Seeber RM, Eidne KA. Bioluminescence resonance energy transfer (BRET) for the real-time detection of protein–protein interactions. Nat Protocols 2006;1:337–45.
26. Liu S, Qi Y, Ge Y, Duplessis T, Rowan BG, Ip C, et al. Telomerase as an important target of androgen signaling blockade for prostate cancer treatment. Mol Cancer Ther 2010;9:2016–25.
27. Dong Y, Zhang H, Gao AC, Marshall JR, Ip C. Androgen receptor signaling intensity is a key factor in determining the sensitivity of prostate cancer cells to selenium inhibition of growth and cancer-specific biomarkers. Mol Cancer Ther 2005;4:1047–55.
28. Zhan Y, Cao B, Qi Y, Liu S, Zhang Q, Zhou W, et al. Methylselenol prodrug enhances MDV3100 efficacy for treatment of castration-resistant prostate cancer. Int J Cancer 2013;133:2225–33.
29. Dong Y, Zhang H, Hawthorn L, Ganther HE, Ip C. Delineation of the molecular basis for selenium-induced growth arrest in human prostate cancer cells by oligonucleotide array. Cancer Res 2003;63:52–9.
30. Dong Y, Lee SO, Zhang H, Marshall J, Gao AC, Ip C. Prostate specific antigen expression is downregulated by selenium through disruption of androgen receptor signaling. Cancer Res 2004;64:19–22.
31. Vichai V, Kirtikara K. Sulforhodamine B colorimetric assay for cytotoxicity screening. Nat Protoc 2006;1:1112–6.
32. van Royen ME, van Cappellen WA, de VC, Houtsmuller AB, Trapman J. Stepwise androgen receptor dimerization. J Cell Sci 2012;125:1970–9.
33. Hamdan FF, Percherancier Y, Breton B, Bouvier M. Monitoring protein–protein interactions in living cells by bioluminescence resonance energy transfer (BRET). Curr Protoc Neurosci 2006;Chapter 5:UInit 5.23.
34. van der Steen T, Tindall DJ, Huang H. Posttranslational modification of the androgen receptor in prostate cancer. Int J Mol Sci 2013;14:14833–59.

Investigative Urology

A Whole Blood Assay for AR-V7 and AR^{v567es} in Patients with Prostate Cancer

Xichun Liu,* Elisa Ledet,* Dongying Li, Ary Dotiwala, Allie Steinberger, Allison Feibus, Jianzhuo Li, Yanfeng Qi, Jonathan Silberstein, Benjamin Lee, Yan Dong, Oliver Sartor and Haitao Zhang†

From the Departments of Pathology (XL, DL, JL, HZ), Structural and Cellular Biology (YQ, YD), Medicine (EL, AD, AS, OS) and Urology (EL, AD, AS, AF, JS, BL, OS) and Tulane Cancer Center (XL, EL, DL, AD, AS, JL, YQ, YD, OS, HZ), Tulane University School of Medicine, New Orleans, Louisiana

Abbreviations and Acronyms

AR-FL = full-length androgen receptor

CRPC = castration resistant prostate cancer

CTC = circulating tumor cell

EMT = epithelial-to-mesenchymal transition

EpCAM = epithelial cell adhesion molecule

mCRPC = metastatic castration resistant prostate cancer

PCR = polymerase chain reaction

PSA = prostate specific antigen

RP = radical prostatectomy

Purpose: Most prostate cancer mortality can be attributed to metastatic castration resistant prostate cancer, an advanced stage that remains incurable despite recent advances. The AR (androgen receptor) signaling axis remains active in castration resistant prostate cancer. Recent studies suggest that expression of the AR-V (AR splice variant) AR-V7 may underlie resistance to abiraterone and enzalutamide. However, controversy exists over the optimal assay. Our objective was to develop a fast and sensitive assay for AR-Vs in patients.

Materials and Methods: Two approaches were assessed in this study. The first approach was based on depletion of leukocytes and the second one used RNA purified directly from whole blood preserved in PAXgene® tubes. Transcript expression was analyzed by quantitative reverse transcription-polymerase chain reaction.

Results: Through a side-by-side comparison we found that the whole blood approach was suitable to detect AR-Vs. The specificity of the assay was corroborated in a cancer-free cohort. Using the PAXgene assay samples from a cohort of 46 patients with castration resistant prostate cancer were analyzed. Overall, AR-V7 and AR^{v567es} were detected in 67.53% and 29.87% of samples, respectively. Statistical analysis revealed a strong association of AR-V positivity with a history of second line hormonal therapies.

Conclusions: To our knowledge this is the first study to demonstrate that PAXgene preserved whole blood can be used to obtain clinically relevant information regarding the expression of 2 AR-Vs. These data on a castration resistant prostate cancer cohort support a role for AR-Vs in resistance to therapies targeting the AR ligand-binding domain.

Accepted for publication June 30, 2016.

No direct or indirect commercial incentive associated with publishing this article.

The corresponding author certifies that, when applicable, a statement(s) has been included in the manuscript documenting institutional review board, ethics committee or ethical review board study approval; principles of Helsinki Declaration were followed in lieu of formal ethics committee approval; institutional animal care and use committee approval; all human subjects provided written informed consent with guarantees of confidentiality; IRB approved protocol number; animal approved project number.

Supported by Grants ACS RSG-07-218-01-TBE, Department of Defense W81XWH-12-1-0275 and W81XWH-14-1-0480, Louisiana BoR LEQSF(2012-15)-RD-A-25 and National Institutes of Health/National Institute of General Medical Sciences 5P20GM103518-10, and the Oliver Sartor Prostate Cancer Research Fund.

* Equal study contribution.

† Correspondence: 1430 Tulane Ave., SL-79, New Orleans, Louisiana 70112 (e-mail: hzhang@tulane.edu).

See Editorial on page 1606.

0022-5347/16/1966-1758/0
THE JOURNAL OF UROLOGY®

http://dx.doi.org/10.1016/j.juro.2016.06.095
Vol. 196, 1758-1763, December 2016
Printed in U.S.A.

Key Words: prostatic neoplasms; receptors, androgen; blood; biomarkers, tumor; protein isoforms

PROSTATE cancer is the second leading cause of cancer mortality in men in the United States. Most disease related deaths can be attributed to mCRPC, which is marked by increasing serum PSA levels approximately 16 months after initial androgen deprivation therapy. Despite recent advances mCRPC remains the most critical challenge in the clinical management of prostate cancer.

It is well accepted that the AR signaling axis has a critical role in CRPC. Through a number of ligand dependent and independent mechanisms cancer cells adapt to low circulating androgens and maintain activation of AR. Particularly, a number of AR-Vs that are devoid of a functional ligand-binding domain have been identified.[1–4] Two major variants, AR-V7 and AR^{v567es}, have been shown to be capable of regulating target gene expression independent of AR-FL.[2–5] Recent studies suggest that the expression of these AR-Vs underlies resistance to second line hormonal therapies.[6,7]

CTCs are shed from solid tumors into the circulation. A number of CTC detection technologies have been developed in recent years. To date the most widely adopted is surface marker based CTC capturing, which relies on cell surface antigens such as EpCAM, cytokeratin, PSMA (prostate specific membrane antigen) or a combination of these markers.[8] Alternatively, CTCs can be enriched by depleting hematopoietic cells. For this purpose CD45, which is expressed on the surface of all leukocytes and their progenitors,[9] is commonly used.[10,11] Yet other studies have demonstrated the validity of using whole blood derived RNA from patients for reverse transcription-PCR analyses without CTC selection or enrichment.[12–14] The results of these series, which focused on genes highly expressed in prostate cancer, were clinically relevant and highly concordant with CTC enumeration analyses.[13,14]

In this study we sought to detect the expression of AR-V7 and AR^{v567es} in the circulation. We evaluated the CD45 based negative selection approach and the whole blood approach. Based on the results we chose the whole blood approach and analyzed blood samples obtained from a cohort of patients with CRPC.

MATERIALS AND METHODS

RNA Extraction from Whole Blood

From each patient 5 ml blood were collected into 2 PAXgene Blood RNA Tubes. The tubes were gently inverted and incubated at room temperature for 2 to 24 hours or stored at −20C before processing. Prior to RNA isolation frozen samples were brought to room temperature for 2 hours and centrifuged at 3,000 × gravity for 10 minutes. RNA isolation was performed using the PAXgene Blood RNA Kit.

Leukocyte Depletion

CTC enrichment was performed using a 2-step procedure as described[11] with modifications.

Red Blood Cells Lysis. Patient blood (10 ml) was collected in sodium citrate tubes (BD™) for immediate processing. Red blood cells were removed by adding lysis buffer composed of 154 mM NH_4Cl, 10 mM $KHCO_3$ and 0.1 mM EDTA (ethylenediaminetetraacetic acid) in 25 ml buffer per ml blood. After 5 minutes at room temperature the remaining cells were collected by centrifugation at 300 × gravity for 5 minutes. The pellet was washed twice with the labeling buffer (phosphate buffered saline with 2 mM EDTA and 0.5% bovine serum albumin, Ca^{2+}/Mg^{2+} free) and resuspended. Cells were counted and the concentration was adjusted to 1×10^8 cells per ml.

Leukocyte Removal. Following red blood cell lysis cell suspension was transferred to a round-bottom tube (BD). For every 10^8 cells 200 μl FcR Blocking Reagent (Miltenyi Biotec, Bergisch Gladbach, Germany) and 50 μl EasySep™ CD45 Depletion Cocktail were added and incubated at room temperature for 30 minutes. For immunomagnetic labeling EasySep Magnetic Nanoparticles were added at 100 μl/ml and mixed by pipetting. The suspension was incubated at room temperature for 15 minutes and volume was adjusted to 2.5 ml. The tube was placed in an EasySep magnet for 10 minutes. Labeled cells (CD45+) were separated by decanting the supernatant (CD45−) into a new tube. RNA was extracted from the CD45+ and CD45− fractions using the RNeasy® Mini Kit.

Quantitative Reverse Transcription-Polymerase Chain Reaction

RNA samples were quantitated by a NanoDrop™ 2000 spectrophotometer. Subsequently, 0.5 μg RNA was reverse-transcribed using SuperScript® III and random hexamers. The TaqMan® assay was chosen as the quantitative PCR technology to ensure the specificity of detection. PCR reactions were performed on a CFX96 Touch™ Real-Time PCR Detection System. The primers for AR-FL and AR-V7 were previously published.[3] Primers for AR^{v567es} were forward, 5′-CTACTCCGGACCTTACGGGGACATGCG-3′ and reverse 5′-TTGGGCACTTGCACAGAGAT-3′. The probe for all 3 amplicons, which was designed in our laboratory, was 5′-AAGAGCCGCTGAAGGGAAACAGAAGTACTTG-3′. RPL30 (ribosomal protein L30) was used as the housekeeping gene and the assay for RPL30 (Applied Biosystems®) was used. A total of 40 cycles served as the detection limit. Expression levels of the same transcript measured by the 2 approaches were compared using the $2^{-\Delta CT}$ method[15] and adjusted for the difference in starting blood volume.

Subjects

A total of 46 patients with CRPC were selected for study and provided consent via the Tulane Cancer Center

Table 1. *Patient demographics*

	Overall		White		Black	
No. pts	46		41		5	
Median age at diagnosis (range)	60	(43–77)	61.1	(46–77)	57.8	(43–66)
Median total Gleason score (range)	8	(6–9)	8	(6–9)	7	
No. family history (%):						
Yes	12	(26)	11	(27)	1	(20)
No	33	(72)	29	(71)	4	(80)
Unknown	1	(2)	1	(2)		
Median ng/ml PSA at sampling (range)	60.8 (less than 0.01–greater than 3,000)		59.7 (less than 0.01–3,000)		184.4 (48.9–2,050)	
Median days diagnosis-sampling (range)	1,877.5	(230–7,781)	1,877.5	(230–7,781)	2,424	(691–7,080)

and/or the urology clinic at Tulane University Hospital. For each patient 5 ml blood were collected in PAXgene tubes. When feasible, serial samples were collected. A total of 73 blood samples were collected and clinically annotated. Table 1 lists patient demographics. Supplementary tables 1 and 2 (http://jurology.com/) show the history of treatment with abiraterone acetate and enzalutamide, and the complete treatment history, respectively. Additionally, blood samples from 21 patients after RP with undetectable PSA (less than 0.01 ng/ml) were analyzed.

Statistical Analysis

All statistical analyses, including descriptive statistics, the Student t-test and the Fisher exact test, were performed with SAS®, version 9.4. All tests were 2-tailed with p values less than the α ($p \leq 0.05$) considered statistically significant. The median and range are reported for all continuous variables and the percent is reported for all categorical variables.

RESULTS

Selection of Whole Blood Approach to AR-V Detection

To identify a protocol for detecting AR-Vs in blood we evaluated the whole blood approach (ie the PAXgene approach) and the CTC enrichment approach based on the depletion of leukocytes (ie the CD45 depletion approach). Ten patients with mCRPC who had progressed to taxane chemotherapy and received multiple rounds of abiraterone and/or enzalutamide were identified for this purpose. Blood samples obtained from the same patient were analyzed side by side (supplementary figure, http://jurology.com/). AR-V7 transcripts were detected in 9 of 10 samples by both methods (supplementary table 3, http://jurology.com/). However, 2 samples were found to be positive for AR^{v567es} by the PAXgene approach but only 1 by the CD45 depletion approach, suggesting that the leukocyte depletion process may lead to loss of sensitivity. Indeed, AR-V transcript levels measured by the CD45 depletion approach were consistently lower than those measured by the PAXgene approach. The estimated decrease in AR-V7 was approximately 40% (supplementary table 4, http://jurology.com/).

The separation of CD45− and CD45+ cells during leukocyte depletion provided an opportunity to investigate the sources of AR transcripts. In 7 of 9 samples the AR-V7 signal was exclusively from the CD45− fraction (table 2). In the remaining samples the levels of AR-V7 measured in the CD45+ fraction were markedly lower than in the CD45− fraction. Similarly, most of the AR^{v567es} transcript was found in the CD45− fraction. In contrast, AR-FL was abundantly expressed in both fractions (table 2). The presence of AR-FL transcripts in CD45+ cells is consistent with studies documenting AR expression in lymphocytes and macrophages.[16,17]

Collectively, these results suggest that the AR-V transcripts in the CD45+ fraction are barely detectable, implying that depleting hematopoietic cells offers little improvement in specificity to detect AR-Vs. Furthermore, performing this procedure could lead to loss of sensitivity.

Whole Blood Assay Sensitivity and Specificity

To assess the sensitivity of this assay 22Rv1 cells, which express AR-V7, were spiked into 5 ml blood from a healthy donor. Figure 1 shows that this assay could detect 5 to 50 AR-V7+ cells in 5 ml blood or 1 to 10 cells per ml.

To evaluate specificity we analyzed blood samples from patients after RP who had undetectable PSA. Neither AR-V7 nor AR^{v567es} was detected in this cohort (table 3). Similarly, AR-V was not detected in

Table 2. *Distribution of AR transcripts in CD45− and CD45+ fractions*

Sample No.	% AR-V7		% AR^{v567es}		% AR-FL	
	CD45−	CD45+	CD45−	CD45+	CD45−	CD45+
1	100.00	0.00	—	—	46.05	53.95
2	100.00	0.00	—	—	29.21	70.79
3	100.00	0.00	—	—	63.96	36.04
4	85.93	14.07	96.16	3.84	55.55	44.45
5	—	—	—	—	65.27	34.73
6	100.00	0.00	—	—	54.75	45.25
7	100.00	0.00	—	—	20.02	79.98
8	91.65	8.35	—	—	76.71	23.29
9	100.00	0.00	—	—	75.59	24.41
10	100.00	0.00	—	—	31.34	68.66

Calculated from expression ratio between 2 fractions with total of 100%.

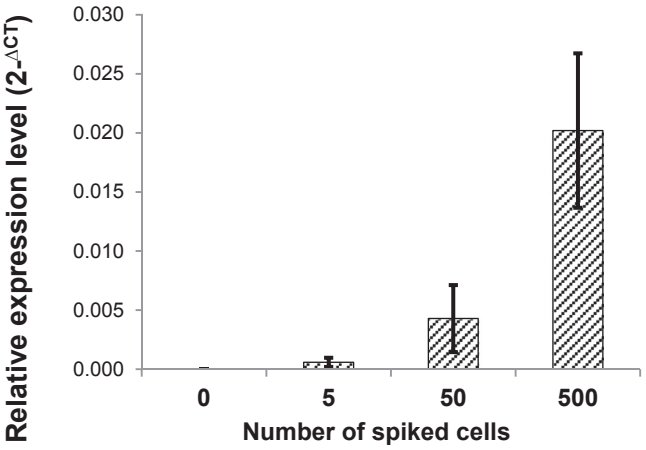

Figure 1. PAXgene assay sensitivity to detect AR-V7. Before transfer to PAXgene tubes 22RV1 cells were spiked into 5 ml blood from healthy donor. RNA extraction and quantitative reverse transcription-PCR analysis were performed as described.

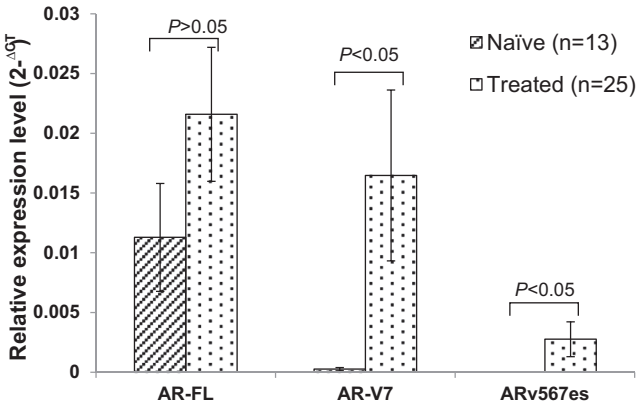

Figure 2. Increased expression of AR-Vs in patients with mCRPC treated with second line hormonal therapy. Naïve patients had never received treatment with abiraterone acetate, ketoconazole or enzalutamide. Treated patients had received these treatments but progressed. Statistical analysis was performed using 2-tailed Student t-test.

blood from 5 healthy donors (data not shown). These results suggest that this assay specifically detects AR-Vs expressed in cancer cells.

AR-V Expression Correlation with Prior Abiraterone and Enzalutamide Treatments

To investigate the clinical relevance of AR-V expression in whole blood we analyzed a total of 73 samples from 46 patients with CRPC. In this cohort 69 samples (94.52%) were positive for AR-FL, 50 (68.49%) were positive for AR-V7 and 23 (31.51%) were positive for AR^{v567es} (table 3). Of the 73 samples 53 (70%) expressed at least 1 variant and 20 (27.40%) expressed both variants. Notably, 20 of the 23 samples that expressed AR^{v567es} were also positive for AR-V7).

Based on the history of second line hormonal therapies, that is abiraterone, ketoconazole and enzalutamide, the CRPC cohort was categorized into naïve and treated groups. Due to a recent report demonstrating an association of AR-V7 expression with prior treatment with docetaxel,[18] patients who had received docetaxel or cabazitaxel were excluded from analysis. The expression level of both variants but not that of AR-FL was higher in the treated group than in the naïve group (fig. 2). In the treated group AR-V7 transcripts were expressed in 17 of 25 samples (68%) compared to 3 of 13 (23.08%) in the naïve group. The Fisher exact test revealed a strong association of AR-V7 positivity with a history of second line hormonal therapies (table 4). Similarly, AR^{v567es} positivity was associated with a history of these therapies, including 9 of 25 treated patients and 0 of 13 naïve patients. Additionally, patients who had been treated with second line hormonal therapies were more likely to express 1 (AR-V+) or both (AR-V7+/AR^{v567es}+) AR-V isoforms.

Table 3. *AR transcript detection in 2 cohorts*

	Post-RP		mCRPC		p Value	
Median age at sampling (range)	65.05 (53–76)		68.52 (47–86)		0.1559	(Student t-test)
No. samples (%):	21		73		–	
AR-FL+	17	(80.95)	69	(94.52)	0.0712	(Fisher exact test)
AR-V7+			50	(68.49)	<0.0001	(Fisher exact test)
AR^{v567es}+	0		23	(31.51)	0.0014	(Fisher exact test)
AR-V+	0		53	(72.60)	<0.0001	(Fisher exact test)
AR-V7+, AR^{v567es}+	0		20	(27.40)	0.0051	(Fisher exact test)

DISCUSSION

As noted by many groups, the development of predictive biomarkers is critical to optimal clinical decision making. The study by Antonarakis et al clearly represents a step forward in this direction.[7] Based on this ground breaking study the AR-V7 transcript in CTCs predicts resistance to abiraterone and enzalutamide. However, a potential shortcoming of this assay is dependence on the selection

Table 4. *AR-V positivity correlated with prior history of second line hormonal treatments*

	No. Naïve	No. Treated	p Value (Fisher exact test)
Overall	13	25	–
AR-FL+	12	24	1.0000
AR-V7+	3	17	0.0156
AR^{v567es}+	0	9	0.0159
AR-V+	3	18	0.0062
AR-V7+/AR^{v567es}+	0	8	0.0335

of EpCAM+ or Her2+ CTCs,[19] which likely represent only a fraction of the entire CTC population. In addition, the use of an epithelial marker such as EpCAM may exclude the population that underwent EMT. This is particularly relevant since studies have shown that AR-V7 and AR^{v567es} promote EMT in prostate cancer cells,[20–23] raising concern that AR-V expressing CTCs may not be captured efficiently by epithelial markers. Furthermore, it is clear from studies of CTCs using immunodetection methodologies that not all patients have detectable CTCs,[24] thus, limiting the number of patients in whom these AR-V7 assays can be performed.

To avoid the problems associated with CTC positive selection we tested a whole blood based approach and a negative selection approach by depleting lymphocytes. A comparison of these approaches led us to conclude that the whole blood approach performed at least as well as the CD45 depletion approach with regard to the sensitivity of AR-V detection (supplementary table 3, http://jurology.com/). The expression of AR-Vs was found predominantly in the CD45− population (table 2), suggesting that depleting CD45+ cells is unnecessary. Furthermore, the variants were detected at lower levels by the CTC enrichment protocol (supplementary table 4, http://jurology.com/), possibly due to the lack of RNA preservation during the enrichment process.

In a few cases we detected variants in the CD45+ fraction (table 2). This was most likely a result of cross contamination rather than expression of the variants by CD45+ cells. This is supported by data on the post-RP cohort showing that neither AR-V was detectable in whole blood derived RNA (table 3). Cross contamination could be caused by nonspecific binding of the CD45 antibodies, aberrant expression of CD45 by cancer cells[25,26] or the formation of lymphocyte/cancer cell microemboli.[27] Regardless, this observation suggests that CTCs could be lost during negative selection.

Recently, Steinestel et al reported using AR-V7 and AR mutations in CTCs to guide a therapy switch in patients.[18] The estimated overall benefit of the molecularly informed treatment decision was 27% over the uninformed decision. This study along with that of Antonarakis et al[7] highlights the importance of incorporating AR-V profiling into individualized treatment decision making. Although our assay is not complement-dependent cytotoxicity based, the findings are in line with complement-dependent cytotoxicity based studies, supporting a role of AR-V7 expression in resistance to second line hormonal therapies.

The current findings have several limitations. 1) This is a cross-sectional rather than a prospective study. A prospective study with longitudinal evaluation of patients is needed to establish the expression of AR-Vs in whole blood as a biomarker of treatment responsiveness. 2) Cells expressing the AR transcripts are not assessable by this assay. As a result some questions could not be properly addressed, such as whether AR-FL and AR-Vs are coexpressed in the same cells. These questions are clinically significant because AR-Vs have been shown to heterodimerize with AR-FL[28] and facilitate its nuclear translocation.[29] 3) There is no tissue confirmation using direct biopsies of tumors.

CONCLUSIONS

Despite the shortcomings, the current study is novel. To our knowledge this is the first report of AR-V7 detection using a whole blood assay that also detected AR^{v567es} in a significant proportion of patients. Eliminating the CTC selection process decreases hands-on time and improves assay sensitivity, enabling more patients to benefit from such assays. Indeed, the percent of AR-V7+ patients in this study was higher than for both CTC based assays (68.49% vs 50% and 49%, respectively).[7,18] The small volume of blood needed and the stability of RNA in PAXgene tubes make it practical to incorporate this assay into routine patient monitoring. In view of the potential benefits it is necessary to further evaluate and refine this assay in a prospective study with an adequate cohort.

REFERENCES

1. Dehm SM, Schmidt LJ, Heemers HV et al: Splicing of a novel androgen receptor exon generates a constitutively active androgen receptor that mediates prostate cancer therapy resistance. Cancer Res 2008; **68:** 5469.
2. Hu R, Dunn TA, Wei S et al: Ligand-independent androgen receptor variants derived from splicing of cryptic exons signify hormone-refractory prostate cancer. Cancer Res 2009; **69:** 16.
3. Guo Z, Yang X, Sun F et al: A novel androgen receptor splice variant is up-regulated during prostate cancer progression and promotes androgen depletion-resistant growth. Cancer Res 2009; **69:** 2305.
4. Sun S, Sprenger CC, Vessella RL et al: Castration resistance in human prostate cancer is conferred by a frequently occurring androgen receptor splice variant. J Clin Invest 2010; **120:** 2715.
5. Hu R, Lu C, Mostaghel EA et al: Distinct transcriptional programs mediated by the ligand-dependent full-length androgen receptor and its splice variants in castration-resistant prostate cancer. Cancer Res 2012; **72:** 3457.
6. Li Y, Chan SC, Brand LJ et al: Androgen receptor splice variants mediate enzalutamide resistance in castration-resistant prostate cancer cell lines. Cancer Res 2013; **73:** 483.

7. Antonarakis ES, Lu C, Wang H et al: AR-V7 and resistance to enzalutamide and abiraterone in prostate cancer. N Engl J Med 2014; **371:** 1028.

8. Harouaka R, Kang Z, Zheng SY et al: Circulating tumor cells: advances in isolation and analysis, and challenges for clinical applications. Pharmacol Ther 2014; **141:** 209.

9. Thomas ML: The leukocyte common antigen family. Annu Rev Immunol 1989; **7:** 339.

10. Lara O, Tong X, Zborowski M et al: Enrichment of rare cancer cells through depletion of normal cells using density and flow-through, immunomagnetic cell separation. Exp Hematol 2004; **32:** 891.

11. Yang L, Lang JC, Balasubramanian P et al: Optimization of an enrichment process for circulating tumor cells from the blood of head and neck cancer patients through depletion of normal cells. Biotechnol Bioeng 2009; **102:** 521.

12. Gandhok NK, Looney S, Koochekpour S et al: Relationships between reverse transcriptase-polymerase chain reaction for prostate specific antigen, survival, and various prognostic laboratory factors in patients with hormone refractory prostate cancer. Urol Oncol Semin Orig Investig 2005; **23:** 163.

13. Helo P, Cronin AM, Danila DC et al: Circulating prostate tumor cells detected by reverse transcription-PCR in men with localized or castration-refractory prostate cancer: concordance with CellSearch assay and association with bone metastases and with survival. Clin Chem 2009; **55:** 765.

14. Danila DC, Anand A, Schultz N et al: Analytic and clinical validation of a prostate cancer-enhanced messenger RNA detection assay in whole blood as a prognostic biomarker for survival. Eur Urol 2014; **65:** 1191.

15. Livak KJ and Schmittgen TD: Analysis of relative gene expression data using real-time quantitative PCR and the 2(-Delta Delta C(T)) method. Methods San Diego Calif 2001; **25:** 402.

16. Zhou Z, Shackleton CHL, Pahwa S et al: Prominent sex steroid metabolism in human lymphocytes. Mol Cell Endocrinol 1998; **138:** 61.

17. Smithson G, Couse JF, Lubahn DB et al: The role of estrogen receptors and androgen receptors in sex steroid regulation of B lymphopoiesis. J Immunol 1998; **161:** 27.

18. Steinestel J, Luedeke M, Arndt A et al: Detecting predictive androgen receptor modifications in circulating prostate cancer cells. Oncotarget 2015; doi: 10.18632/oncotarget.3925.

19. Todenhöfer T, Hennenlotter J, Feyerabend S et al: Preliminary experience on the use of the Adnatest® system for detection of circulating tumor cells in prostate cancer patients. Anticancer Res 2012; **32:** 3507.

20. Liu G, Sprenger C, Sun S et al: AR variant ARv567es induces carcinogenesis in a novel transgenic mouse model of prostate cancer. Neoplasia 2013; **15:** 1009.

21. Cottard F, Asmane I, Erdmann E et al: Constitutively active androgen receptor variants upregulate expression of mesenchymal markers in prostate cancer cells. PLoS ONE 2013; **8:** e63466.

22. Sun F, Chen H, Li W et al: Androgen receptor splice variant AR3 promotes prostate cancer via modulating expression of autocrine/paracrine factors. J Biol Chem 2014; **289:** 1529.

23. Kong D, Sethi S, Li Y et al: Androgen receptor splice variants contribute to prostate cancer aggressiveness through induction of EMT and expression of stem cell marker genes. Prostate 2015; **75:** 161.

24. Galletti G, Portella L, Tagawa ST et al: Circulating tumor cells in prostate cancer diagnosis and monitoring: an appraisal of clinical potential. Mol Diagn Ther 2014; **18:** 389.

25. Ngo N, Patel K, Isaacson PG et al: Leucocyte common antigen (CD45) and CD5 positivity in an "undifferentiated" carcinoma: a potential diagnostic pitfall. J Clin Pathol 2007; **60:** 936.

26. Danbara M, Yoshida M, Kanoh Y et al: Flow cytometric detection of small cell lung cancer cells with aberrant CD45 expression in micrometastatic bone marrow. Jpn J Clin Oncol 2009; **39:** 771.

27. Krebs MG, Metcalf RL, Carter L et al: Molecular analysis of circulating tumour cells—biology and biomarkers. Nat Rev Clin Oncol 2014; **11:** 129.

28. Xu D, Zhan Y, Qi Y et al: Androgen receptor splice variants dimerize to transactivate target genes. Cancer Res 2015; **75:** 3663.

29. Cao B, Qi Y, Zhang G et al: Androgen receptor splice variants activating the full-length receptor in mediating resistance to androgen-directed therapy. Oncotarget 2014; **5:** 1646.

Membrane-associated androgen receptor (AR) potentiates its transcriptional activities by activating heat shock protein 27 (HSP27)

Received for publication, March 22, 2018, and in revised form, May 14, 2018 Published, Papers in Press, June 22, 2018, DOI 10.1074/jbc.RA118.003075

Jianzhuo Li[‡¶§§], Xueqi Fu[‡], Subing Cao[‖§§], Jing Li[§], Shu Xing[‡], Dongying Li[¶§§1], Yan Dong[‖§§], Derrick Cardin[¶§§], Hee-Won Park[**], Franck Mauvais-Jarvis[‡‡¶¶], and Haitao Zhang[¶§§2]

From the [‡]School of Life Sciences and [§]School of Medicine, Jilin University, Changchun, China 130012, the Departments of [¶]Pathology and Laboratory Medicine, [‖]Structural and Cellular Biology, [**]Biochemistry and Molecular Biology, and [‡‡]Medicine and [§§]Tulane Cancer Center, Tulane University School of Medicine, New Orleans, Louisiana 70112, and the [¶¶]Southeast Louisiana Veterans Health Care System, New Orleans, Louisiana 70119

Edited by Phyllis I. Hanson

The androgen receptor (AR) is a ligand-activated nuclear receptor that plays a critical role in normal prostate physiology, as well as in the development and progression of prostate cancer. In addition to the classical paradigm in which AR exerts its biological effects in the nucleus by orchestrating the expression of the androgen-regulated transcriptome, there is considerable evidence supporting a rapid, nongenomic activity mediated by membrane-associated AR. Although the genomic action of AR has been studied in depth, the molecular events governing AR transport to the plasma membrane and the downstream AR signaling cascades remain poorly understood. In this study, we report that AR membrane transport is microtubule-dependent. Disruption of the function of kinesin 5B (KIF5B), but not of kinesin C3 (KIFC3), interfered with AR membrane association and signaling. Co-immunoprecipitation and pulldown assays revealed that AR physically interacts with KIF5B and that androgen enhances this interaction. Furthermore, we show that heat shock protein 27 (HSP27) is activated by membrane-associated AR and that HSP27 plays an important role in mediating AR-mediated membrane-to-nuclear signal transduction. Together, these results indicate that AR membrane translocation is mediated by the microtubule cytoskeleton and the motor protein KIF5B. By activating HSP27, membrane-associated AR potentiates the transcriptional activity of nuclear AR. We conclude that disruption of AR membrane translocation may represent a potential strategy for targeting AR signaling therapeutically in prostate cancer.

This work was supported by American Cancer Society Grants RSG-14-016-01-CCE, DOD W81XWH-12-1-0275, and W81XWH-14-1-0480; Louisiana Cancer Research Consortium Fund; and the Tulane University Carol Lavin Bernick Faculty Grants (to H. Z.). This work was also supported by National Institutes of Health Grants R01 DK074970 and DK107444 (to F. M.-J.) and Department of Veterans Affairs Merit Review Award BX003725. The authors declare that they have no conflicts of interest with the contents of this article. The content is solely the responsibility of the authors and does not necessarily represent the official views of the National Institutes of Health.

This article contains Figs. S1–S9.

[1] Present address: National Center for Toxicological Research, U.S. Food and Drug Administration, Jefferson, AR 72079

[2] To whom correspondence should be addressed: 1430 Tulane Ave., New Orleans, LA 70112. Tel.: 504-988-7696; E-mail: hzhang@tulane.edu.

The androgen receptor (AR),[3] along with the estrogen receptor (ER), glucocorticoid receptor (GR), progesterone receptor (PR), and the mineralocorticoid receptor (MR), is a member of the Type I nuclear receptor subfamily (1, 2). AR plays an important role in the development and maintenance of the male sexual phenotype (3, 4). Similar to other steroid hormone receptors, AR is located in the cytoplasm in the absence of androgens, forming a complex with chaperones and co-chaperones such as heat shock proteins and immunophilins (5). Upon androgen binding, AR undergoes conformational changes and translocates to the nucleus, where it binds to the androgen response elements (AREs) as a homodimer; activates the expression of AR target genes; and induces cell proliferation, differentiation, and survival (6, 7). This mode of action is the classical AR signaling pathway, also known as the genomic action. In addition to the classical pathway, many observations suggest androgens, as well as some other steroid hormones, can affect cellular processes in a nongenomic fashion (8). Cinar *et al.* found that within minutes of androgen stimulation, AR is localized to the membrane lipid rafts microdomain, interacts with AKT, and activates AKT signaling (9). Pedram *et al.* showed palmitoylation of a conserved motif in the ligand-binding domain is critical for membrane localization of estrogen receptor, progesterone receptor, and AR (10). Additionally, studies have shown AR interacts with caveolin-1 (Cav-1), a major component of the caveolae membrane structure (11, 12). Down-regulation of Cav-1 decreases AR membrane localization (11, 12). Overall, studies on membrane-associated AR are limited and very little is understood regarding the mechanisms underlying AR translocation to the plasma membrane.

In this study, we investigated the mechanism involved in AR plasma membrane trafficking. We found that the AR plasma membrane translocation depends on the microtubules and the KIF5B motor protein. We also identified membrane-associated

[3] The abbreviations used are: AR, androgen receptor; IF, immunofluorescence; TS, Triton X-100–soluble; TI, Triton X-100–insoluble/octylglucoside-soluble; 2-BP, 2-bromopalmitate; co-IP, co-immunoprecipitation; NTD, N-terminal domain; CRPC, castration-resistant prostate cancer; CTB, Cholera Toxin Subunit B; cs-FBS, charcoal-stripped fetal bovine serum; DHT, dihydrotestosterone; PSA, prostate-specific antigen.

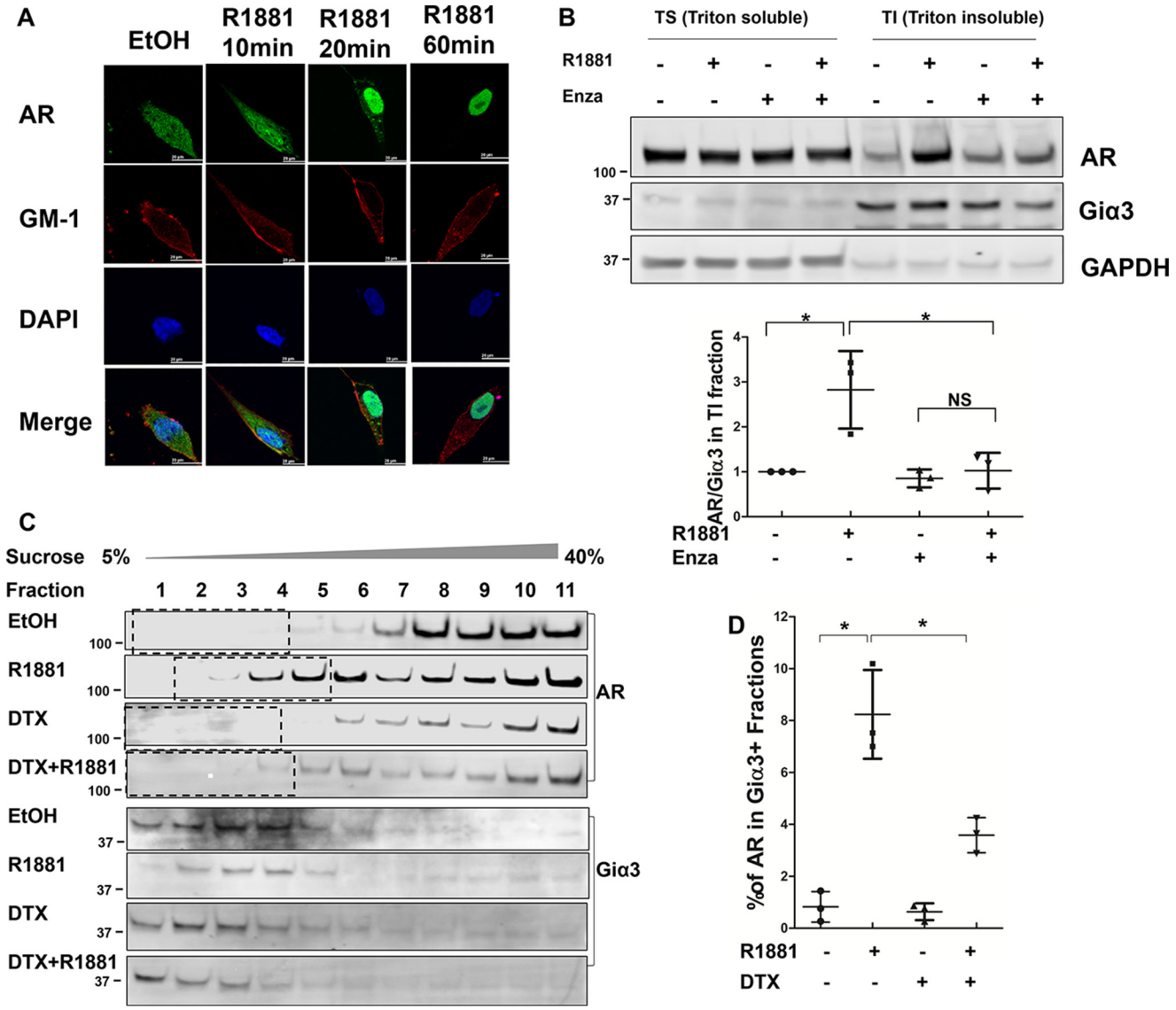

Figure 1. Androgen induces AR membrane translocation. *A*, intracellular localization of AR by immunofluorescence. LNCaP cells were cultured on chamber slides in phenol-red free RPMI 1640 containing 5% charcoal-stripped FBS and treated with 1 nM R1881 for the indicated times. Following fixation, the slides were stained for AR by an anti-AR antibody (*green*), for membrane marker GM-1 by Cholera Toxin Subunit B (*red*), and for nuclei by DAPI (*blue*). Co-localization of AR and GM-1 was visible after R1881 treatment for 10 and 20 min. *Scale bar* is 20 μm. *B*, *top*, Western blot analysis of AR in Triton X-100 soluble (*TS*) and Triton X-100 insoluble/octylglucoside soluble (*TI*) fractions isolated from LNCaP cells. Giα3 was used as the membrane marker and GAPDH as the cytoplasm marker. *Bottom*, AR levels in TI fractions were calculated as the AR/Giα3 ratios and expressed relative to that of the *leftmost* group. *C*, Western blot analysis of AR in LNCaP lysates fractionated by the sucrose gradient ultracentrifugation. Giα 3 was used as the membrane marker. *D*, AR levels in Giα3-positive fractions were quantitated by densitometry and expressed as % of total AR. The mean ± S.D. from three experiments are plotted. *, $p < 0.05$.

AR potentiates the transcriptional activities of AR by enhancing AR nuclear import.

Results

Androgen induces AR plasma membrane translocation

We first employed an immunofluorescence (IF) assay to visualize androgen-induced AR membrane localization in LNCaP cells. As shown in Fig. 1*A*, when the cells were cultured in an androgen-depleted condition, AR was primarily in the cytoplasm. Ten min after the addition of R1881, a synthetic androgen, a fraction of AR could be observed at the periphery of cells, overlapping with the staining for ganglioside GM-1, a membrane lipid raft marker (13). At 20 min, as the majority of cytoplasmic AR had translocated to the nucleus, the membrane pool became more distinguishable. This fraction of AR appeared to peak at around 20 min after androgen stimulation, as the intensity declined after longer incubations. Similar observations were made in COS-7 cells transfected with AR (Fig. S1), suggesting AR membrane translocation is not unique to LNCaP cells.

To confirm the IF results, we performed two membrane fractionation assays based on the low-density and Triton X-100–insoluble properties of membrane domains enriched with cytoplasmically oriented signaling molecules (9). LNCaP cells were lysed 20 min after the addition of R1881 and separated into Triton X-100–soluble (TS) and Triton X-100–insoluble/octylglucoside-soluble (TI) fractions. We first confirmed that there was no contamination from cytoplasmic and nuclear proteins

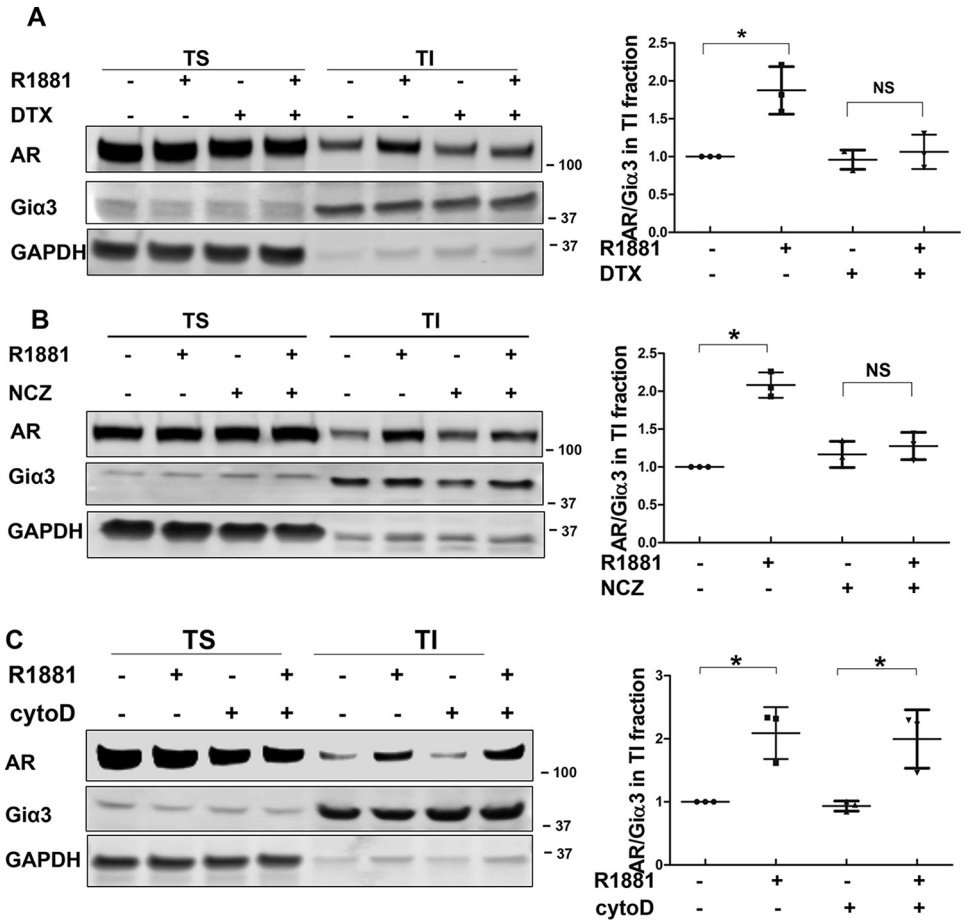

Figure 2. AR membrane translocation is microtubule-dependent. *A–C*, the effects of docetaxel (*DTX*), nocodazole (*NCZ*), and cytochalasin D (*cytoD*) on AR membrane translocation. LNCaP cells were pretreated with 10 nM docetaxel, 50 ng/ml nocodazole , or 0.5 μg/ml cytochalasin D for 16 h, then stimulated with 1 nM R1881 for 20 min. TS/TI fractions were extracted and analyzed by Western blotting. *Left*, representative blots are shown. *Right*, AR levels in TI fractions were calculated as the AR/Giα3 ratios and expressed relative to that of the *leftmost* group. The mean ± S.D. from three experiments are plotted. *, $p < 0.05$.

in the TI fraction, which contains the membrane fraction (Fig. S2). As shown in Fig. 1*B*, AR level was low in the TI fraction under the androgen-depleted condition, but it was markedly induced by the addition of R1881. The induction was blocked by enzalutamide, a potent antiandrogen. Consistent with a previous report showing palmitoylation is critical for AR membrane translocation (10), treatment with 2-bromopalmitate (2-BP), a palmitoylation inhibitor, blocked the androgen-induced increase of AR in the TI fraction (Fig. S3).

Next, LNCaP lysates were fractionated by the sucrose gradient ultracentrifugation method and analyzed by Western blotting. As shown in Fig. 1*C*, AR was present at a very low level in Giα3-positive fractions under the androgen-depleted condition, and treatment with androgen significantly increased AR distribution in these fractions (Fig. 1*C*). When compared against AR in all fractions, we estimated the pool of membrane-associated AR accounted for 8–10% of total AR at 20 min after androgen stimulation (Fig. 1*D*).

The above analyses show AR undergoes a transient, ligand-induced membrane translocation, as previously reported by others (9). To determine the physiological relevance of this phenomenon, we performed the TS/TI fractionation assays with LNCaP cells treated with different concentrations of androgens. As shown in Fig. S4, AR membrane localization could be induced by dihydrotestosterone (DHT) as low as 1 nM, and by R1881 as low as 100 pM, suggesting AR membrane translocation occurs at both physiological and castrate levels of androgen (14, 15).

Microtubule cytoskeleton is involved in AR membrane transport

Studies have established that the microtubules play a critical role in facilitating the nuclear import of steroid receptors such as AR (16–18). However, little is known about the mechanism of AR membrane translocation. To test whether microtubules are involved in this process, LNCaP cells were treated with microtubule inhibitors docetaxel (stabilizes microtubules) and nocodazole (depolymerizes microtubules). As shown in Fig. 1*C*, treatment with docetaxel blocked the androgen-induced AR distribution in the membrane fractions. Similarly, both docetaxel and nocodazole abolished androgen induction of AR in the TI fraction (Fig. 2, *A* and *B*), suggesting microtubule dynamics are critical for AR trafficking to the membrane. The involvement of the microtubule cytoskeleton seems to be unique, as inhibition of actin cytoskeleton, which has been shown to be involved in protein transport (19), did not interfere with AR membrane translocation (Fig. 2*C* and Fig. S5).

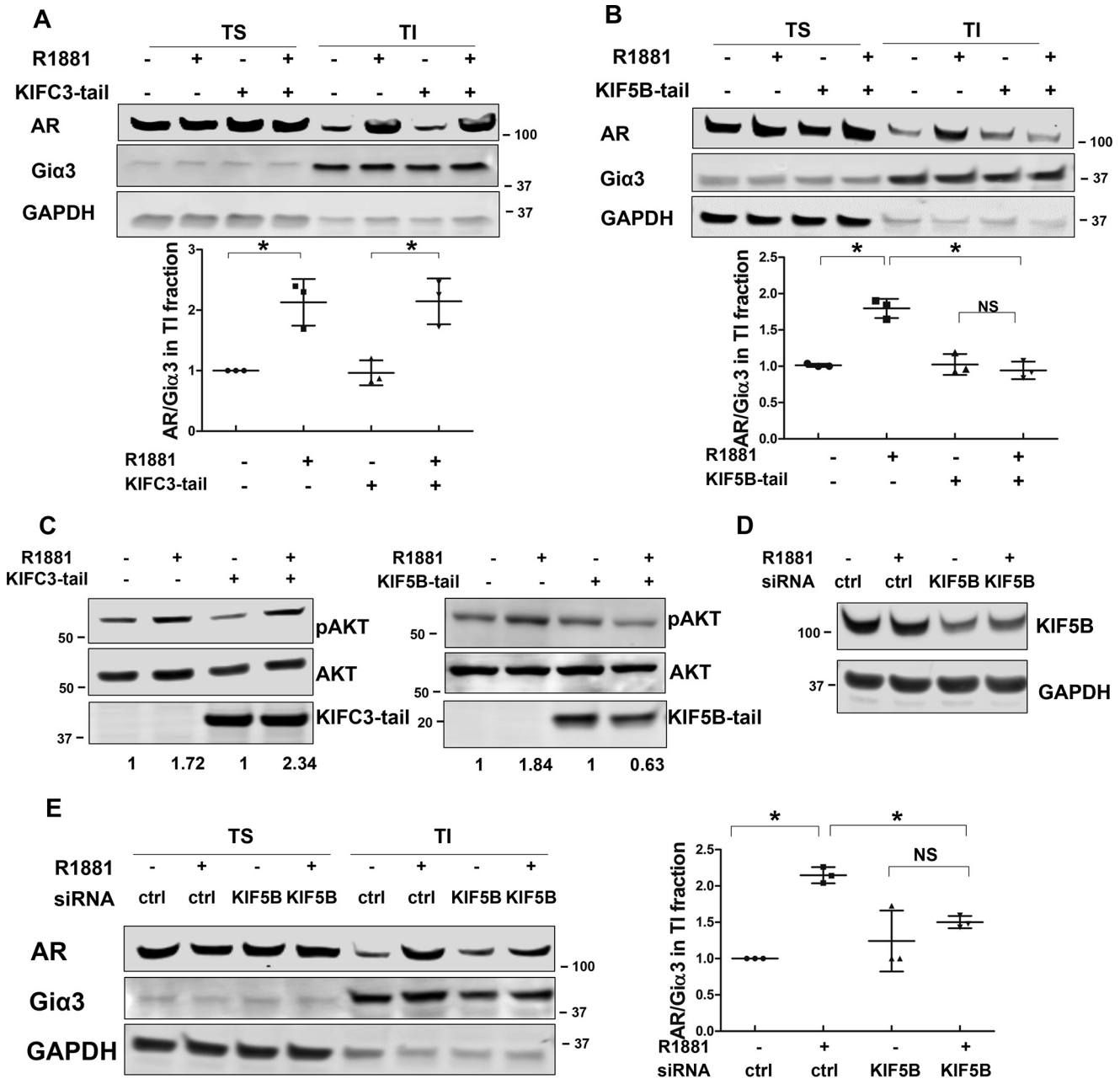

Figure 3. KIF5B mediates AR membrane transport. *A* and *B*, the effects of KIFC3-tail and KIF5B-tail on AR membrane translocation. LNCaP cells were transiently transfected with KIFC3-tail or KIF5B-tail for 48 h, and treated with 1 nM R1881 for 20 min. TS/TI fractions were extracted and analyzed by Western blotting. Membrane AR levels were calculated as AR/Giα3 ratios and expressed relative to that of the *leftmost* group. *C*, KIF5B-tail, but not KIFC3-tail, interferes with rapid activation of AKT. LNCaP cells were transfected with KIF5B-tail or KIFC3-tail, and treated with 1 nM R1881 treatment for 30 min. Whole cell lysates were collected and probed with antibodies against p-AKT and AKT. *D*, KIF5B knockdown. After LNCaP cells were transfected with siRNAs for 48 h, lysates were analyzed by Western blotting to confirm the knockdown of KIF5B. *E*, KIF5B knockdown interrupts AR membrane translocation. LNCaP cells were transfected siRNAs for 48 h and treated with 1 nM R1881 for 20 min. TS/TI fractions were extracted and analyzed for AR distribution. *Left*, representative blots are shown. *Right*, AR levels in TI fractions were calculated as the AR/Giα3 ratios and expressed relative to that of the *leftmost* group. The mean ± S.D. from three experiments are plotted. *, $p < 0.05$.

AR membrane transport is mediated by kinesin 5B

Protein movement along the microtubules is mediated by direction-specific motor proteins, which largely fall into two families, dyneins and kinesins. Whereas dyneins mediate cargo transport to the minus end of the microtubules, kinesins direct movement toward the plus end (20, 21). Among kinesin family proteins, KIF5B and KIFC3 have been shown to transport protein cargos to the plasma membrane (22, 23). To identify the specific motor protein mediating the transport of AR to the plasma membrane, we took advantage of the tail-domain mutants of KIF5B and KIFC3 (KIF5B-tail and KIFC3-tail, respectively). Because of the truncation of the motor domain, these mutants are capable of cargo binding but not transporting, thus acting as dominant-negative mutants (24). When they were co-expressed with AR, the KIFC3-tail had no effect on androgen-induced AR membrane translocation (Fig. 3*A* and Fig. S6*A*). In contrast, AR membrane translocation was abolished in the presence of the KIF5B-tail (Fig. 3*B* and Fig. S6*B*). A

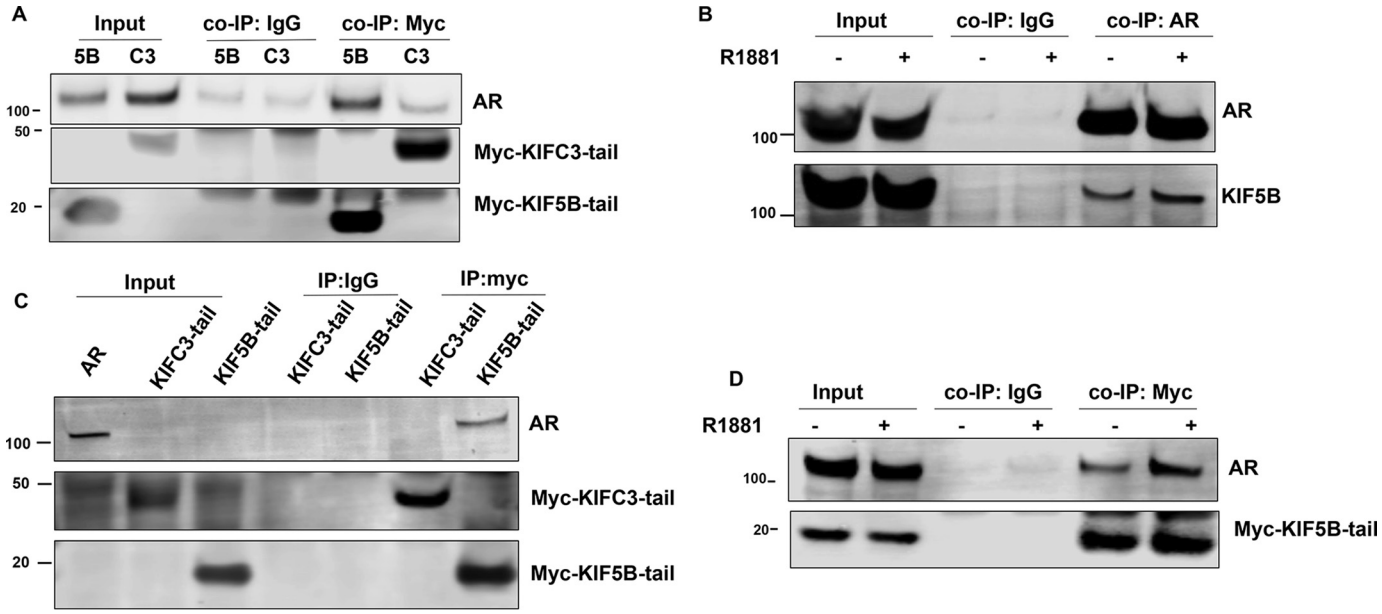

Figure 4. AR interacts with KIF5B. *A*, co-immunoprecipitation (co-IP) of KIF5B-tail or KIFC3-tail with AR. COS-7 cells were co-transfected with Myc-tagged KIF5B-tail or KIFC3-tail with AR. Co-IP assays were performed with an antibody against Myc-tag, followed by immunoblot with antibodies against AR and Myc-tag. *Input*, cell lysates were analyzed for the expression of AR and KIF5B-tail or KIFC3-tail. A control co-IP experiment was performed with a mouse IgG. *B*, the endogenous AR-KIF5B interaction. LNCaP cells were treated with EtOH or R1881 20 min, and a reciprocal co-IP assay was performed with an antibody against AR, followed by Western blot analyses for AR and KIF5B. *C*, *In vitro* pulldown assay for AR. Myc-tagged KIF5B-tail or KIFC3-tail was expressed in COS-7 cells, and enriched by protein G magnetic beads coated with an anti-Myc-tag antibody. The magnetic beads were subsequently incubated with lysates from COS-7 cells transfected with AR, and the eluted proteins were analyzed by immunoblotting. *D*, the KIF5B-tail–AR interaction is enhanced by androgen. COS-7 cells co-transfected with KIF5B-tail and AR were cultured in RPMI 1640 supplemented with 10% cs-FBS, and treated with EtOH or R1881 for 20 min. The lysates were analyzed by the co-IP assay.

previous report has shown membrane-associated AR mediates rapid AKT activation stimulated by androgen (9, 25). Consistent with this study, we found androgen-induced AKT phosphorylation at 30 min was blocked in the presence of the KIF5B-tail, but not the KIFC3-tail (Fig. 3*C*). Additionally, KIF5B knockdown by an siRNA led to a significant reduction of androgen-induced AR membrane localization in LNCaP cells (Fig. 3, *D* and *E*). Collectively, these results show that AR transport to the membrane is mediated by the KIF5B motor protein.

AR interacts with KIF5B through the N-terminal domain

If KIF5B is the motor protein responsible for the anterograde transport of AR, as suggested by the previous section, an interaction would be expected between AR and the KIF5B-tail domain, which is responsible for cargo recognition and binding. This appeared to be the case. In COS-7 cells co-transfected with AR and the KIF5B-tail or the KIFC3-tail plasmids (both are Myc-tagged), AR was co-precipitated with the KIF5B-tail, but not with the KIFC3-tail, by an anti-Myc antibody (Fig. 4*A*), suggesting there is a specific interaction between KIF5B and AR. A reciprocal co-immunoprecipitation (co-IP) assay performed with an antibody against AR in LNCaP cells demonstrated an interaction of endogenous AR and KIF5B (Fig. 4*B*). Additionally, we performed an *in vitro* Myc-pulldown assay. When protein G magnetic beads coated with the KIF5B-tail or KIFC3-tail were incubated with AR-expressing COS-7 lysates, AR was pulled down by the KIF5B-tail, but not by the KIFC3-tail (Fig. 4*C*), further supporting an interaction between AR and KIF5B.

We next investigated the effect of androgen on the AR–KIF5B association. As shown in Fig. 4*D*, a weak AR band co-precipitated with the KIF5B-tail under the androgen-deprived condition; however, a discernible stronger interaction was observed after the addition of androgen, suggesting that the AR–KIF5B interaction is ligand-dependent. A similar observation was made with the endogenous proteins (Fig. 4*B*).

To identify the domain(s) of AR mediating the interaction with KIF5B, a series of AR deletion constructs were generated (Fig. 5*A*) and used in the pulldown assay. As shown in Fig. 5, *B* and *C*, the full-length AR, as well as constructs containing the N-terminal domain (NTD) and the NTD plus the DNA-binding domain (DBD), were pulled down by the KIF5B-tail. In contrast, none of the constructs lacking the NTD were pulled down by the KIF5B-tail. These data suggest AR interacts with KIF5B through the NTD. Interestingly, the AR-NDH (NTD plus DBD and Hinge domain) construct was not pulled down by the KIF5B-tail, suggesting an inhibitory role of the hinge domain in the AR-KIF5B interaction.

Membrane-associated AR cross-talks with nuclear-destined AR

Pedram *et al.* have previously identified a conserved motif in the ligand-binding domain of steroid hormone receptors that is critical for ligand-induced translocation to the plasma membrane (10). For AR, substituting the cysteine residue at position 807 with an alanine abolished AR palmitoylation, leading to reduced membrane localization (10). We believe this membrane-deficient mutant is suitable for understanding the functional relevance of membrane-associated AR. In our lab, we first confirmed that AR–C807A was defective in androgen-induced membrane localization by IF and TS/TI fractionation assays (Fig. S7, *A* and *B*). Subsequently, we performed the ligand-binding assay with AR–C807A, because the mutation is

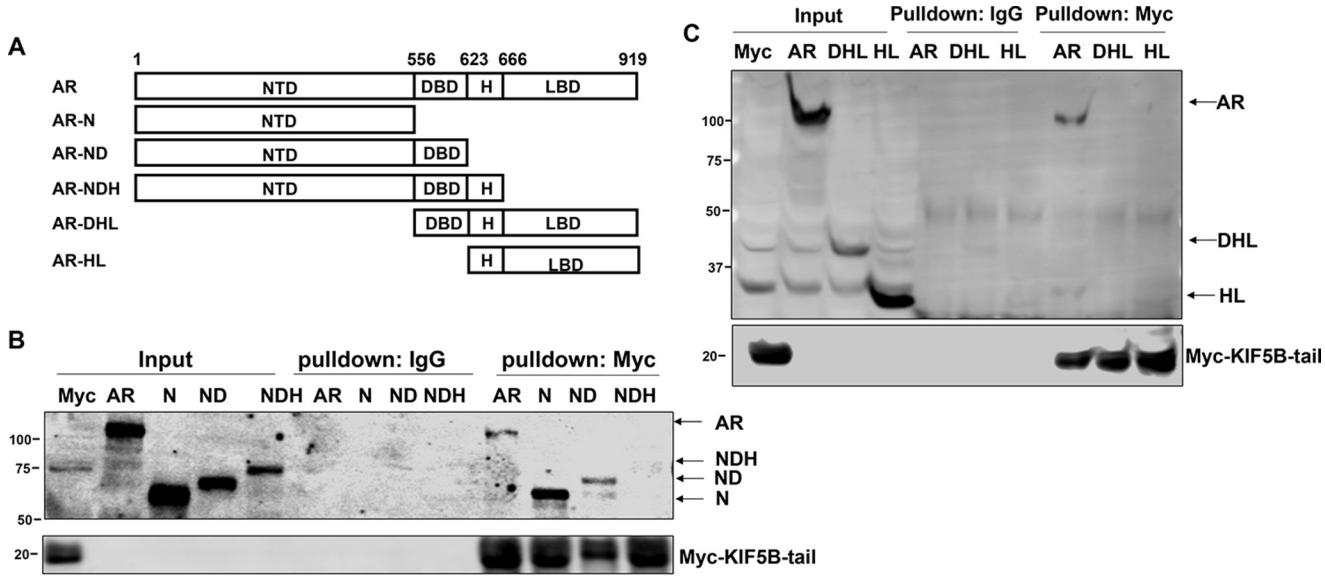

Figure 5. AR binds to KIF5B via the N-terminal domain. *A*, a series of AR deletion constructs were generated by deleting progressively from the C and N termini. *B* and *C*, these constructs were expressed in COS-7 cells and analyzed by the *in vitro* pulldown assay with KIF5B-tail–coated magnet beads. Western blots were probed with the N-20 (*B*) and C-19 (*C*) antibodies, which recognized the N and C termini of AR, respectively. Control pulldowns were performed with a mouse IgG. *H*, Hinge domain; *LBD*, ligand-binding domain; *N*, NTD only; *ND*, NTD and DBD; *NDH*, NTD plus DBD and H; *DHL*, DBD plus H and LBD; *HL*, H and LBD.

in the ligand-binding domain. Analysis of the data revealed similar binding curves and disassociation constants (K_d) for AR–C807A and AR–WT (Fig. S7, *C* and *D*), thus excluding the possibility that the observed deficiency in membrane localization of AR–C807A was because of decreased ligand-binding capacity. Furthermore, the cycloheximide chase assay showed that the protein stability was similar between AR–WT and AR–C807A (Fig. S7*E*).

When the transcriptional activity of AR–C807A was analyzed in COS-7 cells by the luciferase reporter assay, we found that although their activities were similar in the absence of androgen, the R1881-induced activity of AR–C807A was significantly less than that of the WT counterpart (Fig. 6*A*). This was confirmed by the expression of TMPRSS2, an AR-regulated gene, in DU145 cells ectopically expressing AR–WT or AR–C807A (Fig. 7*C*). Consistent with these results, treatment of LNCaP cells with the palmitoylation inhibitor 2-BP, which was shown to inhibit AR membrane localization, inhibited androgen-induced prostate-specific antigen (PSA) mRNA expression (Fig. 7*D*). These results suggest that abolishing AR membrane localization may ultimately impair the activity of AR as a transcriptional activator, supporting a cross-talk between membrane-associated and nuclear-destined AR.

To understand how the nuclear function of AR is weakened by the lack of AR membrane localization, we looked into nuclear translocation by using an IF assay. In the absence of androgen, AR–WT and AR–C807A were both predominantly localized to the cytoplasm (Fig. S8*A*). Following androgen stimulation, AR–WT underwent a robust nuclear translocation, and became predominantly nuclear localized after 1 h. In comparison, the translocation of AR–C807A to the nucleus was much slower (Fig. S8*A* and Fig. 6*B*). Similar observations were made in COS-7 cells by using the subcellular fractionation assay (Fig. 6*C* and Fig. S8, *B* and *C*). These results suggest membrane-associated AR plays a critical role in potentiating the nuclear import of AR.

HSP27 mediates membrane-to-nuclear AR cross-talk

It has been previously reported that androgen induces phosphorylation of heat shock protein 27 (HSP27), which in turn facilitates AR nuclear translocation (26). However, it remains unclear whether HSP27 phosphorylation is mediated by membrane-associated AR. To address this question, we blocked AR membrane transport with the dominant-negative KIF5B-tail and examined HSP27 phosphorylation. As shown in Fig. 7*A*, androgen induced a rapid and robust induction of HSP27 phosphorylation in cells expressing the KIF3C-tail, which did not affect AR membrane localization (Fig. 3*A*). In contrast, androgen treatment failed to induce HSP27 phosphorylation in cells expressing the KIF5B-tail (Fig. 7*A*). Similarly, COS-7 cells expressing AR-C807A showed subdued HSP27 phosphorylation following androgen stimulation as opposed to those expressing AR-WT (Fig. 7*B*). These results suggest androgen-stimulated HSP27 phosphorylation is mediated by membrane-associated AR.

If HSP27 functions as a key mediator of AR signaling from the membrane to nucleus, it would be expected that expression of constitutive active HSP27 will at least in part rescue the defects of membrane-deficient AR. To this end, we performed rescue assays with HSP27-D (phosphorylation mimicking) and HSP27-A (phosphorylation deficient) mutants (27). As mentioned previously, androgen-induced TMRPSS2 expression was muted in AR–C807A–expressing DU145 cells. The co-transfection of HSP27-D, but not HSP27-A, rescued the expression of TMRPSS2 (Fig. 7*C*). Similarly, in LNCaP cells treated with 2-BP, the expression of PSA mRNA was rescued by HSP27-D, but not HSP27-A (Fig. 7*D*). Furthermore, although they grew similarly in an androgen-depleted condition (Fig. S9),

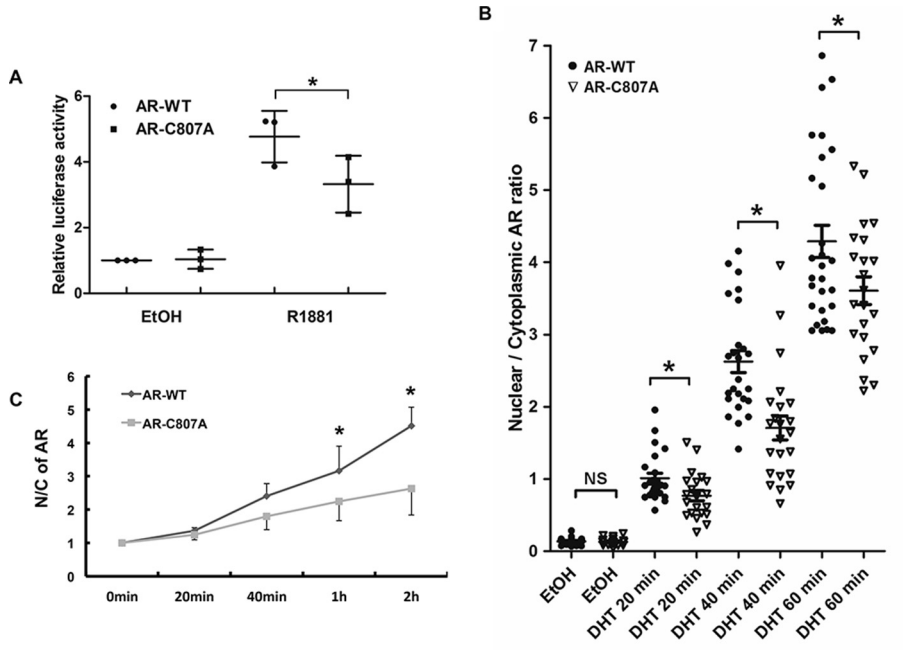

Figure 6. Loss of AR membrane association impairs its nuclear activity. *A*, luciferase reporter assay. COS-7 cells were co-transfected with the ARR3 luciferase reporter, pRL–TK, along with WT AR (*AR–WT*) or the AR–C807A mutant. Dual-Luciferase assays were performed 24 h after the cells were treated with the solvent (EtOH) or 1 nM R1881. The normalized luciferase activities were expressed relative to the *leftmost* group. *B*, IF analyses of COS-7 cells transfected with AR–WT or AR–C807A. Transfected cells were cultured on chamber slides for 48 h, and treated with 10 nM DHT for the indicated times. Following fixation, the slides were stained by an anti-AR, by CTB (for defining cell boundary), and by DAPI (for nuclei). The images were analyzed by the Image J software to quantitate the nuclear and cytoplasmic AR signals. At least 20 cells per group were analyzed. *C*, subcellular fractionation assay of COS-7 cells transfected with AR–WT or AR–C807A. Cells were stimulated by 1 nM R1881 for the indicated times and levels of AR were determined by Western blotting. The nuclear/cytoplasmic AR ratios were calculated relative to the 0 min time point. The mean ± S.D. from three experiments are plotted. *, $p < 0.05$.

AR–WT– expressing DU145 cells proliferated at a higher rate than those expressing AR–C807A in the presence of androgen (Fig. 7*E*), suggesting membrane localization is critical for the proliferative effects of AR. Co-expression of HSP27-D partially restored cell proliferation, whereas the co-transfection of HSP27-A failed to do so (Fig. 7*E*). Collectively, these results provide evidence supporting HSP27 as a key mediator of the AR membrane-to-nuclear signaling.

Discussion

As a member of the nuclear receptor superfamily, AR is best known for its activity in the nucleus as a ligand-dependent transcription factor, orchestrating the expression of androgen-regulated transcriptome which is critical for prostate development, homeostasis, and carcinogenesis (1, 15, 28). In recent years, AR's actions outside the nucleus, also known as the non-genomic function, have been increasingly recognized. A previous study has shown that upon androgen stimulation, AR appears in the membrane fraction within minutes, forms a complex with AKT, and induces the phosphorylation and activation of AKT (9, 25). However, the mechanism of AR transport to the plasma membrane and the downstream events regulated by membrane-associated AR are largely unknown. In this study, we are the first to demonstrate that AR membrane transport is microtubule-dependent, a similarity shared with its nuclear import. However, this anterograde transport of AR is mediated by the motor protein KIF5B, as opposed to dynein, which mediates the retrograde transport (17).

Previously, Lu *et al.* showed that caveolin-1 (Cav-1) knockdown by shRNAs decreased the amount of AR localized to the membrane, suggesting Cav-1 is involved in AR membrane trafficking (11). In our study, AR membrane translocation was observed in both Cav-1–positive COS-7 cells and Cav-1–negative LNCaP cells, indicating Cav-1 is not necessary for this process. Cav-1 may stabilize AR in the plasma membrane in Cav-1– expressing cells.

Our study also presents the first evidence that membrane-associated AR potentiates the classical AR actions by enhancing the nuclear import and activity of AR through the activation of HSP27. HSP27 is an ATP-independent molecular chaperone involved in cytoprotection in stress conditions (29). The activity of HSP27 is regulated by phosphorylation and phospho-HSP27 has been shown to suppress apoptosis, enhance invasion and survival of cancer cells (30). HSP27 is believed to drive prostate cancer cell metastasis through its regulation of MMP-2 (31). Particularly, HSP27 has been shown to be activated by androgen stimulation, and to enhance AR nuclear import and transcriptional activity through its interaction with AR (26). In our study, we found the phosphorylation of HSP27 is mediated by membrane-associated AR. However, the exact kinase(s) responsible for HSP27 phosphorylation remains to be elucidated. A possible candidate is ERK, which has been shown to phosphorylate HSP27 (32). Deng *et al.* showed testosterone induces rapid AR membrane association and phosphorylation of AKT and ERK (25).

As shown in Fig. 1*A*, androgen-induced AR membrane localization is transient. However, by using a novel androgen dendrimer conjugate (ADC) that selectively binds AR in the cytoplasm but prevents AR from being imported to the nucleus (33,

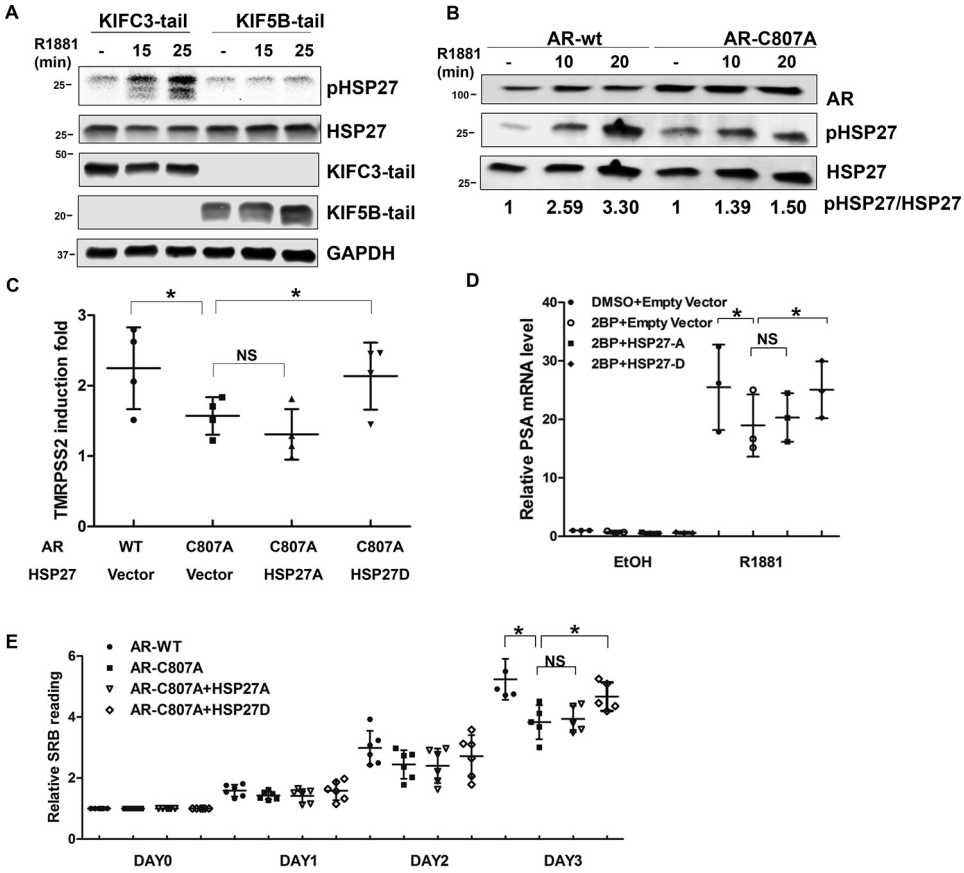

Figure 7. HSP27 mediates cross-talk between membrane-associated and nuclear-destined AR. *A*, KIF5B-tail blocks androgen-induced phosphorylation of HSP27. LNCaP cells transfected with KIF5B-tail or KIFC3-tail were treated with 1 nM R1881 for 15 and 25 min, and analyzed by Western blotting for total and phosphorylated HSP27. *B*, AR–WT, but not AR–C807A, induces HSP27 phosphorylation. COS-7 cells transfected with AR–WT or AR–C807A were treated with 1 nM R1881 for 0, 10, 20 min, and analyzed by Western blotting for total and phosphorylated HSP27. *C*, rescue of TMPRSS2 expression by HSP27D. DU145 cells were transfected with AR–WT/AR–C807A with vector/HSP27A/HSP27D, and treated with EtOH or 1 nM R1881 for 24 h. Following qRT-PCR, normalized TMPRSS2 mRNA levels were expressed relative to the leftmost group. *D*, inhibition of androgen-induced PSA expression by 2-BP is rescued by constitutively active HSP27. LNCaP cells were transfected with HSP27A/HSP27D or empty vector, treated with 10 μM 2-BP or DMSO for 16 h, followed by 1 nM R1881 or EtOH treatment for an additional 24 h. Following qRT-PCR, normalized PSA mRNA levels (by RPL30 housekeeping gene) were expressed relative to the *leftmost* group. *E*, HSP27D rescued cell growth. DU145 cells were transfected with AR/AR–C807A with vector/HSP27A/HSP27D, cultured in RPMI supplemented with 10% cs-FBS and treated with 1 nM R1881 for 1 to 3 days, and the SRB assay was performed. The data were expressed as -folds of the day 0 readings. The mean ± S.D. from at least three experiments are plotted. *, $p < 0.05$.

34), we found AR remained in the membrane fractions for longer periods (data not shown). This result suggests a feedback signal transmitted from nuclear AR to inhibit AR membrane association.

In addition to the canonical full-length AR, at least two AR isoforms have been found on the plasma membrane. AR8, a novel AR splice variant that contains the NTD and a unique 33 amino acid C terminus, is expressed in both clinical samples and prostate cancer cell lines (35). Localized primarily to the plasma membrane, AR8 promotes the association of Src and AR with EGFR in response to EGF stimulation, and is required for the optimal AR transcriptional activity induced by EGF or DHT (35). This is similar to our finding that membrane-associated AR potentiates the transcriptional activity of nuclear-destined AR. Another AR splice variant found on the plasma membrane is AR45, which lacks the NTD (36). A recent study identified AR45 in the plasma membrane lipid rafts of neuronal cells (37). Functionally, AR45 is postulated to play a role in the regulation of intracellular calcium signaling through its interactions with the membrane-associated Gαo and Gαq proteins (37). The molecular mechanisms of membrane transport of AR8 and AR45 have not been studied. However, based on our data that KIF5B interacts with the AR NTD, it is likely AR8 is transported by KIF5B.

Based on the current study and previous work from our lab and others, we propose a working model for role of the microtubule cytoskeleton in the regulation of AR intracellular localization and activity (Fig. 8). In the absence of androgen, AR is associated with the microtubules (16), which retains AR in the cytoplasm. Following androgen stimulation, AR undergoes conformational changes, which reduce AR binding to the microtubules but allow it to interact with KIF5B via the NTD. KIF5B then transports AR to the plasma membrane, where AR initiates a signaling cascade, possibly through interaction with AKT, leading to the phosphorylation and activation of ERK and HSP27, the latter of which further facilitates AR nuclear transport.

It is now widely accepted that the AR signaling pathway remains active in castration-resistant prostate cancer (CRPC). Our study demonstrated that AR membrane transport can be induced by DHT concentrations found in CRPC tissues (38) (Fig. S4). Based on the existing evidence, we propose that mem-

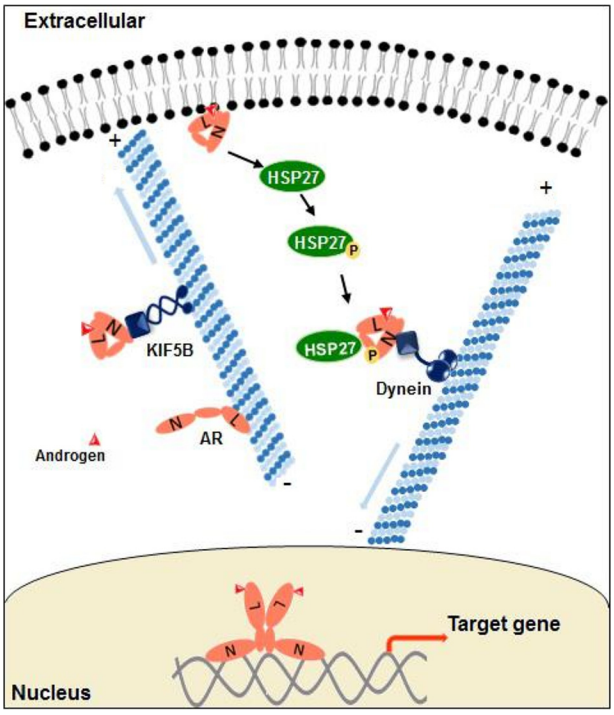

Figure 8. Schematic illustration of the anterograde AR transport and the cross-talk between membrane-associated and nuclear-destined AR.

brane-associated AR plays a critical role in sustaining AR signaling in CRPC through at least two mechanisms. First, membrane AR potentiates the AR transcriptional activity in the presence of low levels of androgen by enhancing the nuclear translocation. Second, AR activates AKT, ERK, and Src pathways at the membrane, thereby promoting cell proliferation, invasion, and survival through these pathways (39). Therefore, targeting AR membrane transport represents a novel strategy to fully suppress AR signaling in CRPC.

Experimental procedures

Cell lines and reagents

LNCaP, DU-145, and COS-7 cells were obtained from American Type Culture Collection. The suppliers for the antibodies used in this study include Santa Cruz Technology (for AR N-20 and GAPDH antibodies), EMD Millipore (AR PG-21, Giα3, and Myc-tag), Cell Signaling Technology (AKT, phospho-AKT (Ser-473), HSP27, and phospho-HSP27 (Ser-82)), GeneTex (anti-LSD1), and Abcam (anti-KIF5B). Docetaxel was obtained from Selleck Chemicals (Houston, TX); nocodazole, protease inhibitor cocktails, and KIF5B siRNA were from Sigma Aldrich; and Alexa Fluor® 594 conjugated Cholera Toxin Subunit B (CTB) was from Thermo Fisher Scientific. For plasmids, pRK–Myc–KIFC3-tail was kindly provided by Dr. Kristen Verhey (University of Michigan), Myc–KIF5B-tail by Dr. Geri E. Kreitzer (Weill Cornell Medical College, Cornell University), and AR–C807A was a gift from Dr. Ellis Levin (University of California at Irvine). The pFLAG-CMV2-Hsp27-S15D/S78D/S82D and pFLAG-CMV2-Hsp27-S15A/S78A/S82A plasmids were obtained from Addgene (85188, 84997, supplied by Ugo Moens's lab).

Immunofluorescence

Cells were cultured on chamber slides at 37 °C and stained with CTB for 30 min at 4 °C. Following CTB staining, cells were washed with phosphate-buffered saline (PBS) once, fixed with 4% paraformaldehyde for 10 min at room temperature, and permeabilized with 0.2% Triton X-100 for 10 min at room temperature. Cells were then blocked with 5% BSA in PBST buffer (PBS with Tween 20) for 1 h, and incubated with anti-AR overnight at 4 °C, followed by staining with the Alexa Fluor® 488–labeled secondary antibody for 1 h at room temperature. The fluorescence signal was detected by using a Nikon A1 confocal microscope.

Membrane fractionation by serial detergent extraction

The membrane fractions were extracted by using the successive detergent method as previously described (40). Briefly, cells were washed with PBS and suspended in buffer A (25 mM morpholinoethanesulfonic acid, 150 mM NaCl, pH 6.5, 1% Triton X-100, 1 mM Na_3VO_4, 1 mM phenylmethylsulfonyl fluoride, and protease inhibitor cocktails) and incubated on ice for 30 min. The Triton-insoluble fractions were collected by centrifugation at 14,000 × *g* for 20 min at 4 °C. The supernatant (Triton soluble) was transferred to a new tube and the pellet (Triton insoluble) was resuspended in buffer B (10 mM Tris, pH 7.6, 1% Triton X-100, 500 mM NaCl, 1 mM Na_3VO_4, 60 mM *n*-octyl-β-D-glucoside, 1 mM phenylmethylsulfonyl fluoride, and protease inhibitor mixture) and incubated on ice for 30 min. The debris (octylglucoside insoluble) was cleared by centrifugation at 14,000 × *g* for 20 min at 4 °C.

Sucrose gradient ultracentrifugation

Low-density membrane fractions enriched with lipid rafts were isolated by using the sucrose gradient ultracentrifuge method as described previously (41). Briefly, cells were washed once with PBS and suspended in lysis buffer (50 mM HEPES, 300 mM KCl, 0.1 mM EDTA, 1 mM PMSF, 0.1% Nonidet P-40, and protease inhibitor cocktails). Lysates were scraped from the dishes and cleared by centrifugation at 3000 × *g* at 4 °C for 10 min. The supernatant was mixed with an equal volume of 80% sucrose (in HEPES buffer), placed at the bottom of an ultracentrifuge tube, and layered with 4 ml each of 35 and 5% sucrose. Samples were centrifuged at 120,000 × *g* at 4 °C for 18 h in a swing bucket rotor (Beckman SW41 Ti). After ultracentrifugation, the layers were carefully collected and analyzed by Western blotting.

Western blotting

Cells were washed with ice-cold PBS and lysed with 1× Cell Lysis Buffer (Cell Signaling Technology) containing a phosphatase inhibitor and the protease inhibitor mixture (Sigma). After incubating the cells on ice for 30 min, lysates were collected by centrifugation at 12,000 × *g* for 10 min. Protein concentrations were determined by the BCA Protein Assay kit (Pierce). The samples were separated on 10% SDS-polyacrylamide gels and transferred onto polyvinylidene fluoride (PVDF) membranes. After blocking in TBST buffer (150 mM NaCl, 10 mM Tris, pH 7.4, 0.1% Tween 20) containing 5% nonfat milk, the blots were

incubated with a primary antibody overnight at 4 °C and a fluorescent-labeled secondary antibody for 1 h at room temperature. The fluorescent signals were obtained by the Odyssey IR Imaging System (LI-COR Biosciences).

Cell culture, transient transfection, and luciferase reporter assay

LNCaP and DU-145 cells were cultured in RPMI 1640 and COS-7 cells in Dulbecco's modified Eagle's medium (high glucose), supplemented with antibiotics (penicillin and streptomycin) and 10% fetal bovine serum. Transient transfection was performed by using TurboFect (Thermo Scientific) or Lipofectamine 3000 (Invitrogen) for plasmids, and X-tremeGENE (Roche) for siRNAs, following the manufacturers' instructions.

For reporter gene assay, cells were co-transfected with the ARR3-luc luciferase reporter construct and pRL-TK, along with a plasmid encoding for AR–WT or AR–C807A. After incubating with the transfection mixture for 4 h, cells were replated in culture medium containing 10% charcoal-stripped fetal bovine serum (cs-FBS) and treated with 0 or 1 nM R1881. Dual-Luciferase assay was performed at 24 h post treatment using the Dual-Luciferase Reporter Assay System (Promega). The Firefly luciferase activity was normalized by the Renilla luciferase.

Co-immunoprecipitation

Cells were prepared in lysis buffer (50 mM Tris-HCl, pH 8.0, 120 mM NaCl, 0.5% Nonidet P-40, and protease inhibitor cocktails), precleared with anti-mouse IgG antibody for 1 h at 4 °C, and immunoprecipitated with an anti–Myc-tag antibody at 4 °C overnight. The antibody and associated complex were collected by protein G beads (Thermo Fisher), washed three times with the lysis buffer, and analyzed by Western blotting.

In vitro pulldown assay

Myc-tagged KIF5B-tail was expressed in COS-7 cells, and enriched by protein G magnetic beads coated with an anti-Myc-tag antibody. The enriched kinesin was further incubated with lysates from COS-7 cells transfected with AR or AR deletion constructs, and the proteins pulled down by kinesin were analyzed by Western blotting.

Ligand-binding assay

COS-7 cells transfected with AR–WT and AR–C807A were cultured in a 6-well plate for 48 h. Cells were washed twice in serum-free medium and incubated with 0.25, 0.5, 1, 2.5, 5, and 7.5 nM [^{3}H]R1881 (methyltrienolone, Perkin-Elmer) in the presence or absence of 200-fold cold R1881 at 37 °C in a CO_2 incubator for 1 h. At the end of incubation, cells were washed three times with ice-cold PBS and the wash solution was completely removed after each wash. Seven hundred μl absolute ethanol was added to each well and the cells were incubated at room temperature with gentle rocking for 30 min. The ethanoic extracts were transferred to scintillation vials with 4 ml scintillation fluid for radioactivity counting.

Nuclear and cytoplasmic fractionation

Nuclear and cytoplasmic factions were extracted by NE-PER™ Nuclear and Cytoplasmic Extraction kit (Thermo Fischer Scientific) according to the manufacturer's instructions. GAPDH was used as the cytoplasmic marker, and LSD1 as the nuclear marker.

Statistical analysis

Statistical analysis was performed using GraphPad Prism and Microsoft Excel. The Student's two-tailed t test was used to determine the difference in means between two groups. $p < 0.05$ is considered significant. Data are presented as mean ± S.D. from at least three independent experiments.

Author contributions—Jianzhuo Li, X. F., H.-W. P., F. M.-J., and H. Z. conceptualization; Jianzhuo Li and S. C. data curation; Jianzhuo Li, Jing Li, S. X., D. L., and Y. D. formal analysis; Jianzhuo Li validation; Jianzhuo Li, S. C., and Y. D. methodology; Jianzhuo Li writing-original draft; Jianzhuo Li, D. L. C., and H. Z. writing-review and editing; H. Z. supervision; H. Z. funding acquisition.

Acknowledgments—We are indebted to Dr. Kristen Verhey for providing the pRK–Myc–KIFC3-tail plasmid, to Dr. Dr. Geri E. Kreitzer for the Myc–KIF5B-tail plasmid, and to Dr. Ellis Levin for the AR–C807A expression vectors. We thank Sudurika Mukhopadhyay for help with manuscript preparation.

References

1. Tan, M. H. E., Li, J., Xu, H. E., Melcher, K., and Yong, E.-L. (2015) Androgen receptor: Structure, role in prostate cancer and drug discovery. *Acta Pharmacol. Sin.* **36,** 3–23 CrossRef Medline
2. Mangelsdorf, D. J., Thummel, C., Beato, M., Herrlich, P., Schütz, G., Umesono, K., Blumberg, B., Kastner, P., Mark, M., Chambon, P., and Evans, R. M. (1995) The nuclear receptor superfamily: The second decade. *Cell* **83,** 835–839 CrossRef Medline
3. Yeh, S., Tsai, M.-Y., Xu, Q., Mu, X.-M., Lardy, H., Huang, K.-E., Lin, H., Yeh, S.-D., Altuwaijri, S., Zhou, X., Xing, L., Boyce, B. F., Hung, M.-C., Zhang, S., Gan, L., and Chang, C. (2002) Generation and characterization of androgen receptor knockout (ARKO) mice: An *in vivo* model for the study of androgen functions in selective tissues. *Proc. Natl. Acad. Sci. U.S.A.* **99,** 13498–13503 CrossRef Medline
4. Notini, A. J., Davey, R. A., McManus, J. F., Bate, K. L., and Zajac, J. D. (2005) Genomic actions of the androgen receptor are required for normal male sexual differentiation in a mouse model. *J. Mol. Endocrinol.* **35,** 547–555 CrossRef Medline
5. Pratt, W. B., and Toft, D. O. (1997) Steroid receptor interactions with heat shock protein and immunophilin chaperones. *Endocr. Rev.* **18,** 306–360 CrossRef Medline
6. Beato, M. (1989) Gene regulation by steroid hormones. *Cell* **56,** 335–344 CrossRef Medline
7. Foradori, C. D., Weiser, M. J., and Handa, R. J. (2008) Non-genomic actions of androgens. *Front. Neuroendocrinol.* **29,** 169–181 CrossRef Medline
8. Simoncini, T., and Genazzani, A. R. (2003) Non-genomic actions of sex steroid hormones. *Eur. J. Endocrinol.* **148,** 281–292 CrossRef Medline
9. Cinar, B., Mukhopadhyay, N. K., Meng, G., and Freeman, M. R. (2007) Phosphoinositide 3-kinase-independent non-genomic signals transit from the androgen receptor to Akt1 in membrane raft microdomains. *J. Biol. Chem.* **282,** 29584–29593 CrossRef Medline
10. Pedram, A., Razandi, M., Sainson, R. C. A., Kim, J. K., Hughes, C. C., and Levin, E. R. (2007) A conserved mechanism for steroid receptor translocation to the plasma membrane. *J. Biol. Chem.* **282,** 22278–22288 CrossRef Medline
11. Lu, M. L., Schneider, M. C., Zheng, Y., Zhang, X., and Richie, J. P. (2001) Caveolin-1 interacts with androgen receptor. A positive modulator of androgen receptor mediated transactivation. *J. Biol. Chem.* **276,** 13442–13451 CrossRef Medline

12. Deng, Q., Wu, Y., Zhang, Z., Wang, Y., Li, M., Liang, H., and Gui, Y. (2017) Androgen receptor localizes to plasma membrane by binding to caveolin-1 in mouse Sertoli cells. *Int. J. Endocrinol.* **2017,** 3985916 CrossRef Medline
13. Moreno-Altamirano, M. M. B., Aguilar-Carmona, I., and Sánchez-García, F. J. (2007) Expression of GM1, a marker of lipid rafts, defines two subsets of human monocytes with differential endocytic capacity and lipopolysaccharide responsiveness. *Immunology* **120,** 536–543 CrossRef Medline
14. Nishiyama, T. (2014) Serum testosterone levels after medical or surgical androgen deprivation: A comprehensive review of the literature. *Urol. Oncol.* **32,** 38.e17–38.e28 CrossRef Medline
15. Heinlein, C. A., and Chang, C. (2004) Androgen receptor in prostate cancer. *Endocr. Rev.* **25,** 276–308 CrossRef Medline
16. Zhang, G., Liu, X., Li, J., Ledet, E., Alvarez, X., Qi, Y., Fu, X., Sartor, O., Dong, Y., and Zhang, H. (2015) Androgen receptor splice variants circumvent AR blockade by microtubule-targeting agents. *Oncotarget* **6,** 23358–23371 CrossRef Medline
17. Thadani-Mulero, M., Nanus, D. M., and Giannakakou, P. (2012) Androgen receptor on the move: Boarding the microtubule expressway to the nucleus. *Cancer Res.* **72,** 4611–4615 CrossRef Medline
18. Harrell, J. M., Murphy, P. J. M., Morishima, Y., Chen, H., Mansfield, J. F., Galigniana, M. D., and Pratt, W. B. (2004) Evidence for glucocorticoid receptor transport on microtubules by dynein. *J. Biol. Chem.* **279,** 54647–54654 CrossRef Medline
19. Pollard, T. D., and Cooper, J. A. (2009) Actin, a central player in cell shape and movement. *Science* **326,** 1208–1212 CrossRef Medline
20. Gennerich, A., and Vale, R. D. (2009) Walking the walk: How kinesin and dynein coordinate their steps. *Curr. Opin. Cell Biol.* **21,** 59–67 CrossRef Medline
21. Soldati, T., and Schliwa, M. (2006) Powering membrane traffic in endocytosis and recycling. *Nat. Rev. Mol. Cell Biol.* **7,** 897–908 CrossRef Medline
22. Noda, Y., Okada, Y., Saito, N., Setou, M., Xu, Y., Zhang, Z., and Hirokawa, N. (2001) KIFC3, a microtubule minus end–directed motor for the apical transport of annexin XIIIb–associated Triton-insoluble membranes. *J. Cell Biol.* **155,** 77–88 CrossRef Medline
23. Schmidt, M. R., Maritzen, T., Kukhtina, V., Higman, V. A., Doglio, L., Barak, N. N., Strauss, H., Oschkinat, H., Dotti, C. G., and Haucke, V. (2009) Regulation of endosomal membrane traffic by a Gadkin/AP-1/kinesin KIF5 complex. *Proc. Natl. Acad. Sci.* **106,** 15344–15349 CrossRef Medline
24. Gelfand, V. I., Le Bot, N., Tuma, M. C., and Vernos, I. (2001) A dominant negative approach for functional studies of the kinesin II complex. in *Kinesin Protocols* (Vernos, I., ed) pp. 191–204, part of the *Methods in Molecular Biology* series, Humana Press, New York CrossRef
25. Deng, Q., Zhang, Z., Wu, Y., Yu, W.-Y., Zhang, J., Jiang, Z.-M., Zhang, Y., Liang, H., and Gui, Y.-T. (2017) Non-genomic action of androgens is mediated by rapid phosphorylation and regulation of androgen receptor trafficking. *Cell. Physiol. Biochem.* **43,** 223–236 CrossRef Medline
26. Zoubeidi, A., Zardan, A., Beraldi, E., Fazli, L., Sowery, R., Rennie, P., Nelson, C., and Gleave, M. (2007) Cooperative interactions between androgen receptor (AR) and heat-shock protein 27 facilitate AR transcriptional activity. *Cancer Res.* **67,** 10455–10465 CrossRef Medline
27. Jovcevski, B., Kelly, M. A., Rote, A. P., Berg, T., Gastall, H. Y., Benesch, J. L. P., Aquilina, J. A., and Ecroyd, H. (2015) Phosphomimics destabilize Hsp27 oligomeric assemblies and enhance chaperone activity. *Chem. Biol.* **22,** 186–195 CrossRef Medline
28. Pomerantz, M. M., Li, F., Takeda, D. Y., Lenci, R., Chonkar, A., Chabot, M., Cejas, P., Vazquez, F., Cook, J., Shivdasani, R. A., Bowden, M., Lis, R., Hahn, W. C., Kantoff, P. W., Brown, M., Loda, M., Long, H. W., and Freedman, M. L. (2015) The androgen receptor cistrome is extensively reprogrammed in human prostate tumorigenesis. *Nat. Genet.* **47,** 1346–1351 CrossRef Medline
29. Konda, J. D., Olivero, M., Musiani, D., Lamba, S., and Di Renzo, M. F. (2017) Heat-shock protein 27 (HSP27, HSPB1) is synthetic lethal to cells with oncogenic activation of MET, EGFR and BRAF. *Mol. Oncol.* **11,** 599–611 CrossRef Medline
30. Katsogiannou, M., Andrieu, C., and Rocchi, P. (2014) Heat shock protein 27 phosphorylation state is associated with cancer progression. *Front. Genet.* **5,** 346 CrossRef Medline
31. Voll, E. A., Ogden, I. M., Pavese, J. M., Huang, X., Xu, L., Jovanovic, B. D., and Bergan, R. C. (2014) Heat shock protein 27 regulates human prostate cancer cell motility and metastatic progression. *Oncotarget* **5,** 2648–2663 CrossRef Medline
32. Robitaille, H., Simard-Bisson, C., Larouche, D., Tanguay, R. M., Blouin, R., and Germain, L. (2010) The small heat-shock protein Hsp27 undergoes ERK-dependent phosphorylation and redistribution to the cytoskeleton in response to dual leucine Zipper-bearing kinase expression. *J. Invest. Dermatol.* **130,** 74–85 CrossRef Medline
33. Harrington, W. R., Kim, S. H., Funk, C. C., Madak-Erdogan, Z., Schiff, R., Katzenellenbogen, J. A., and Katzenellenbogen, B. S. (2006) Estrogen dendrimer conjugates that preferentially activate extranuclear, nongenomic versus genomic pathways of estrogen action. *Mol. Endocrinol.* **20,** 491–502 CrossRef Medline
34. Navarro, G., Xu, W., Jacobson, D. A., Wicksteed, B., Allard, C., Zhang, G., De Gendt, K., Kim, S. H., Wu, H., Zhang, H., Verhoeven, G., Katzenellenbogen, J. A., and Mauvais-Jarvis, F. (2016) Extranuclear Actions of the androgen receptor enhance glucose-stimulated insulin secretion in the male. *Cell Metab.* **23,** 837–851 CrossRef Medline
35. Yang, X., Guo, Z., Sun, F., Li, W., Alfano, A., Shimelis, H., Chen, M., Brodie, A. M. H., Chen, H., Xiao, Z., Veenstra, T. D., and Qiu, Y. (2011) Novel membrane-associated androgen receptor splice variant potentiates proliferative and survival responses in prostate cancer cells. *J. Biol. Chem.* **286,** 36152–36160 CrossRef Medline
36. Ahrens-Fath, I., Politz, O., Geserick, C., and Haendler, B. (2005) Androgen receptor function is modulated by the tissue-specific AR45 variant. *FEBS J.* **272,** 74–84 CrossRef Medline
37. Garza-Contreras, J., Duong, P., Snyder, B. D., Schreihofer, D. A., and Cunningham, R. L. (2017) Presence of androgen receptor variant in neuronal lipid rafts. *eNeuro* **4,** ENEURO.0109–17.2017 CrossRef Medline
38. Mohler, J. L., Gregory, C. W., Ford, O. H., 3rd, Kim, D., Weaver, C. M., Petrusz, P., Wilson, E. M., and French, F. S. (2004) The androgen axis in recurrent prostate cancer. *Clin. Cancer Res.* **10,** 440–448
39. Zarif, J. C., Lamb, L. E., Schulz, V. S., Nollet, E. A., and Miranti, C. K. (2015) Androgen receptor non-nuclear regulation of prostate cancer cell invasion mediated by Src and matriptase. *Oncotarget* **6,** 6862–6876 CrossRef Medline
40. Zhuang, L., Lin, J., Lu, M. L., Solomon, K. R., and Freeman, M. R. (2002) Cholesterol-rich lipid rafts mediate Akt-regulated survival in prostate cancer cells. *Cancer Res.* **62,** 2227–2231 CrossRef Medline
41. Song, K. S., Li, S., Okamoto, T., Quilliam, L. A., Sargiacomo, M., and Lisanti, M. P. (1996) Co-purification and direct interaction of Ras with caveolin, an integral membrane protein of caveolae microdomains: Detergent-free purification of caveolae membranes. *J. Biol. Chem.* **271,** 9690–9697 CrossRef Medline

Membrane-associated androgen receptor (AR) potentiates its transcriptional activities by activating heat shock protein 27 (HSP27)

Jianzhuo Li, Xueqi Fu, Subing Cao, Jing Li, Shu Xing, Dongying Li, Yan Dong, Derrick Cardin, Hee-Won Park, Franck Mauvais-Jarvis and Haitao Zhang

J. Biol. Chem. 2018, 293:12719-12729.
doi: 10.1074/jbc.RA118.003075 originally published online June 22, 2018

Figure S1

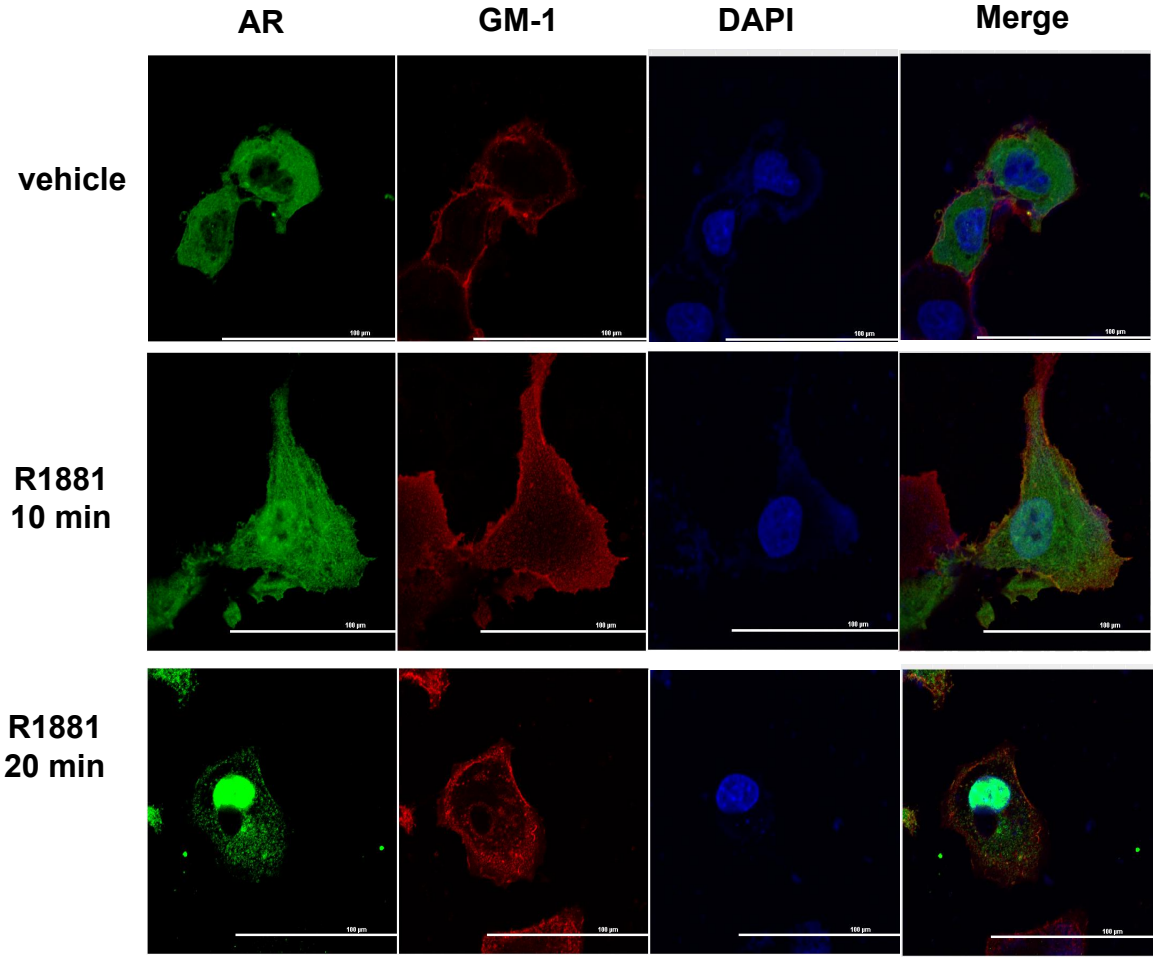

Figure S1. Intracellular localization of AR by immunofluorescence. COS-7 cells transfected with AR were cultured on chamber slides in phenol-red free DMEM containing 5% charcoal-stripped FBS and treated with 1 nM R1881 for the indicated times. Following fixation, the slides were stained for AR by an anti-AR (green), for membrane marker GM-1 by Cholera Toxin Subunit B (red), and for nuclei by DAPI (blue). Scale bar is 100 μm.

Figure S2

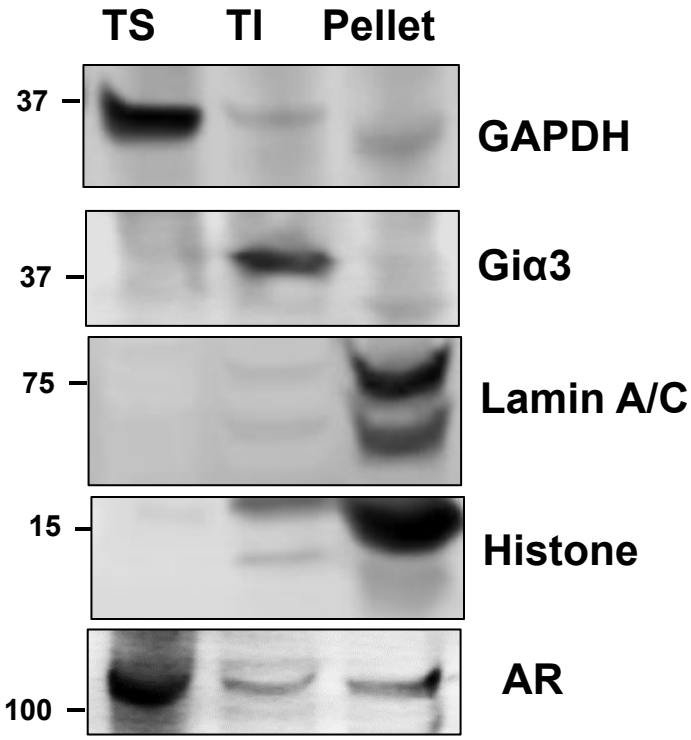

Figure S2. Assessment of the membrane fractionation assay. LNCaP cells cultured in an androgen-depleted condition were separated into Triton X-100-soluble (TS), Triton X-100-insoluble/octylglucoside-soluble (TI) and pellet (insoluable in both Triton X-100 and octylglucoside) fractions. Western blotting was performed to detect the distribution of GAPDH (cytoplasm marker), Giα3 (membrane marker), histone, and lamin A/C (nuclear markers). AR was detected in all three fractions.

Figure S3

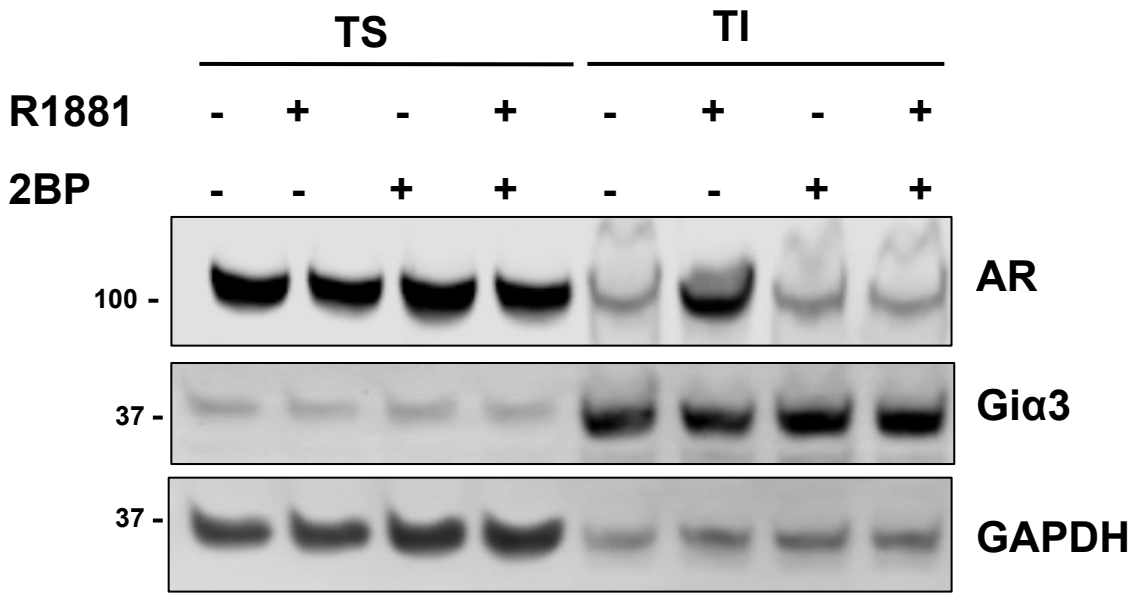

Figure S3. Androgen-induced AR membrane translocation is blocked by a palmitoylation inhibitor. LNCaP cells were pretreated with 10 μM 2-BP for 16 h, then stimulated with 1 nM R1881 for 20 min. TS/ TI fractions were extracted and analyzed by Western blots.

Figure S4

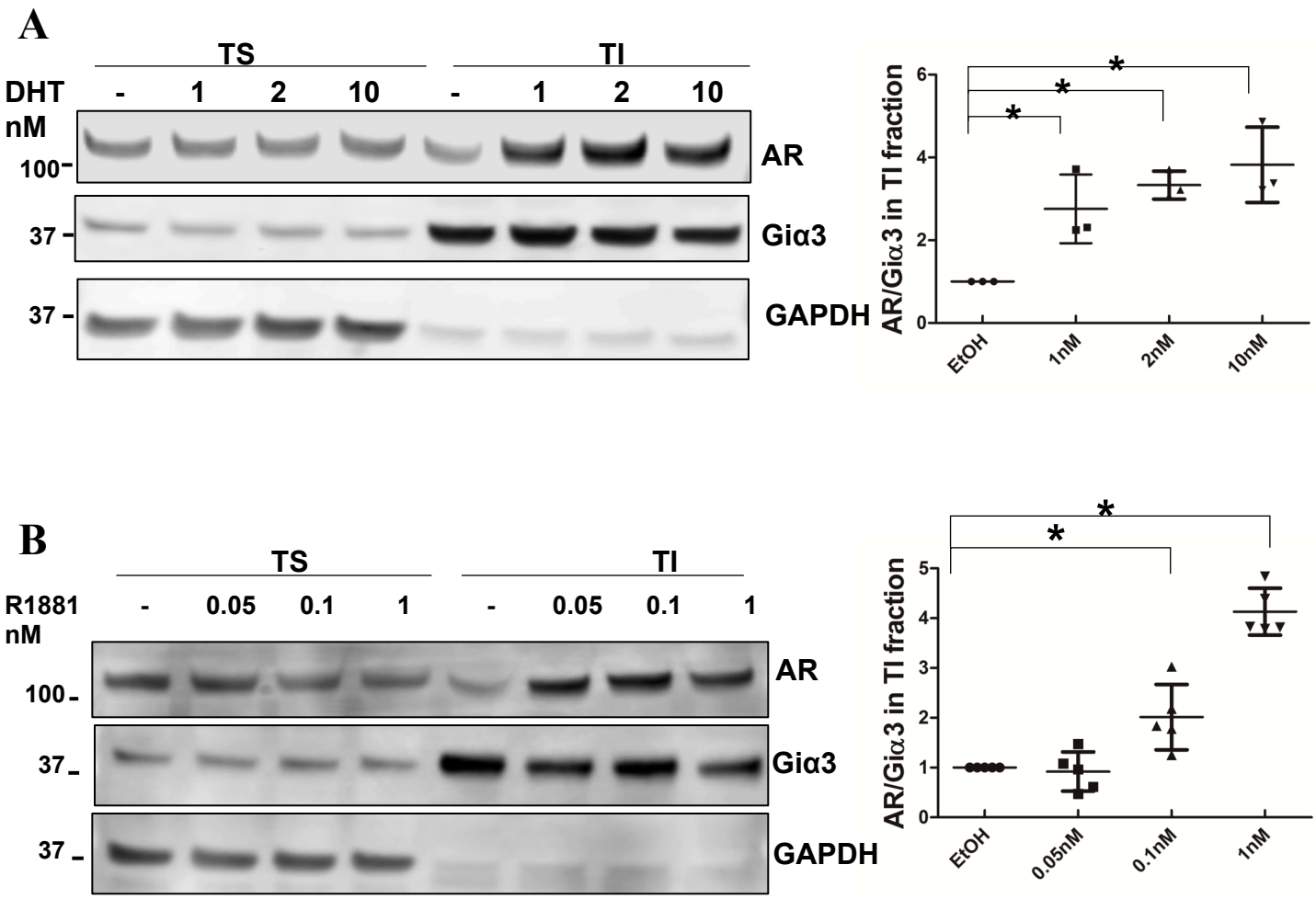

Figure S4. AR membrane transport induced by different concentrations of androgens. LNCaP cells were treated with DHT (1, 2, 10 nM, in panel A) or R1881 (50, 100 pM, 1 nM, in panel B) for 20 min. TS/TI fractions were extracted and analyzed by Western blots. Membrane AR levels were calculated as AR/Giα3 ratios and expressed relative to that of the leftmost group. The mean ± SEM from three experiments are plotted. **, P<0.05.*

Figure S5

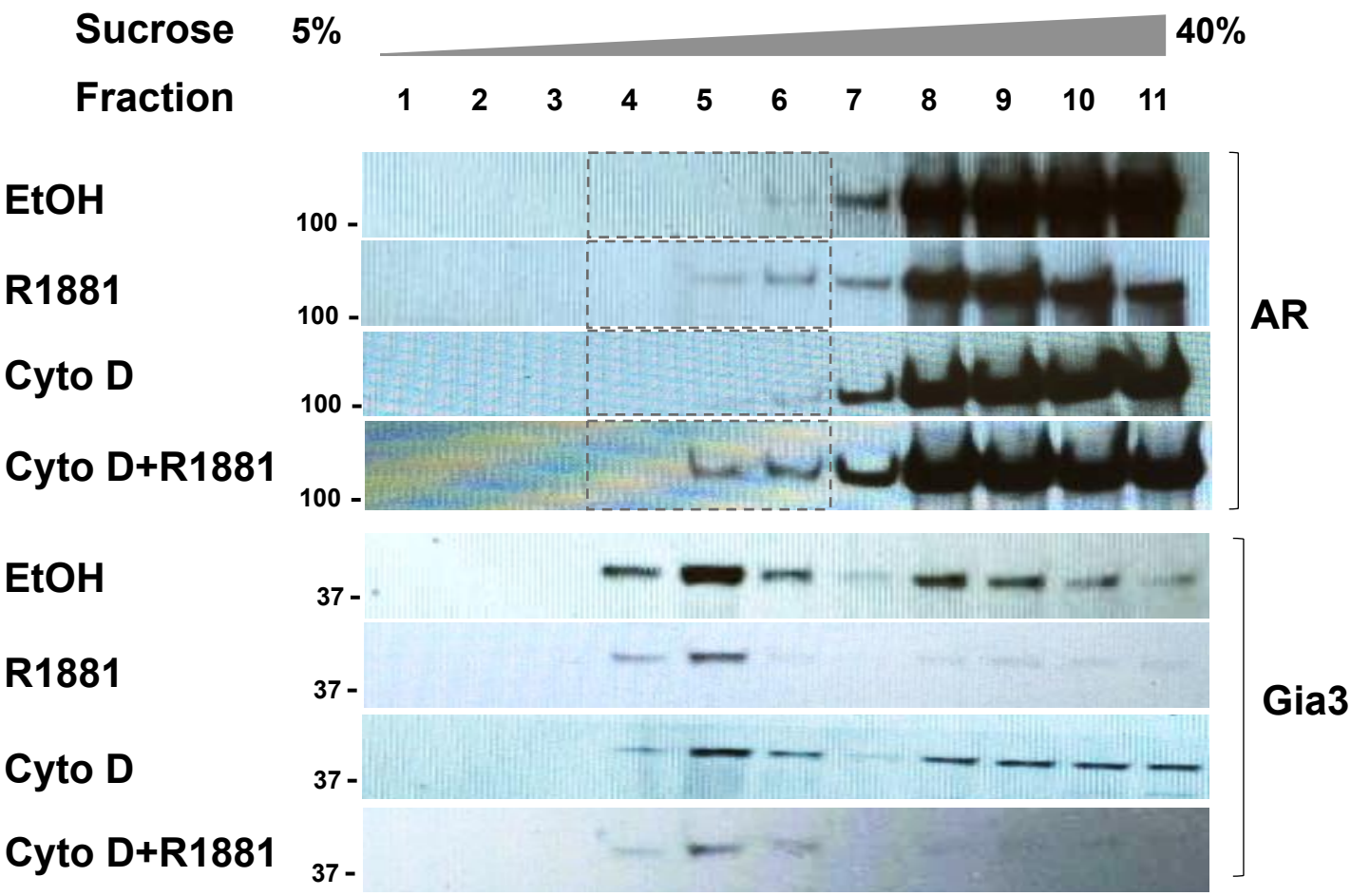

Figure S5. AR transport to the membrane is not affected by cytochalasin D. LNCaP cells were pretreated with EtOH or 0.5 mg/ml cytochalasin D overnight, followed by 1 nM R1881 for an additional 20 min. Cell lysates were subjected to sucrose gradient ultracentrifugation and analyzed by Western blots. Giα3 was used as the membrane marker.

Figure S6

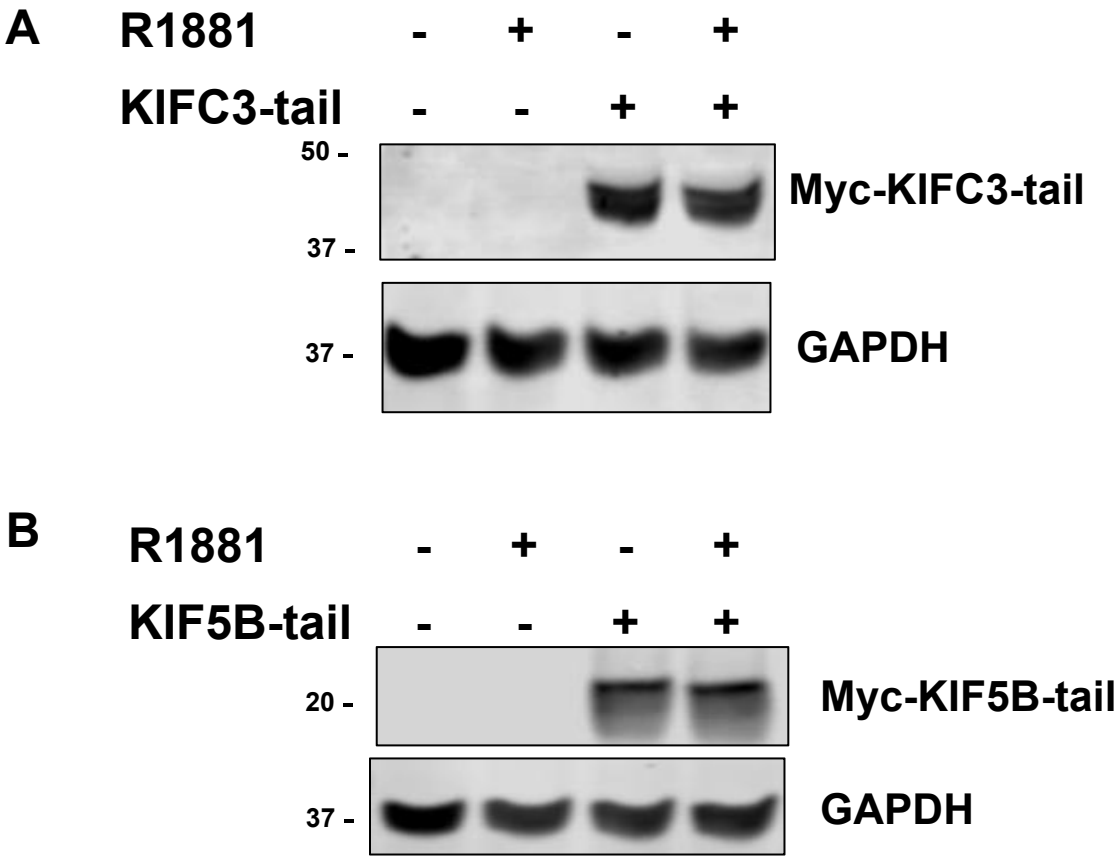

Figure S6. Expression of KIFC3-tail and KIF5B-tail in LNCaP. Cells were transiently transfected with KIFC3-tail or KIF5B-tail. Whole cell lysates were collected after 48 h and analyzed by Western blots to confirm the expression of KIFC3-tail and KIF5B-tail.

Figure S7

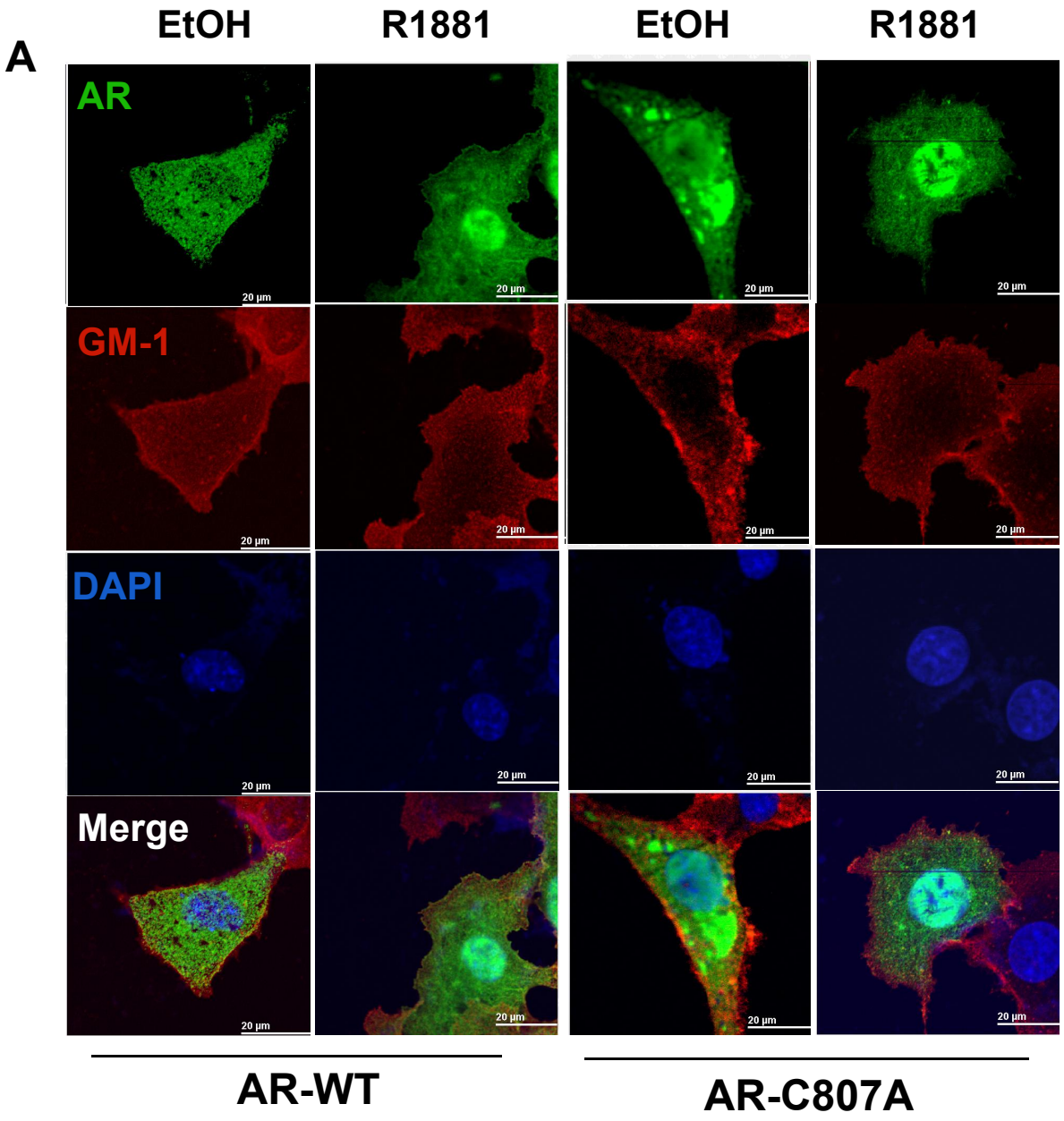

Figure S7 Cont'd

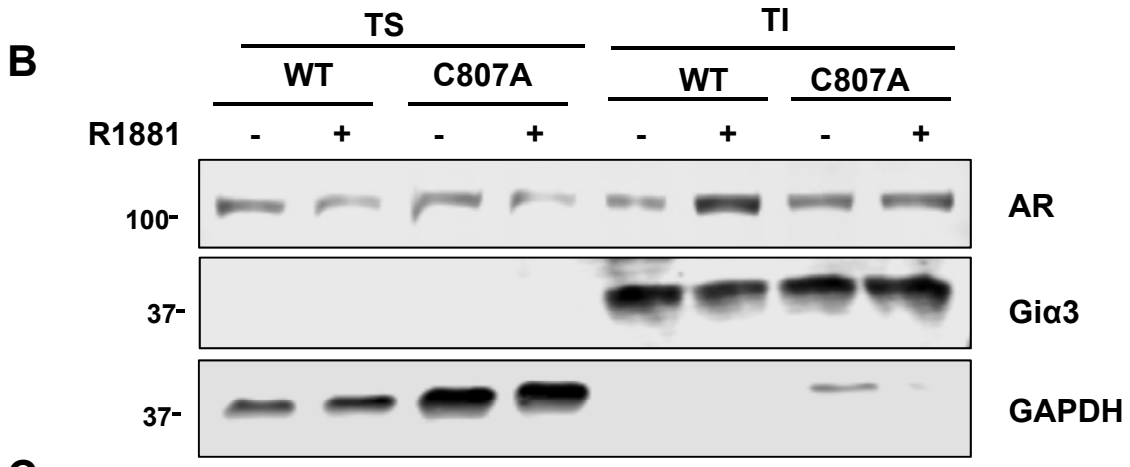

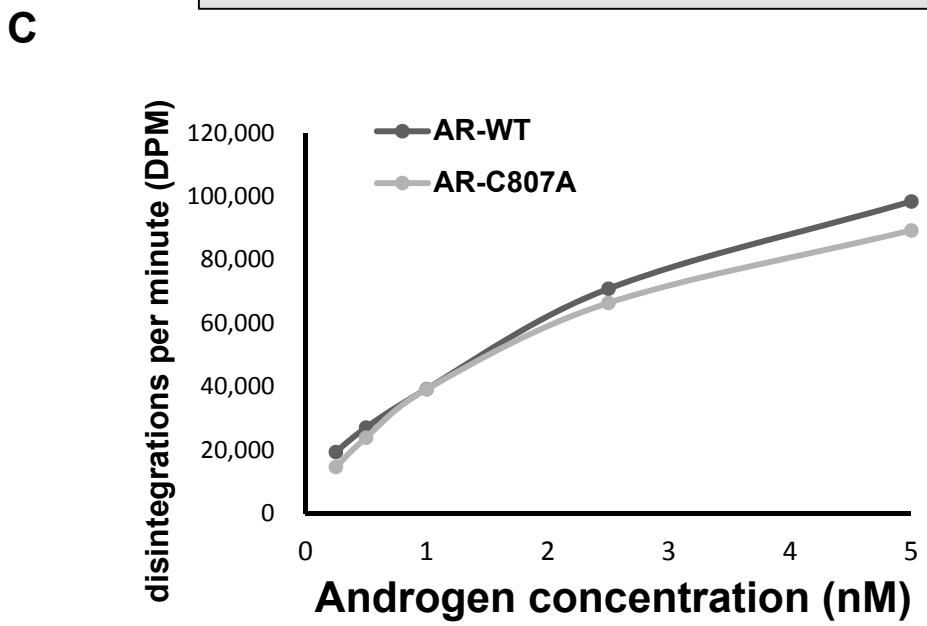

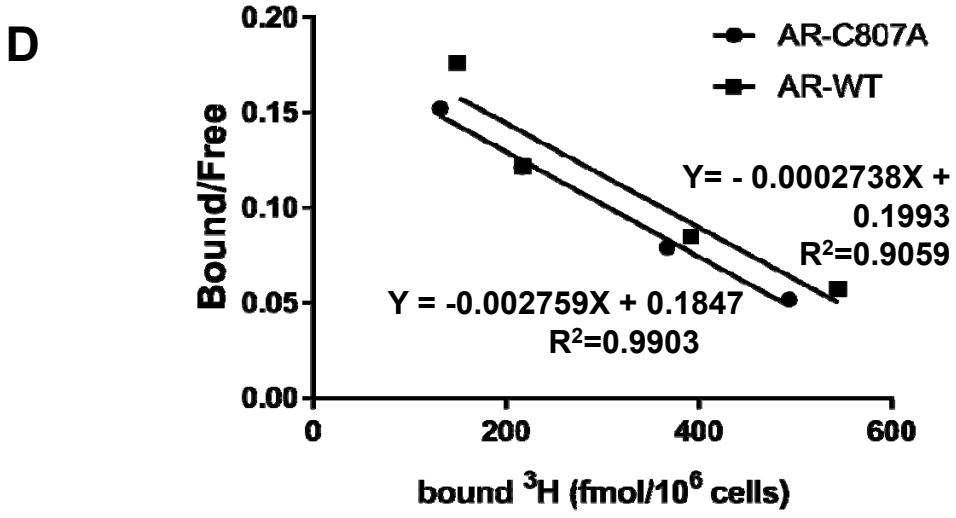

Figure S7 Cont'd

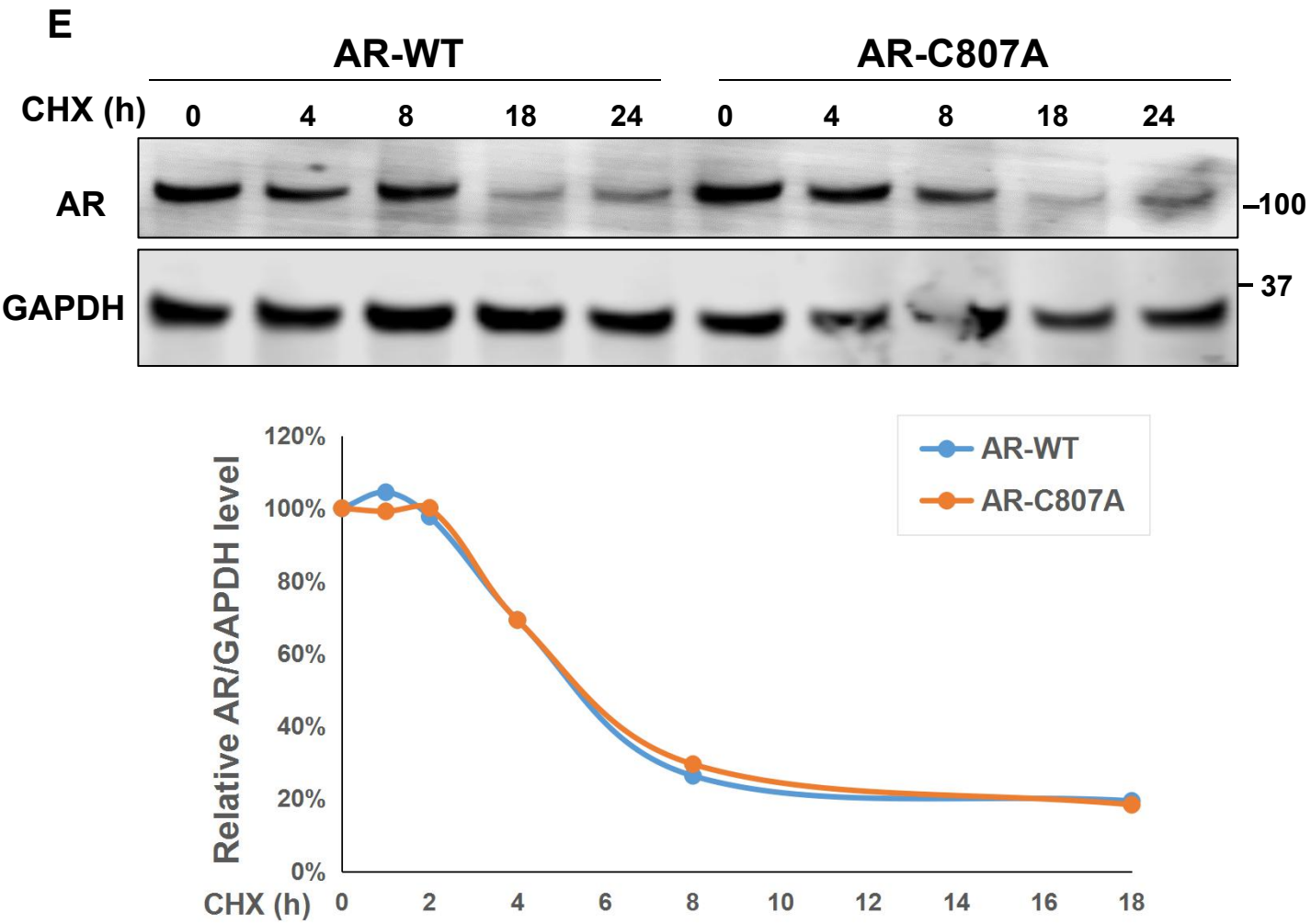

Figure S7. Characterization of the AR-C807A mutant. A, intracellular localization of AR-WT/AR-C807A by immunofluorescence. COS-7 cells were transiently transfected with AR-WT or AR-C807A, cultured in phenol-red free DMEM with 5% cs-FBS for 48 h, and stimulated with 1 nM R1881 for 20 min. Following fixation, cells were stained for AR by an anti-AR (green). B, the localization of AR-WT/AR-C807A at plasma membrane was detected by the TS/TI fractionation assay. C, androgen binding activities of AR-WT and AR-C807A. D, Scatchard plots for AR-WT/AR-C807A ligand binding. The calculated dissociation constant (Kd) is 3.652 pM for AR-WT, and is 3.625 pM for AR-C807A. E, stability of AR-WT and AR-C807A. COS-7 cells were transfected with AR-WT or AR-C807A for 48h, and treated with 20 μg/ml CHX for different times. AR protein in whole cell lysates were analyzed by Western blotting.

Figure S8

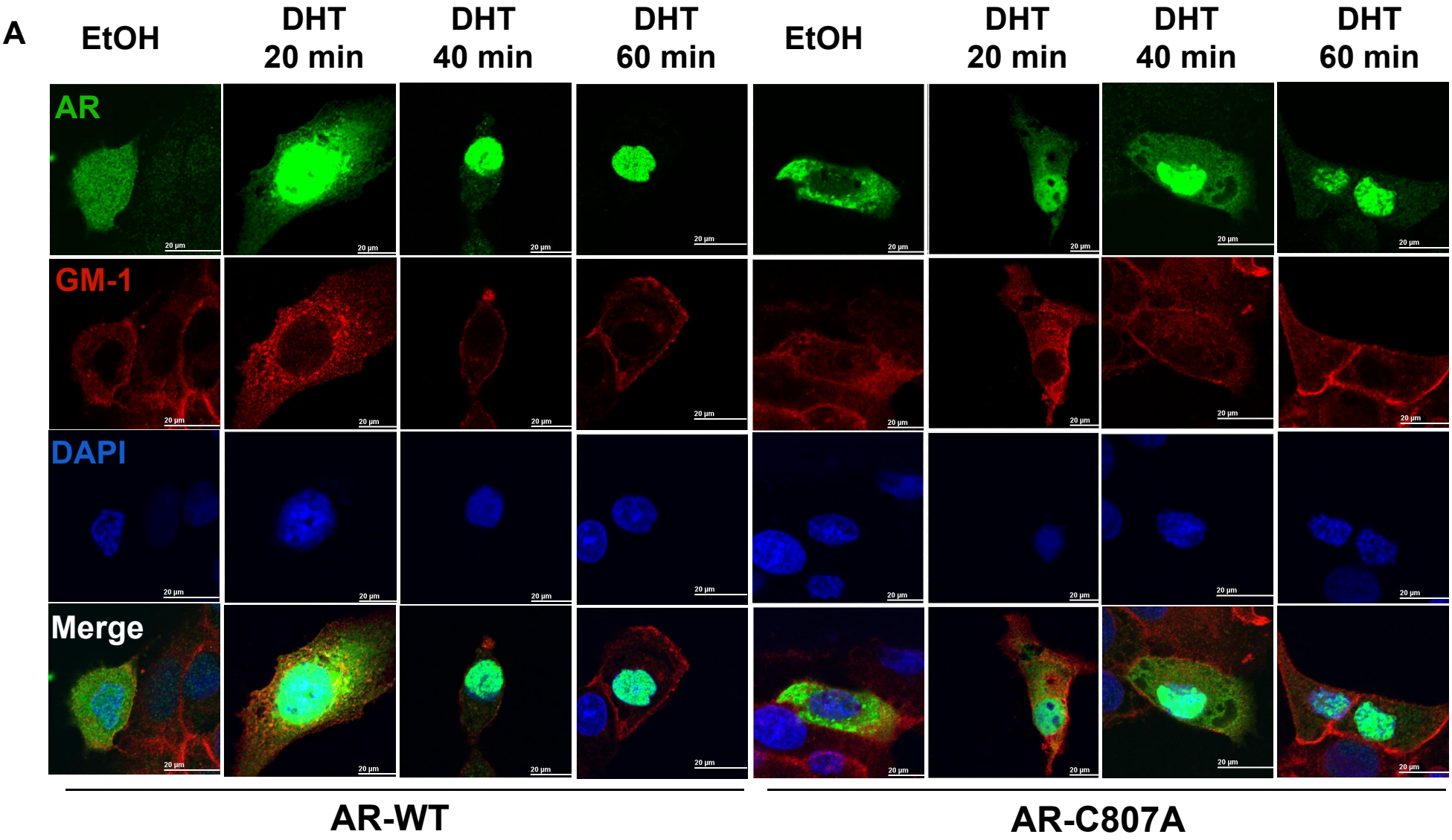
A
EtOH
DHT 20 min
DHT 40 min
DHT 60 min
EtOH
DHT 20 min
DHT 40 min
DHT 60 min
AR
GM-1
DAPI
Merge
20 μm
AR-WT
AR-C807A

Figure S8 Cont'd

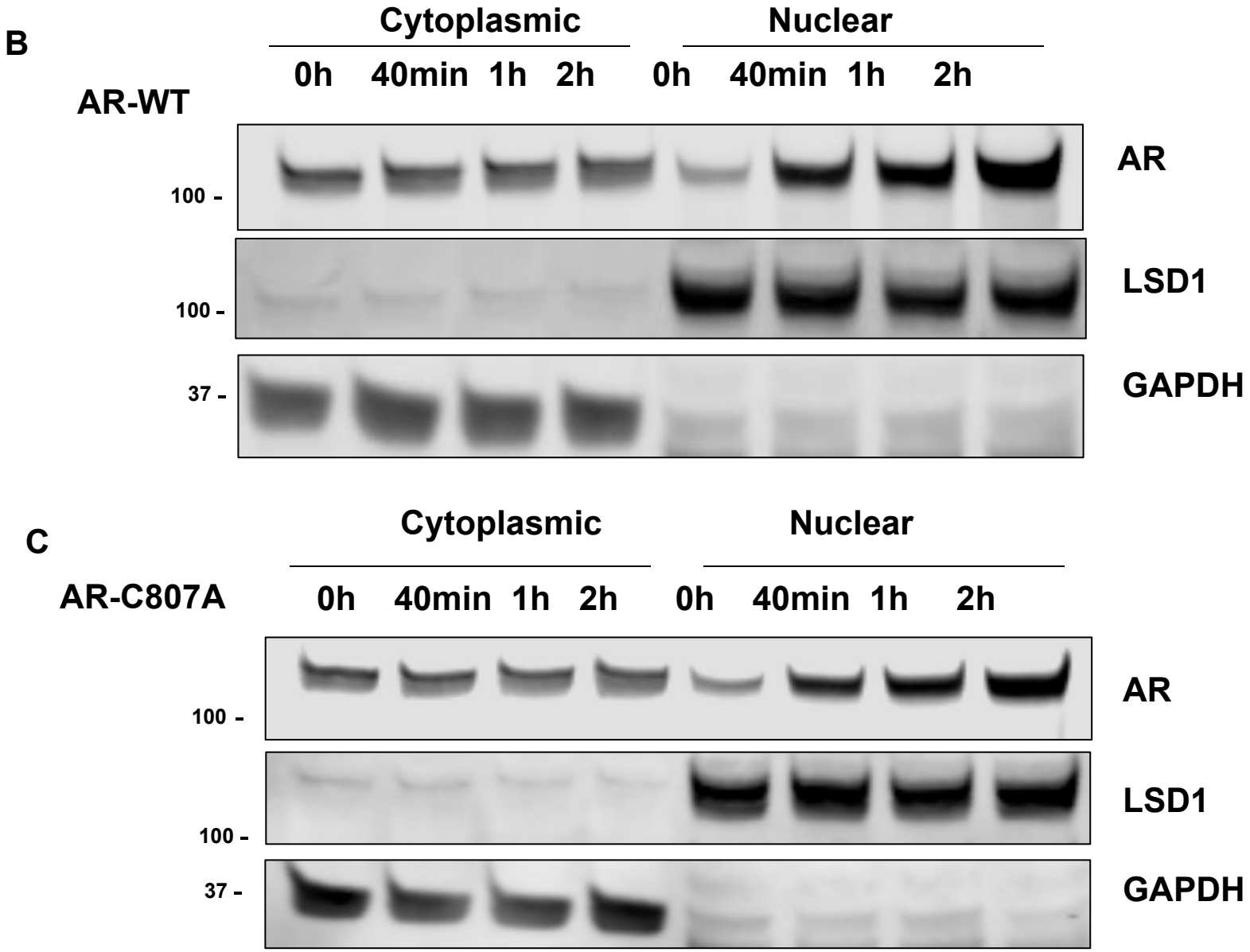

Figure S8. Nuclear import of AR-WT and AR-C807A. A, immunofluorescence assay. Transfected COS-7 cells were treated with 1 nM R1881 for the indicated time points and stained for AR, GM-1, and nuclei. Scale bar is 20 μm. B and C, subcellular fractionation assay. COS-7 cells was treated with 1 nM R1881 for different time points (0, 40 min, 1 h, 2 h), lysed for cytoplasm/nuclear fractionation, and analyzed by Western blots. LSD1 was used as the nuclear marker and GAPDH as the cytoplasmic marker.

Figure S9

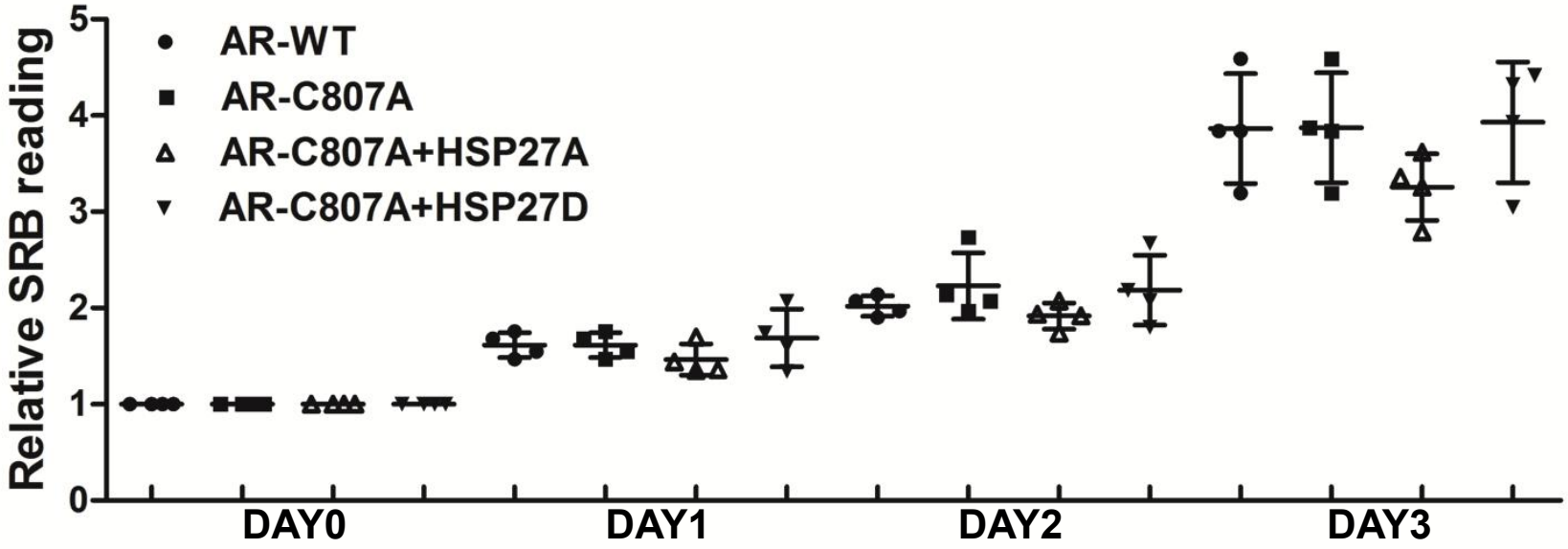

Figure S9. Cell growth assay in DU145 cells without androgen stimulation. Cells were co-transfected with AR-WT/AR-C807A and vector/HSP27A/HSP27D, cultured in RPMI 1640 supplemented with 10% cs-FBS for 1 to 3 days, and the SRB assay was performed. The data were expressed as folds of the day 0 readings and plotted as mean ± SD from three experiments.